

**Combination Therapies Targeting Extracellular Signal Regulated Kinases 1/2 and  
Histone Deacetylase 6 as Potential Therapeutics for B-Cell Lymphoma**

Mariana Asslan

Faculty of Medicine and Health Sciences

Department of Pharmacology and Therapeutics

McGill University, Montreal, Quebec Canada

December 2023

A thesis submitted to McGill University in partial fulfillment of the requirements of the  
degree of Doctor in Philosophy

© Copyright Mariana Asslan 2023

## Table of contents

Table of contents .....	1
Abstract.....	5
Abrégé.....	7
Acknowledgements .....	10
Contribution to original knowledge .....	10
Abbreviation list.....	12
Chapter 1: Introduction.....	18
1.1 Lymphomas .....	18
1.1.1 Introduction .....	18
1.1.2 B lymphocytes maturation, development, and differentiation .....	18
1.1.3 BCR structure and signaling.....	19
1.1.4 Lymphomas and their characteristics .....	21
1.2 Mitogen-activated protein kinases (MAPKs).....	27
1.2.1 Mitogen-activated protein kinase kinase kinase (MAP3K) .....	28
1.2.2 Mitogen-activated protein kinase kinase (MAP2K).....	31
1.2.3 Mitogen-activated protein kinase (MAPK) .....	32
1.2.4 MAPK cascades and tumorigenesis.....	33
1.3 Histone Deacetylases .....	37
1.4 Drug Safety Assessment in Zebrafish Model .....	41
1.5 Hypothesis and Objectives .....	43
Preface .....	44
Chapter 2: Inhibition of the TPL2-MKK1/2-ERK1/2 pathway in B-Cell Lymphomas .....	45
Authors' contributions .....	46
2.1 Abstract.....	46
2.2 Introduction.....	47
2.3 Methods.....	49
2.3.1 Cell culture .....	49
2.3.2 Trypan blue exclusion assay .....	50
2.3.3 Flow cytometry analysis of cell death by propidium iodide (PI) staining.....	50
2.3.4 MTT cell proliferation assay .....	51

2.4 Results.....	51
2.4.1 The susceptibility of the BCWM.1 cell line to TAK1-IKK-TPL2-MKK1/2 pathway inhibitors is dependent on the presence of TLR activation.....	51
2.4.2 TPL2-MKK1/2 inhibition results in cytostatic effect on B-cells isolated from lymphomas.....	56
2.4.3 Dual therapies using BCL2 and TPL2 inhibitors show no interaction towards decreasing OCI-LY2 cell viability. ....	60
2.5 Discussion .....	64
2.6 References .....	66
2.7 Supplementary data.....	71
Preface .....	73
Chapter 3: Single and Dual Inhibition of Extracellular Signal Regulated Kinases 1/2 and Histone Deacetylase 6 as Potential Therapies for Diffuse Large B-Cell Lymphoma .....	74
Authors' contributions .....	75
3.1 Abstract:.....	75
3.2 Introduction.....	76
3.3 Methods and Materials .....	79
3.3.1 Cell culture .....	79
3.3.2 Cell counting assay .....	80
3.3.3 Cell cycle assay .....	80
3.3.4 Apoptosis and necrosis assay .....	81
3.3.5 Nuclear staining .....	81
3.3.6 Immunostaining for flow cytometry analysis .....	82
3.3.6.1 Cytoplasmic proteins .....	82
3.3.6.2 Nuclear proteins .....	82
3.3.7 Proteomic analysis .....	83
3.3.7.1 Whole lysate analysis .....	83
3.3.7.2 Acetylpeptide enrichment analysis.....	84
3.3.8 Statistical analysis.....	85
3.4 Results.....	85
3.4.1 Monotherapies reduce B-cell lymphoma cell line growth in a concentration-dependent manner. ....	85
3.4.2 MKK1/2-HDAC6 inhibitor combinations show additivity in OCI-LY2 and RAMOS cells, but antagonism in BCWM.1 cells. ....	88

3.4.3 Dual therapies increased the percentage of cells at the sub-G1/G1 phase while decreasing the percentage at the S and G2 phases in the OCI-LY2 cell line.	92
3.4.4 Combined therapies exert cytotoxic effects, whereas monotherapies show cytostatic effects.	95
3.4.5 Single and dual therapies affect ERK phosphorylation and ( $\alpha$ -tubulin/H3K14) acetylation.	98
3.4.6 Proteomic analyses after treatment with PD184352 and Sahaquine alone or in combination.	101
3.5 Discussion	103
3.6 References	109
3.7 Supplementary data	122
Preface	131
Chapter 4: Mass spectrometry imaging in zebrafish larvae for assessing drug safety and metabolism	132
Authors' contributions	133
Acknowledgements	133
4.1 Abstract	133
4.2 Introduction	135
4.3 Materials and Methods	138
4.3.1 Materials	138
4.3.2 Zebrafish husbandry	139
4.3.3 Waterborne exposure toxicity assay	139
4.3.4 Sq intravenous (IV) microinjection toxicity assay	140
4.3.5 Larvae embedding, sectioning and confocal microscopy imaging	141
4.3.6 MALDI Mass Spectrometry Imaging	141
4.3.6.1 Sample preparation	141
4.3.6.2 Mass Spectrometry Imaging	142
4.3.7 Xenograft model	142
4.3.7.1 Cells preparation	143
4.3.7.2 Larvae preparation	143
4.3.8 Statistical analysis	144
4.4 Results	144
4.4.1 Sahaquine toxicity in zebrafish larvae evaluated by two exposure routes	144
4.4.2 Development of a MALDI MSI method to study Sq tissue distribution	147
4.4.2.1 DAN matrix was identified as the most suitable matrix for Sq detection	147

4.4.2.2 Optimizing matrix deposition and hexane washes using zebrafish homogenate spiked with Sq .....	150
4.4.2.3 MS/MS identification of Sq injected into larvae yolk .....	152
4.4.3 Sq did not induce tissue specific toxicity .....	152
4.4.4 Glucuronidated Sq was formed and excreted within 72 hpi .....	155
4.4.5 Waterborne exposure was not adequate for Sq to reach therapeutic concentrations in the larval body.....	156
4.5 Discussion .....	157
4.6 References .....	163
4.7 Supplementary data.....	172
Chapter 5: Scholarly Discussion and Conclusion .....	182
5.1 Mechanisms of action involved in cytotoxic effects of dual MKK1/2-HDAC6 inhibition .....	183
5.2 Mechanisms of resistance following NHL first line treatments .....	187
Limitations and future directions .....	189
Conclusion.....	190
Reference list .....	191

## **Abstract**

B cell lymphomas are a heterogeneous group of malignancies affecting B lymphocytes that play an essential role in immune responses as they differentiate into antibody-secreting plasma cells. B cell lymphomas can broadly be divided into B cell Hodgkin lymphoma (HL) and B cell non-Hodgkin lymphoma (NHL) which include more than 50 different types, varying from slow-growing to fast-growing lymphomas. The two most common types of NHL are Diffuse large B cell lymphoma (DLBCL) and follicular lymphoma, whereas some types of NHL are rare such as Burkitt lymphoma and Waldenstrom Macroglobulinemia.

Multiple oncogenic drivers are involved in the formation and progression of these malignancies, such as extracellular signal regulated kinase 1 and 2 (ERK1/2) signaling and histone deacetylase 6 (HDAC6). Deregulation of ERK signaling leading to its constitutive activation is a prominent feature of B-cell lymphomas, including DLBCL. Moreover, mutations of histone-modifying genes promoting malignant transformation are common in B-cell lymphomas, especially in DLBCL. Hence, novel therapies targeting oncogenic mechanisms are particularly attractive as an alternative therapeutic strategy to replace the standard chemotherapies which are associated with a wider range of adverse events and a high rate of relapse after initial therapy in lymphoma patients. Therefore, the central hypothesis in this project is that single and dual inhibition of ERK1/2 signaling and HDAC6 activity will impair the survival of B cell NHL.

For this thesis, I tested the efficacy of pharmacological inhibitors of ERK1/2 signaling and HDAC6 activity as single agents to prevent the proliferation and survival of several B cell NHL cell lines in vitro (Aim 1). Afterwards, I evaluated the combined effect of dual ERK1/2 and HDAC6 inhibition in a cell culture model and characterized the combined mechanisms of action (Aim 2). Finally, I optimized a matrix-assisted laser desorption/ionization mass spectrometry imaging (MALDI MSI) approach specifically designed to detect a novel HDAC6 inhibitor, Sahaquine, in zebrafish larvae to assess its safety and metabolism (Aim 3).

Results show that monotherapies including ERK1/2 cascade inhibitors (Compound 1 and PD184352), and HDAC6 inhibitors (Sahaquine and ACY1215) hinder cell growth and have mainly cytostatic effects. Conversely, dual inhibition of ERK1/2 and HDAC6 induces cell death. To better understand the potential mechanisms of action of this combination, acetylation-affinity purification combined with mass spectrometry was performed. This led to the identification of four proteins of interest, namely Actin-related protein 2/3 complex subunit 2 (ARPC2); Delta(3,5)-Delta(2,4)-dienoyl-CoA isomerase mitochondrial (ECH1); Cathepsin D (CATD/CTSD); and Strawberry notch homolog 1 (SBNO1). These results can help provide an explanation linking the inhibition of HDAC6 and ERK1/2 activity to interference with DNA damage responses and energy production. Safety studies indicate that Sahaquine has a good safety profile in zebrafish larvae. Moreover, MALDI MSI data detected a potential Sahaquine metabolite (glucuronidated form) and identified a distinct protection mechanism that enables zebrafish larvae to eliminate xenobiotics via yolk-intestine translocation associated with intestine metabolic activity.

As a comprehensive body of work, this study provides insight into an innovative strategy and suggests that dual inhibition of ERK1/2 signaling and HDAC6 activity shows promise as a more efficacious strategy than a single therapy for the improvement of lymphoma treatment. In addition, the optimized MALDI MSI protocol applied in a zebrafish safety study can be widely used to study metabolic fate and distribution of other anti-tumorigenic compounds.

## **Abrégé**

Les lymphomes à cellules B constituent un groupe hétérogène de tumeurs malignes affectant les lymphocytes B qui jouent un rôle essentiel dans les réponses immunitaires en se différenciant en plasmocytes sécréteurs d'anticorps. Les lymphomes à cellules B peuvent être divisés en deux grandes catégories : les lymphomes hodgkiniens à cellules B (HL) et les lymphomes non hodgkiniens à cellules B (LNH), qui comprennent plus de 50 types différents, allant des lymphomes à croissance lente aux lymphomes à croissance rapide. Les deux types de LNH les plus courants sont le lymphome diffus à grandes cellules B (DLBCL) et le lymphome folliculaire. Les LNH, comme le lymphome de Burkitt et la macroglobulinémie de Waldenstrom, sont quant à eux plus rares.

De multiples facteurs oncogéniques sont impliqués dans la formation et la progression de ces tumeurs malignes, tels que les signaux extracellulaires régulés par les kinases 1 et 2 (ERK1/2) et histone désacétylase 6 (HDAC6). La dérégulation de la signalisation ERK conduisant à son activation constitutive est une caractéristique majeure des

lymphomes à cellules B, y compris les DLBCL. De plus, les mutations des gènes modifiant les histones et favorisant la transformation maligne sont fréquentes dans les lymphomes à cellules B, en particulier dans les DLBCL. Par conséquent, de nouvelles thérapies ciblant les mécanismes oncogéniques sont particulièrement intéressantes en tant que stratégie thérapeutique alternative pour remplacer les chimiothérapies traditionnelles qui, elles, sont souvent associées à un large éventail d'effets secondaires indésirables et à un taux élevé de rechute après la thérapie initiale chez les patients atteints de lymphome. Ainsi, l'hypothèse centrale de ce projet est que l'inhibition simple et double de la signalisation ERK1/2 et de l'activité HDAC6 réduira la survie des cellules B issues de LNH.

Dans le cadre de cette thèse, j'ai d'abord testé l'efficacité in vitro d'inhibiteurs pharmacologiques de la signalisation ERK1/2 et de l'activité HDAC6 en tant qu'agents uniques pour empêcher la prolifération et la survie de plusieurs lignées cellulaires de LNH à cellules B (Objectif 1). Ensuite, j'ai évalué l'effet combiné de la double inhibition d'ERK1/2 et d'HDAC6 dans un modèle de culture cellulaire et j'ai caractérisé les mécanismes d'action combinés (objectif 2). Enfin, j'ai optimisé une approche d'imagerie par spectrométrie de masse par désorption/ionisation laser assistée par matrice (MALDI MSI) spécialement conçue pour détecter un nouvel inhibiteur de HDAC6, la Sahaquine, dans des larves de poisson zèbre et ce, afin d'évaluer la toxicité et la façon dont ce composé est métabolisé (Objectif 3).

Les résultats montrent que les monothérapies comprenant des inhibiteurs de la cascade ERK1/2 (Compound 1 et PD184352) et des inhibiteurs de HDAC6 (Sahaquine et ACY1215) entravent la croissance cellulaire et ont principalement des effets

cytostatiques. À l'inverse, la double inhibition d'ERK1/2 et d'HDAC6 induit la mort cellulaire. Afin de mieux comprendre les mécanismes d'action potentiels de cette combinaison, une purification par acétylation et affinité combinée à la spectrométrie de masse a été réalisée et a conduit à l'identification de quatre protéines d'intérêt, à savoir la sous-unité 2 du complexe Actin-related protein 2/3 (ARPC2), la Delta(3,5)-Delta(2,4)-dienoyl-CoA isomerase mitochondriale (ECH1), la cathepsine D (CATD/CTSD) et le Strawberry notch homolog 1 (SBNO1). Ces résultats peuvent contribuer à expliquer le lien entre l'inhibition de l'activité de HDAC6 et de ERK1/2 et l'interférence avec les réponses aux lésions de l'ADN et la production d'énergie. Les études de toxicité indiquent que Sahaquine a un bon profil d'innocuité chez les larves de poisson zèbre. En outre, les données MALDI MSI ont permis de détecter un métabolite potentiel de la Sahaquine (forme glucuronidée) et d'identifier un mécanisme de protection distinct qui permet aux larves de poisson zèbre d'éliminer les xénobiotiques via la translocation sac vitellin-intestin associée à l'activité métabolique de l'intestin.

Dans l'ensemble, cette étude propose une stratégie innovante et suggère que la double inhibition de la signalisation ERK1/2 et de l'activité HDAC6 est prometteuse et plus efficace qu'une thérapie unique afin d'améliorer le traitement du lymphome. De plus, le protocole MALDI MSI optimisé appliqué à une étude de sécurité chez le poisson zèbre peut devenir un outil de choix pour étudier la métabolisation et la distribution d'autres composés anti-tumorigènes.

## **Acknowledgements**

I wish to extend big thanks to my supervisor Dr. Simon Rousseau for his guidance and supervision. I am very grateful for the unique perspectives (scientific and personal) he has provided throughout all these years.

Thanks to the entire Department of Pharmacology and Therapeutics for exposing me to the world of pharmacological research and special huge thanks to Tina for her everlasting support.

Thanks to all my advisory committee members for so generously sharing their expertise with me, namely, Dusica Maysinger, Barbara Hales, Wilson Miller, and Maureen Mckeague.

Thanks to the many great friends that I have made during my study.

And finally, thanks to my family for their encouragement and support.

## **Contribution to original knowledge**

The original contribution of my thesis work to general knowledge can be summarized as follows:

1. Targeting ERK1/2 signaling via TPL2 inhibition is an effective therapeutic strategy to inhibit the growth of B cell NHL.

2. The impact of TAK1-IKK-TPL2-MKK1/2 pathway inhibition depends on the presence of TLR activation signals in a lymphoplasmacytic lymphoma cell line with MYD88 mutations.
3. Blocking HDAC6 activity has an inhibitory effect on B cell NHL proliferation in a dose-dependent manner.
4. The dual inhibition of ERK1/2-HDAC6 leads to an additive effect in DLBCL with p53 aberrations and normal NF- $\kappa$ B activity. Therefore, it can be considered as a potential alternative strategy to treat DLBCL patients with similar profiles.
5. The combination of HDAC6 and ERK1/2 inhibitors induces cytotoxic effects, presumably by affecting mechanisms involved in disrupting DNA damage response via targeting ARPC2 and SPNO1 acetylation, in addition to probably reducing metabolic energy production by interfering with cathepsin D and ECH1 functions.
6. Sahaquine has a good safety profile and it did not accumulate in vital organs; instead it was metabolized into a glucuronidated form and excreted, as shown in the zebrafish larvae study. Therefore, it merits further investigations in other disease models.
7. The MALDI MSI study enhanced our understanding of the xenobiotics distribution and elimination in zebrafish larvae by identifying a distinct protection mechanism that enables zebrafish larvae to eliminate xenobiotics via accumulating them in the yolk, then translocating and metabolizing them in the intestine.
8. The optimized MALDI MSI protocol can be widely used to study the distribution and metabolic fate of other Sahaquine-related molecules in the aquatic environment and to understand their potential consequences on aquatic species.

## Abbreviation list

<b>Abbreviation</b>	<b>Name</b>
ABC	Activated B-cell
AKT	Protein kinase B (PKB, or Akt)
ARID1A	AT-Rich Interaction Domain 1A
ARPC2	Actin-related protein 2/3 complex subunit 2
ASK	Apoptosis signal-regulating kinase
Bad	Bcl-2-associated death promoter
Bak	Bcl-2 homologous antagonist/killer
Bax	Bcl-2-associated X protein
BCL	B-cell lymphoma
BCR	B-cell antigen receptor
BET	Bromodomain and extraterminal
BFL-1/A1	Bcl-2-related protein A1
BH	BCL2-homology
Bid	BH3-interacting domain death agonist
Bik	Bcl-2-interacting killer
Bim	Bcl-2 interacting mediator of cell death
BLNK	B-cell linker protein
Bmf	Bcl-2 modifying factor

Bok	BCL-2–related ovarian killer
BTK	Bruton's tyrosine kinase
CATD/CTSD	Cathepsin D
CCND3	Cyclin D3
CD	Cluster of differentiation
CDK	Cyclin dependent kinase
COO	Cell Of Origin
CoREST	co-repressor for element-1-silencing transcription factor
CREBBP	CREB Binding Protein
CTCL	Cutaneous T cell lymphoma
CTLA4	Cytotoxic T-lymphocyte antigen 4
CYP	Cytochrome P
DAG	Diacylglycerol
DEF	Docking site for ERK and FXFP
DLBCL	Diffuse Large B Cell Lymphoma
DLK	Dual leucine kinase
DNA	Deoxyribonucleic acid
dpf	days of post fertilization
ECH1	Delta(3,5)-Delta(2,4)-dienoyl-CoA isomerase mitochondrial
EGFP	Enhanced green fluorescent protein
ELK-1	ETS Like-1 protein
EMA	European Medicines Agency
EP300	E1A binding protein p300

ERK	Extracellular signal-regulated kinase
FDA	Food and Drug Administration
FL	Follicular Lymphoma
Fos	Finkel-Biskis-Jinkins osteosarcoma
GCB	Germinal center B-cell
GCs	Germinal centres
Grb2/SOS	Growth factor receptor-bound protein/Son of Sevenless
HATs	Histone Acetyltransferases
HDACs	Histone Deacetylases
HL	Hodgkin lymphoma
HPFB	Health Products and Food Branch
Hrk	Harakiri protein
ID3	Inhibitor Of DNA Binding 3
Ig	Immunoglobulin
IKK	Inhibitor of nuclear factor- $\kappa$ B (I $\kappa$ B) kinase
ITAM	Immunoreceptor tyrosine-based activation motif
ITO	Indium tin oxide
JNK	Jun N-terminal kinase
KMT2D	Lysine methyltransferase 2D
KSR	Kinase suppressor of Ras
LAG3	Lymphocyte-activation gene 3
LYN	Lck/Yes novel tyrosine kinase
LZK	Leucine zipper kinase

MALDI MSI	matrix-assisted laser desorption/ionization mass spectrometry imaging
MAP2K	Mitogen Activated Protein Kinase Kinase
MAP3K	Mitogen Activated Protein Kinase Kinase Kinase
MAPK	Mitogen Activated Protein Kinase
Mcl-1	Myeloid leukemia 1
MHC	Major histocompatibility complex
MKP3	MAPK phosphatase 3
MLK	Mixed lineage kinase
MLL2	Mixed Lineage Leukemia 2
MNK	MAPK interacting kinase
MOS	Moloney murine sarcoma
MP1	MEK Partner-1
MSK	Mitogen- and stress-activated kinases
mTOR	Mammalian target of rapamycin
MYC	Myelocytomatosis oncogene
MYC	Myelocytomatosis
MYD88	Myeloid differentiation primary response gene 88
NAD <sup>+</sup>	Nicotinamide adenine dinucleotide
NF- $\kappa$ B	Nuclear Factor kappa B
NHL	Non-Hodgkin lymphoma
NLK	Nemo-like kinase
Noxa	Phorbol-12-myristate-13-acetate-induced protein 1

NuRD	nucleosome remodeling and deacetylation
P53	tumor protein 53
PARP	poly (ADP-ribose) polymerase
PCR	Polymerase chain reaction
PD1	Programmed cell death protein 1
PI3K	Phosphoinositide 3-kinase
PIP2	Phosphatidylinositol 4,5-bisphosphate
PKC $\beta$	Protein kinase C beta
PLC $\gamma$ 2	Phospholipase C gamma 2
PTCL	Peripheral T cell lymphoma
PTEN	Phosphatase and TENsin homolog
Puma	P53 upregulated modulator of apoptosis
RAF	Rapidly Accelerated Fibrosarcoma
RAS	Rat sarcoma
RSK	Ribosomal S6 kinase
SBNO1	Strawberry notch homolog 1
Sin3	Swi-independent 3
SIRT	Sirtuins
SMARCA4	SWI/SNF related, matrix associated, actin dependent regulator of chromatin, subfamily a, member 4
SRC	Sarcoma
SYK	Spleen tyrosine kinase
T7E1	T7 Endonuclease I

TAK1	Transforming growth factor $\beta$ -activated kinase 1
TAO	Thousand and one
TCF3	Transcription factor 3
TIM3	T-cell immunoglobulin and mucin-domain containing protein 3
TLR	Toll-like receptor
TPL2	Tumor Promoting Locus 2
TRIF	TIR domain-containing adaptor protein inducing interferon- $\beta$
WM	Waldenstrom Macroglobulinemia
ZAK	Sterile alpha motif and leucine zipper containing kinase AZK

# **Chapter 1: Introduction**

## **1.1 Lymphomas**

### **1.1.1 Introduction**

Lymphomas are malignancies affecting the lymphatic system that consists of lymph nodes, lymphatic organs, and lymphatic vessels [1]. This system circulates the lymphocytes throughout the body to fight infections [2]. Therefore, lymphomas can arise in nodal or extra-nodal sites, such as the gastrointestinal tract, skin, breast, bone, lung, or brain. Lymphocytes belong to a category of white blood cells which are essential components of the immune system. There are three main types of lymphocytes: B lymphocytes (B cells), T lymphocytes (T cells), and natural killer cells. Lymphocytes originate from pluripotent hematopoietic stem cells in the bone marrow that give rise to lymphoid progenitor cells which are the precursor of the lymphocytes [3]. B lymphocytes undergo maturation in the bone marrow, then migrate to peripheral lymphoid tissue to complete their development [4], while T lymphocytes mature in the thymus. B and T lymphocytes are responsible for adaptive immune responses against foreign antigens because they bear antigen receptors [5].

### **1.1.2 B lymphocytes maturation, development, and differentiation**

B lymphocytes have the B-cell antigen receptor (BCR), a membrane immunoglobulin (antibody) that undergoes 3 gene-remodeling processes during maturation and development [6]. The first remodeling (VDJ recombination) takes place in bone marrow

and leads to B cell maturation via the formation of functional BCR. This functional BCR on mature naive B cells can recognize (at low affinity) antigens expressed on T cells, circulating throughout the body [7]. Upon antigen activation, these activated B cells are recruited to secondary lymphoid tissues to undergo a second BCR-gene remodeling event, where they establish germinal centres (GCs). The second remodeling (somatic hypermutation) increases BCR affinity for a cognate antigen and occurs in a specific area of the GC called the dark zone [8].

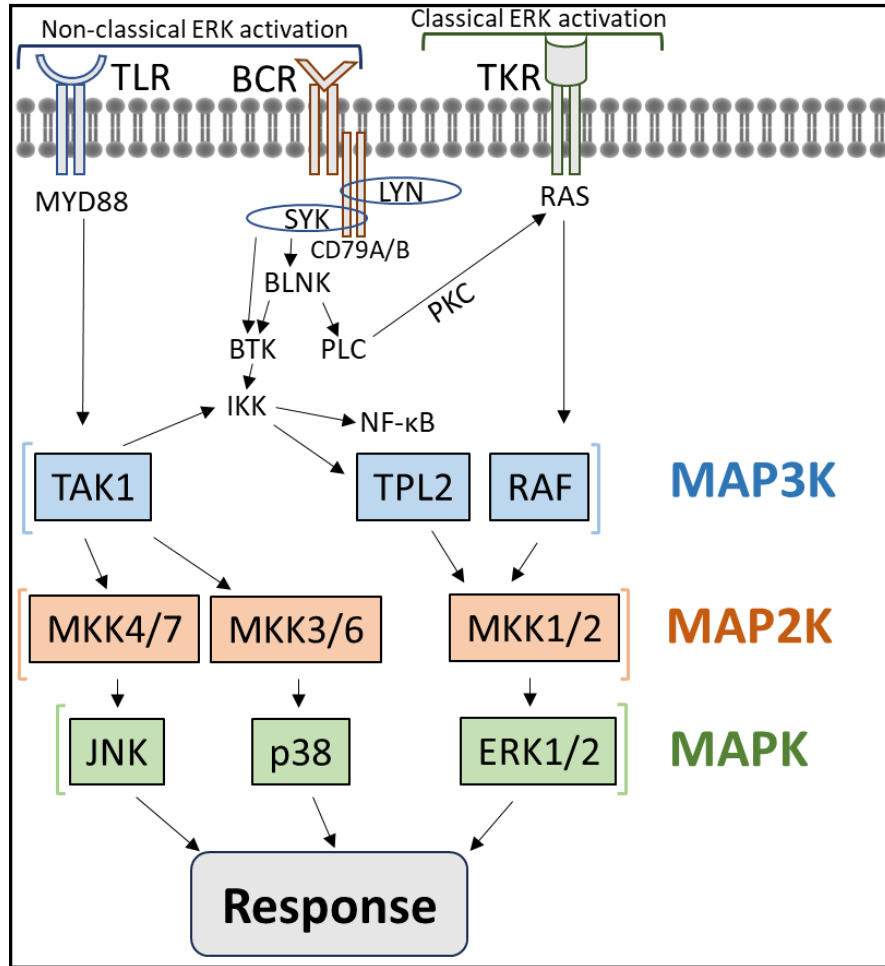
The third BCR-gene remodeling (class switch recombination) also occurs in GCs in a specific area called the light zone. It results in the exchange of IgM and IgD constant regions with IgG, IgA, or IgE leading to the BCR antibody recognizing the same antigen, but it initiates different functions [9]. These developed GC B cells will differentiate into either memory B cells or antibody-secreting plasma cells and will leave the GC microenvironment. The last two remodeling processes with the differentiation steps are known as the GC reaction [10].

### **1.1.3 BCR structure and signaling**

The BCR consists of pair of heavy and light immunoglobulin chains, each chain containing two regions: the variable-region that interacts with the antigen and the constant-region that interacts with downstream effectors. B cells in the bone marrow develop a functional BCR by rearranging DNA segments of the variable-region to form a V, (D), and J gene segment combination known as V(D)J recombination [9]. Following BCR activation, the rearranged variable-region genes are subject to deletions, duplications, or point mutations via a process called somatic hypermutation that occurs

in germinal centers. B cells with favorable somatic hypermutation (higher antigen affinity) will be selected to undergo constant-region exchange to switch from IgM or IgD to IgG, IgA, or IgE, which is known as class switch recombination. This switching is essential to alter BCR effector functions, without affecting the specificity for the antigen [11, 12].

The BCR is coupled with a heterodimer of CD79A (Ig $\alpha$ ) and CD79B (Ig $\beta$ ) subunits that possess a cytoplasmic immunoreceptor tyrosine-based activation motif (ITAM) containing two tyrosine residues [13]. Antigen-dependent activation of the BCR leads to receptor aggregation and phosphorylation of ITAM tyrosine residues by the SRC-family kinases (mainly LYN) [14, 15]. Phosphorylated tyrosine residues on CD79A/CD79B recruit and activate tyrosine kinase SYK, which in turn promotes B-cell linker protein (BLNK) to phosphorylate downstream effectors such as BTK and PLC $\gamma$ 2, in addition to the cytoplasmic tail of CD19, which can activate PI3K. Phosphorylated PLC $\gamma$ 2 cleaves PIP2 to generate DAG and inositol triphosphate which is involved in the regulation of intracellular calcium levels. DAG mediates PKC $\beta$  activation leading to RAS-dependent phosphorylation of ERK1/2, in addition to Nuclear Factor kappa B (NF- $\kappa$ B) pathway activation. ERK1/2 signaling can also be activated by recruiting the Grb2/SOS complex to associate with ITAM or BLNK. Therefore, BCR signaling promotes B cell proliferation, differentiation, and survival [16-18].



#### 1.1.4 Lymphomas and their characteristics

Lymphoma was first reported by Thomas Hodgkin in 1832; therefore, lymphomas have been categorized into two main groups: Hodgkin lymphoma (HL) that affects B cells and non-Hodgkin lymphoma (NHL) that can affect B, T, or natural killer cells. Both types can appear in either adults or children and vary from slow-growing (indolent) to fast-growing (aggressive) lymphomas. The origin of various B-cell lymphomas can be determined based on the stage of GC reaction that is characterized by a specific BCR-structure and expression of B cell cluster of differentiation (CD) markers, in particular histological

structures. B cell CD markers include CD79A/CD79B, CD19, CD20, CD24, CD27, and CD38 [9, 19-21] .

### **Hodgkin Lymphoma (HL)**

HL accounts for 10% of all lymphomas and are distinguished by the presence of pathological Reed-Sternberg cells that are malignant B cells. There are 4 types of classical HL, namely nodular sclerosing, mixed cellularity, lymphocyte rich, and lymphocyte depleted HL, and only one type of non-classical HL that is nodular lymphocyte-predominant. No underlying causes are defined in the majority of cases. Some risk factors are immunodeficiency and Epstein Barr virus infection. HL is mostly curable with combinations of several cytotoxic chemotherapies and radiation therapy. Moreover, relapsing can be effectively treated with chemotherapy followed by autologous stem cell transplantation [22] .

### **Non-Hodgkin Lymphoma (NHL)**

NHL accounts for 90% of all lymphomas, including diverse malignancies that arise from either B cells (90%) or T and natural killer cells (10%). There are more than 60 different NHL types, classified according to histological characteristics. The two most common types are diffuse large B Cell lymphoma and follicular lymphoma, which together represent 65% of all NHL types, whereas some types are rare, such as Burkitt lymphoma and Waldenstrom Macroglobulinemia.

## **Diffuse Large B Cell Lymphoma (DLBCL)**

DLBCL, the most common B cell NHL, is a genetically, clinically, and morphologically heterogeneous aggressive malignancy that arises from mature B lymphocytes during the GC reaction [23, 24]. DLBCL cells express the standard B-cell markers, including CD19, CD20, CD22, CD45, and CD79a [25]. Alterations in histone-modifying genes are among the most frequent genetic mutations in DLBCL, such as genetic inactivation of *EP300* /*CREBBP* (acetyltransferases) and *MLL2* (histone methyltransferase). These mutations prevent B cells from terminating the GC reaction. Therefore, they can promote malignant transformation [25-29]. DLBCL generally escape immune surveillance and become invisible to cytotoxic T lymphocytes and natural killer cells due to genetic lesions affecting the expression of CD58 and major histocompatibility complex (MHC) class I, both of which are necessary for immune system recognition [30].

DLBCLs are classified according to their probable Cell Of Origin (COO) into two main subtypes with distinct genomic profiles and different clinical outcomes, namely the germinal center B-cell (GCB) and activated B-cell (ABC) subtypes. In addition, one minor subtype consists of DLBCL that cannot be classified as either GCB or ABC. These subtypes are clinically further categorized based on the presence of BCL2, BCL6, and MYC chromosomal translocations and expression [25, 31]. It is postulated that GCB DLBCL affects GC B cells during the second BCR-gene remodeling (somatic hypermutation). GCB DLBCL preferentially express IgG BCR [11, 32] and generally harbor t(14;18) translocation [33-35] leading to the upregulation of BCL2 (anti-apoptotic

protein). Membrane IgG possesses a longer C-terminal cytoplasmic end, containing both a protein–protein interaction domain (PDZ) and a tyrosine phosphorylation site [36]. Therefore, the IgG tail can enhance signaling, including activating the extracellular signal–regulated kinase (ERK) pathway [37, 38], in addition to traditional BCR signaling mediated by CD79A and CD79B. It is postulated that ABC DLBCL is derived from GC B cells either during the third BCR-gene remodeling or immediately after it. Most commonly ABC DLBCL express IgM BCR [11, 32] with NF- $\kappa$ B constitutive activation as a result of variant alterations including MYD88 mutation [39, 40]. IgM BCR signaling is mediated mainly via CD79A and CD79B because IgM has very short cytoplasmic tail that consists of a few amino acids only [36].

The treatment of choice for DLBCL is R-CHOP immunochemotherapy: Rituximab is an anti-CD20 monoclonal antibody; Cyclophosphamide is an alkylating agent; Hydroxydaunorubicin (doxorubicin) is an intercalating agent; Oncovin (vincristine) is an anti-microtubule agent; and Prednisone is an immunosuppressant and anti-inflammatory agent. Although R-CHOP therapy improved the overall survival of DLBCL patients, eventually more than half of them relapse. Recurrent DLBCL is associated with more aggressive characteristics and extremely poor outcomes [41]. After relapsing, salvage immunochemotherapy with autologous stem cell transplantation can cure only 10% of cases [42]. Novel therapeutics targeting DLBCL dysregulated signaling pathways are under investigation, including NF- $\kappa$ B [43-50], BCR [51-53], BCL-2 [54, 55], and PI3K–AKT–mTOR [56, 57] signaling. Clinical trial results showed that these

inhibitors are generally more effective when used in combinations compared into single therapy procedures [43-47, 50-57].

### **Follicular Lymphoma (FL)**

FL, the second most common B cell NHL, is an indolent lymphoma mainly affecting adults with a median survival of 10 years. The initiating genetic translocation t(14;18) occurs in the bone marrow during the first BCR-gene remodeling, leading to the overexpression of the anti-apoptotic protein BCL2. However, this mutation alone is not enough to form FL. The accumulation of further genetic mutations in the GC during the second and third steps of BCR-gene remodeling is essential to complete FL transformation. Moreover, in some cases FL can progressively transform into more aggressive DLBCL [58]. Currently, FL is generally considered an incurable disease. Therefore, for patients without treatment indications, the watchful monitoring strategy is adopted [59]. Upon relapsing, FL patients can be treated with several chemoimmunotherapy regimens, phosphoinositide 3-kinase inhibitors, and lenalidomide plus rituximab [60].

### **Burkitt lymphoma**

Burkitt lymphoma is a GC B-cell non-Hodgkin lymphoma, representing 1% of adult NHL and 30-50% of childhood NHL [61]. Burkitt lymphoma is classified as follows: immunodeficiency (HIV)-related type; Epstein Barr virus-related malaria-endemic type; and developed-nations sporadic type [62]. In Burkitt lymphoma, *MYC* was identified as

an important oncogene due to t(8; 14) chromosomal translocation that constitutively activates the *MYC* gene, leading to rapid cell proliferation, thus making it the fastest growing human tumor [63, 64]. Moreover, frequent mutations of PI3K-AKT signaling (TCF3, ID3, PTEN), epigenetic regulation (ARID1A, SMARCA4, KMT2D), cell cycle progression (CCND3), and apoptosis (TP53) are found in Burkitt lymphoma [65].

TP53 mutations are associated with higher incidence of refractory disease, especially in pediatric cases [66]. Survival has improved for Burkitt lymphoma patients treated with multiagent chemotherapies and Rituximab (anti-CD20 monoclonal antibody); however, the relapsing survival rate remains poor [67, 68].

Preclinical studies have suggested that the inhibition of the PI3K/AKT/mTOR pathway alone [69] or in combination with either chemotherapy [70] or HDAC inhibitors [71] and single or dual [72] inhibition of BET epigenetic readers [73] and cyclin dependent kinases (CDK) [62] can be therapeutic options for Burkitt lymphoma.

### **Lymphoplasmacytic Lymphoma/ Waldenstrom Macroglobulinemia (WM)**

WM is an indolent rare B cell Lymphoma, accounting for 1% of all NHL, with an overall median survival greater than 5 years. WM affects post-germinal-centre B cells which are the B cells that undergone the second BCR-gene remodeling, but are transformed before completing the third BCR-gene remodeling process [74]. In WM patients, the most common mutation, found in >90% of cases, is Gain-of-Function mutation affecting MYD88, which is a Toll-like receptor signaling adapter molecule. The dominant MYD88 mutation is leucine to proline substitution in codon 265 (MYD88[L265P]), which leads to

increased cellular proliferation and survival via activation of the NF- $\kappa$ B and Mitogen Activated Protein Kinase (MAPK) pathways [75]. Currently WM is mainly incurable, with patients often experiencing relapse after initial therapy. Therefore, treatments are focused on controlling the symptoms and improving quality of life. Only patients with symptoms are considered for treatment, whereas asymptomatic patients are followed with surveillance [76]. Frontline therapies include rituximab alone or combined with alkylators, proteasome inhibitors, nucleoside analogs, and ibrutinib, which is the first FDA approved Bruton's tyrosine kinase (BTK) inhibitor [77]. BTK inhibitors play central roles in BCR signaling, leading to several activation cascades, including NF- $\kappa$ B, PI3K, and MAPK-ERK signaling pathways [17]. Moreover, autologous stem cell transplant can be considered in eligible patients [78].

## **1.2 Mitogen-activated protein kinases (MAPKs)**

MAPKs are a family of signal transduction proteins that convert extracellular stimuli into cellular responses via three-tier sequential phosphorylation events. They play key roles in diverse cellular processes including cell growth, development, proliferation, differentiation, survival, and innate immunity [79, 80]. Therefore, dysregulated MAPK signaling is involved in the development and progression of several cancers, including ovarian, breast, colorectal, melanoma, thyroid, and lung cancers [81, 82], and B cell lymphomas including DLBCL [36, 75, 83, 84].

MAPKs transmit signaling via four main cascades, each cascade consisting of three core tiers including from upstream to downstream (closer to nucleus) MAPK kinase kinase (MAP3K), which encompasses serine/threonine kinases; MAPK kinase (MAP2K), which encompasses tyrosine and threonine/serine dual-specificity kinases; and MAPK, which encompasses serine/threonine kinases [85, 86].

The four MAPK cascades are named according to the MAPK tier as follows:

extracellular-signal-regulated kinase 1/2 (ERK1/2) pathway; c-Jun N-terminal kinase (JNK) pathway; p38 pathway; and ERK5 pathway [87]. All MAPK cascades integrate with different signaling pathways to generate more complex networks that regulate physiological functions. The ERK1/2 cascade is primarily involved in proliferation and differentiation processes, but it can also participate in stress and other processes under certain conditions [88]. JNK and p38 MAPK cascades participate mainly in cellular and environmental stress responses, in addition to immune and inflammatory responses [89]. As of now, at least 22 MAP3K, 7 MAP2K, and 14 MAPK have been identified in mammalian cells [90].

### **1.2.1 Mitogen-activated protein kinase kinase kinase (MAP3K)**

MAP3K can be activated by different stimuli, including growth factors, antigens, inflammatory cytokines, and stresses to participate in cellular responses [91]. Currently, 22 MAP3K has been identified, including MEKK(1-4), RAF(A,B,C), TAO(1-3), ASK(1-2), TAK1, TPL2, MOS, MLK(1-4), ZAK, LZK, and DLK. There are 6 MAP3K that regulate the ERK1/2 cascade, whereas 12 and 9 MAP3K regulate JNK and p38 cascades, respectively [92].

### **Rapidly Accelerated Fibrosarcoma (RAF) kinases**

The RAF family, consisting of A-RAF, B-RAF, and C-RAF, is part of the canonical RAS-RAF-MKK1/2-ERK1/2 cascade, which is a critical growth signaling cascade. RAF is activated in response to growth factors (receptor tyrosine kinases) and hormones (G-protein coupled receptors) that stimulate RAS (GTP-binding protein) activity. RAS activation leads to RAF membrane recruitment and stimulation. All the three isoforms of RAF are activated by RAS; however, B-RAF phosphorylates MEK1/2 more efficiently than either A-RAF or C-RAF [93].

B-RAF has high frequency of mutation in human cancer (7%) [94] but A- and C-RAF are rarely mutated. The most common B-RAF somatic point mutation that accounts for 90% of all B-RAF mutations in human cancers is the substitution of valine at position 599 for glutamic acid [V599E], leading to B-RAF constitutive activation. Therefore, B-RAF is considered as an important human oncogene [95-97].

### **Transforming growth factor $\beta$ -activated kinase 1 (TAK1)**

TAK1 is required for the activation of NF- $\kappa$ B [98] and MAPK (ERK1/2, JNK and p38) cascades [99] downstream of tumor necrosis factor receptors [100] and Toll-like receptors (TLRs) [101]. The TLR family, consisting of 10 members, participates in innate immune responses as they recognize foreign invaders to trigger inflammatory signaling via signaling adaptors [102].

Currently, there are five TLR adaptors, the main two being the myeloid differentiation primary response gene 88 (MYD88) and the TIR domain-containing adaptor protein inducing interferon- $\beta$  (TRIF). MyD88 is utilized by all TLRs, excluding TLR3 which employs TRIF as its adaptor for signal transmission. Notably, TLR4 can activate both a MyD88-dependent pathway and a MyD88-independent pathway utilizing TRIF [103]. Activation of TLR pro-inflammatory signaling through an MYD88 adaptor is linked to the development and growth of tumors. Conversely, triggering TLR-mediated Type I interferon production via the TRIF adaptor is related to promoting an immune response against tumors [104, 105]. In the TLR pathways, MYD88 mediates the recruitment and activation of TAK1, which subsequently activates the I $\kappa$ B kinase (IKK) complex, which in turn mediates the activation of both NF- $\kappa$ B and TPL2. Also, TAK1 can directly phosphorylate MKK4/7 and MKK3/6 to activate JNKs and p38 signaling, respectively [106].

### **Tumor Promoting Locus 2 (TPL2)**

TPL2, also known as Cancer Osaka Thyroid (COT) or MAP3K8, is a cytoplasmic kinase that is expressed as long isoform M1-TPL-2 (58 kDa) and short isoform M30-TPL-2 (52 kDa) due to alternative translational initiation at methionine 1 (M1) or methionine 30 (M30) [107]. TPL2 is stabilized by forming a complex with a small proportion of p105 NF- $\kappa$ B1 [108, 109]. p105 NF- $\kappa$ B1 is a precursor of p50 NF- $\kappa$ B1, which is a member of the NF- $\kappa$ B family consisting of five proteins including p65 (RelA), RelB, c-Rel, p105/p50 (NF- $\kappa$ B1), and p100/52 (NF- $\kappa$ B2). These proteins combine to form up to 15 different NF- $\kappa$ B complexes, with p50-p65 being the main canonical complex [110]. TLR ligand-

stimulation activates MYD88/TAK1/IKK signaling. Activated IKK $\beta$  phosphorylates p105 NF- $\kappa$ B1 lead to its degradation which releases full-length but not short-length TPL2 from this complex [111, 112]. In B cells, the liberated Tpl2 is an essential activator of ERK1/2 via MKK1/2 in response to TLR signals (immune stimuli) but not mitogens [113], in contrast to the canonical RAF-MKK1/2-ERK1/2 pathway that is stimulated by mitogens [108].

### **1.2.2 Mitogen-activated protein kinase kinase (MAP2K)**

The primary function of MAP2K is to transmit signals from the cell surface to the nucleus, therefore orchestrating a range of cellular responses, including growth, differentiation, and stress adaptation. Their role in connecting extracellular signals to intracellular processes makes them critical components in various physiological and pathological contexts. The MAP2K family contains 7 kinases divided into four subfamilies based on their homology and substrate specificity, including ERK-activating MAP2Ks (MKK1/2); JNK-activating MAP2Ks (MKK4/7); p38-activating MAP2Ks (MKK3/6); and MKK5 which activate ERK5.

### **Mitogen-activated protein kinase kinase 1 and 2 (MKK1/2)**

MKK1 and MKK2 are tyrosine and threonine/serine dual-specificity kinases that transmit signals specifically to ERK1/2 downstream of RAF(A,B,C), TPL2, MEKK1, and MOS kinases [92]. The RAF-MKK1/2 tier amplifies the signal, while the MKK1/2-ERK1/2 tier enhances the cooperativity of activation by involving other modulation events [91].

MKK1/2 are activated by phosphorylation of either serine 217 or 221 residues within

their activation loops, whereas ERK1/2 dual phosphorylation is required for full activity [114, 115].

### **1.2.3 Mitogen-activated protein kinase (MAPK)**

MAPKs are the effector proteins of the MAPK cascades, and they are divided into conventional and atypical MAPK subfamilies according to their ability to be activated by MAP2K. The conventional MAPK family consists of four main subgroups: ERK(1/2); JNK(1-3); p38( $\alpha, \beta, \gamma, \delta$ ); and ERK5. Atypical MAPK include ERK(3,4 and 7) and Nemo-like kinase (NLK) which are not substrates for MAP2K; therefore, they have different regulatory mechanisms and their activation does not require MAP2K phosphorylation [116, 117].

### **Extracellular signal-regulated kinase 1 and 2 (ERK1/2)**

ERK1 and ERK2 are closely related kinases that are activated specifically by MKK1/2 via the dual phosphorylation of threonine (T202) and tyrosine (Y204) residues or T185 and Y187 residues within ERK1 and ERK2 activation loops, respectively. Most frequently, the ERK1/2 pathway is primarily activated by RAF isoforms. However, other MAP3Ks can activate ERK1/2 in specific cell types or under specific stimulations. For example, during oocyte maturation, MOS activates ERK1/2 in response to steroid receptor stimulation leading to meiotic progression [118]. In B cells and macrophages, following TLR stimulation, ERK1/2 is activated via Tpl2 [119]. Under stress situations, MEKK1 activates ERK1/2 in neuronal cells [120].

Phosphorylation of ERK1/2 initiates a variety of cellular responses. These responses are regulated by several factors, including docking motifs, scaffold proteins, and protein phosphatases. Docking motifs can modulate substrate affinity for ERK1/2, such as the docking site for ERK and FXFP (DEF) which was identified in many ERK1/2 substrates including ELK-1 and KSR [121]. Scaffold proteins are critical signal transducers that facilitate the assembly of ERK1/2 signaling components, which in turn allows for phosphorylation and activation of specific pathways such as KSR, MP1, and  $\beta$ -arrestins scaffolding proteins [122]. Phosphatases play regulatory roles in ERK1/2 signaling as they can directly impact ERK1/2 functions, such as the dual-specificity MAPK phosphatase 3 (MKP3) that acts as a negative regulator of ERK1/2 [123].

Phosphorylated ERK1/2 catalyzes the activation of hundreds of nuclear and cytoplasmic substrates. Nuclear substrates of ERK1/2 include transcription factors and regulatory molecules, such as Elk1, c-Fos, and c-MYC. Cytosolic ERK1/2 substrates include RSK1-4, MNK1/2, and MSK1/2, in addition to the cytoskeletal elements such as paxillin. Activation of these substrates plays a key role in regulating cellular growth, proliferation, motility, and survival [124].

#### **1.2.4 MAPK cascades and tumorigenesis**

Dysregulated ERK1/2 cascade signaling is involved in various diseases, including inflammation and developmental and neurological disorders [80]. The discovery of oncogenic mutations leading to ERK1/2 constitutive activation or elevated expression [80] linked ERK1/2 signaling to multiple forms of cancer, including colorectal, ovarian, melanoma, pancreatic, thyroid [125], and lung cancers [126], as well as to

hematological malignancies [127]. Therefore, targeting the ERK1/2 signaling pathway has received widespread attention.

Mutations affecting RAS and RAF are most common in the classical RAS-RAF-MEK1/2-ERK1/2 pathway. Currently, three B-RAF inhibitors, namely Vemurafenib (Zelboraf), dabrafenib (Tafinlar), and encorafenib (Braftovi), are FDA-approved for the treatment of B-RAF-mutant melanoma [128]. In addition, three MKK1/2 inhibitors have received FDA approval to be used as a treatment for B-RAFV-mutant diseases, including Trametinib (Mekinist), Cobimetinib (Cotellic) and Binimetinib (Mektovi) [129]. However, the efficacy of these inhibitors is limited by their adverse effects and the emergence of drug resistance [130]. Therefore, in order to improve their therapeutic effectiveness, they have been combined with other agents such as chemotherapy, immunotherapy, and small molecule inhibitors including PI3K and B-cell lymphoma-2 (BCL2) inhibitors [131-136].

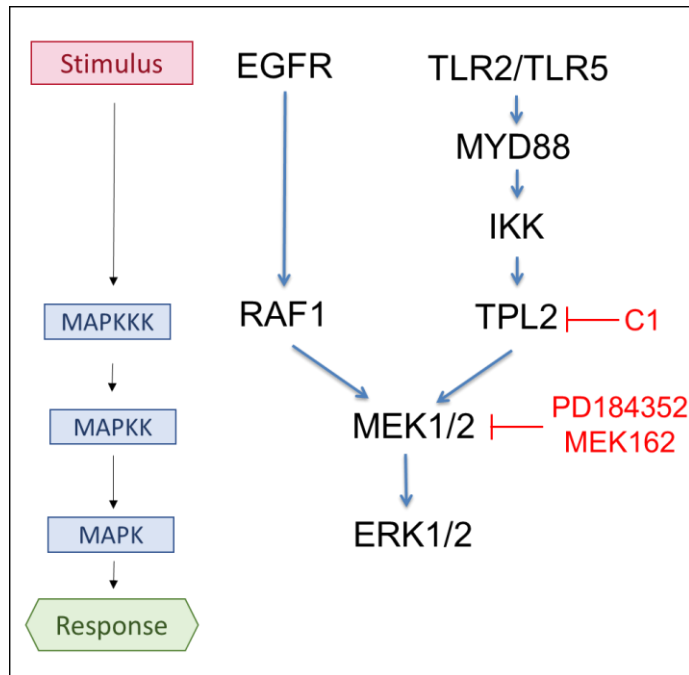
### **BCL2 inhibitors in combination with ERK1/2 signaling inhibitors**

The B-cell lymphoma-2 (BCL-2) family comprises pro-apoptotic and anti-apoptotic members responsible for regulating mitochondrial outer membrane permeability, thereby controlling the release of pro-apoptotic factors and influencing B-cell survival. These family members share conserved BCL2-homology (BH) domains, categorized by BH1, BH2, BH3, and BH4 motifs, determining their classification and functions [137]. Anti-apoptotic proteins possess BH(1-4) domains, including Bcl-2, Bcl-w, Bcl-xL, Mcl-1, and BFL-1/A1. Pro-apoptotic proteins can be divided into multidomain effector subsets including Bax, Bak, and Bok, and the BH3-only subset including Bad, Bid, Bik, Bim, Bmf, Hrk, Noxa, and Puma. Notably, the "BH3-only subset" shares homology primarily

at the BH3 domain and serves as an initiator of apoptosis in response to cellular stress. Naturally, the BH3-only subset neutralizes anti-apoptotic proteins through direct binding which tightly regulates apoptosis [138]. However, this balance is disrupted in various hematological malignancies including DLBCL [139, 140]. For example in DLBCL, BCL2 protein is overexpressed due to t(14;18) translocation, *BCL2* gene amplification, and/or BCL2 transcriptional upregulation via NF- $\kappa$ B constitutive activation, all of which shift the balance in favor of anti-apoptotic signals, leading to survival following cellular insults [141, 142]. BCL-2 protein is the first identified major anti-apoptotic regulator, composed of 239 amino acids with a molecular weight of approximately 26 kDa [143]. Recently, BCL2 inhibitors showed anticancer effects, such as the BH3 mimetics ABT199 (Venetoclax) and ABT263 (Navitoclax), which bind to anti-apoptotic proteins and effectively counteract their apoptotic inhibitory effects, thus promoting cell death induction [140, 144]. However, the therapeutic benefit of BCL2 inhibitors alone, ABT263 being a case in point, is limited due to acute toxicity including dose-dependent thrombocytopenia; therefore, they are used in combination with other agents [145]. The combination of BCL2 and ERK1/2 inhibitors has enhanced their efficacy and showed promising results in several cancers, including acute myeloid leukemia and colorectal and lung cancers [146-148]. This approach holds promise, particularly in cancer therapy, where BH3 mimetics disrupt the survival advantage conferred by anti-apoptotic BCL-2 family members, ultimately facilitating apoptotic pathways and combating cell proliferation.

### **Targeting ERK1/2 via TPL2**

An alternative therapeutic target to control ERK1/2 pathway activation is via TPL2, especially in immune cells. Downstream of the TLR pathway, MYD88 activates the IKK complex which in turn mediates parallel activation of both NF- $\kappa$ B and TPL2 [75, 119]. This has led to an overestimation of the role of NF- $\kappa$ B and an underestimation of TPL2-ERK1/2 roles in the scientific literature investigating the role of MYD88 in cancer [149, 150]. Recent studies highlight the importance of the TPL2-MKK1/2-ERK1/2 pathway in cancers, including ovarian carcinomas [151], melanoma [152], leukemias [153], and lymphomas [75]. Previous analysis from our lab, investigating the mutations found downstream of MYD88[L265P], identified 7 genes which are likely oncogenic drivers that can all be linked to the TPL-ERK1/2 pathways. This analysis identified the ERK pathway as a major target of TLR-driven lymphocyte transformation [75]. TPL2 inhibitors have been developed and they are under investigation in pre-clinical models [154, 155]. In chapter 2, we studied the anti-lymphoma activity of novel TPL2 inhibitors (tested in pre-clinical studies) and classical ERK1/2 pathway inhibitors alone or in the presence of either TLRs agonists or BCL2 inhibitors in cell culture.



### 1.3 Histone Deacetylases

HDACs are a family of enzymes that play a critical role in regulating diverse cellular functions, including cell survival, proliferation, inflammation, and immunity. HDACs control these functions by catalyzing the removal of acetyl groups from histone and nonhistone proteins to counteract the effects of Histone Acetyltransferases (HATs) that add acetyl groups. This modification can alter the structure of proteins and change their accessibility to the machinery that activates or suppresses them. In histones, generally speaking, deacetylation restores the positive charges of histones, thus increasing the affinity for negatively charged DNA, resulting in a more compact and less accessible

chromatin structure that usually leads to the repression of gene expression and vice versa for acetylation induced by HATs [156-158].

In humans, currently, 18 HDAC proteins have been identified, and they are classified into four classes based on their sequence homology and enzymatic activity. The four classes include class I HDACs (HDAC1, 2, 3, and 8); class II HDACs that are further divided into class IIa (HDAC4, 5, 7 and 9) and class IIb (HDAC6, and 10); class III HDACs (Sirtuins SIRT1-7); and class IV HDAC (HDAC11) [159].

Class I HDACs are primarily localized in the nucleus and mainly regulate gene expression. Class II HDACs are found in both the cytoplasm and nucleus, and they play a role in various cellular processes such as cytoskeleton organization and stress response [160]. Class III comprises the only class that depends on NAD<sup>+</sup> as a cofactor instead of Zn<sup>2+</sup> and they are involved in regulating metabolism [161] and aging [162]. Class IV HDAC consists of a sole member HDAC11 that has both class I and II characteristics and participates in the regulation of immune functions [163].

### **HDAC 1 and HDAC2 (HDAC1/2)**

HDAC1/2 share structural and functional characteristics, making them closely related members of the class I HDAC family. They often collaborate in the regulation of gene expression and can be found together in several major co-repressor complexes such as Swi-independent 3 (Sin3); nucleosome remodeling and deacetylation (NuRD); and the co-repressor for element-1-silencing transcription factor (CoREST) [164-166]. This repression is important for maintaining proper gene expression patterns and cellular functions. HDAC1/2 are particularly important for the control of cell growth and

differentiation. Consequently, dysregulation of HDAC1/2 has been linked to various diseases including cancer and neurological disorders [167, 168].

## **HDAC6**

HDAC6 is the largest enzyme of the HDAC family (1215 amino acids) that plays a critical role as a non-histone deacetylase with mainly cytoplasmic localization. Currently, HDAC6 and HDAC10 (class IIb) are the only members that have two catalytic domains. The HDAC10 second catalytic site is not functional, making HDAC6 the only HDAC protein with two catalytically active domains [169]. HDAC6 C-terminal end contains a ubiquitin-binding zinc finger domain that is involved in ubiquitination-mediated degradation. Both the deacetylase and ubiquitin-binding activities are necessary for HDAC6 regulation of aggresomal formation in response to misfolded protein stress which affects cell viability [170].

HDAC6 is a microtubule-associated deacetylase that specifically removes the acetyl group from  $\alpha$ -tubulin lysine 40 (K40) residue located on the luminal surface of the microtubule hollow tube which is composed of  $\alpha$ -tubulin and  $\beta$ -tubulin dimers [171, 172]. Acetylation stabilizes microtubules by improving flexibility and resilience, whereas deacetylation decreases the rigidity of microtubules, rendering them more susceptible to breakage after stresses [173-175]. The second catalytic domain of HDAC6 is responsible for catalyzing  $\alpha$ -tubulin deacetylation [176], which regulates mitosis, motility, and intracellular transport [177]. Moreover, HDAC6 can target ERK1 acetylation and regulates c-Myc expression and NF- $\kappa$ B activity (more details in chapter 3) [178-180].

## HDACs and tumorigenesis

Targeting HDACs has been identified as a potential therapeutic strategy for a variety of diseases, including inflammatory conditions [181], cardiac diseases [182], neurodegenerative disorders [183], and cancers [184]. Altered HDAC expression or activity is frequently observed in various human cancers, such as gastric [185], breast [186], and colon [187] cancers, as well as hematological malignancies [188-191].

To date, four HDAC inhibitors have received FDA approval, namely Vorinostat (Zolinza), a pan HDAC inhibitor (hydroxamic acid family) approved for the treatment of cutaneous T cell lymphoma (CTCL); Romidepsin (Istodax), a class 1 selective HDAC inhibitor (cyclic peptide family) approved for the treatment of CTCL and peripheral T cell lymphoma (PTCL); Belinostat (Beleodaq), a pan HDAC inhibitor (hydroxamic acid family) approved for the treatment of PTCL; and Panobinostat (Farydak), a pan HDAC inhibitor (hydroxamic acid family) approved for the treatment of multiple myeloma in combination with other drugs [192].

FDA-approved HDAC inhibitors are widely used; however, resistance to treatments and toxicity remain key problems [193]. Therefore, experimental HDAC inhibitors are under investigation as single agents or in combination with other therapeutics as potential treatments for various malignancies [194]. Based on the chemical structures, HDAC inhibitors can be divided into five groups: hydroxamates, cyclic tetrapeptides, benzamides, aliphatic acids, and electrophilic ketones [195].

As a group, hydroxamates constitute the most widely explored HDAC inhibitors due to the encouraging results obtained from clinical trials [196, 197]. Recently, the novel selective HDAC6 inhibitor, Sahaquine, has been synthesized by combining hydroxamic acid with primaquine [198]. In chapter 3, we investigate the effectiveness of Sahaquine (tested in pre-clinical studies) as a single agent on inhibiting cell growth in several B-cell NHL cell lines and in combination with ERK1/2 inhibitors.

#### **1.4 Drug Safety Assessment in Zebrafish Model**

Drug safety assessment is an important step in the drug development process to identify and evaluate the potential risks and side effects associated with drug administration, in order to balance the effectiveness of a drug against its adverse effects [199, 200]. Drug safety information is collected throughout the life cycle of a drug, from preclinical toxicology studies to clinical trials and post-marketing surveillance [201]. The drug safety data is evaluated by regulatory agencies such as the US Food and Drug Administration (FDA), the Health Products and Food Branch (HPFB) of Health Canada, and the European Medicines Agency (EMA), all of which assess the potential benefits and risks of the drug to make decisions about its approval and labeling [202-204].

Preclinical toxicity can be evaluated using in vitro and in vivo models. Cytotoxicity is initially assessed in a cell-culture model, a procedure which is less expensive and faster than in vivo models; however, in vivo models more successfully predict toxicity [205, 206]. Recently, zebrafish (*Danio rerio*) have emerged as an attractive vertebrate model, bridging the gap between in vitro and in vivo studies as this model combines cell culture

convenience with the power of a whole animal model [207, 208]. Zebrafish have a high reproductive capacity allowing them to produce hundreds of embryos from a single mating. Zebrafish embryos are transparent and develop rapidly, with major organ development within the first few days post fertilization (dpf) [209, 210]. Most embryos hatch from the chorion by 2-3 dpf to enter the larval stage. The yolk is the main source of nutrients up to 5 dpf; therefore, the non-feeding life-stages are not subject to regulations for animal experimentation and do not need ethical approval [211]. These unique features make the zebrafish model ideal for studying drug efficacy and safety in zebrafish larvae or xenografted larvae models (more details in chapter 4) [212-214].

Zebrafish share a relatively high degree of genetic similarity with humans, with approximately 70% of human genes having a zebrafish counterpart [215]. The zebrafish genome contains HDAC genes which are orthologs of human HDACs (except HDAC2) [216]. Zebrafish HDAC6 catalytic domain 2 is a well-studied substitute for human HDAC6 catalytic domain 2, as the active site structures of both zebrafish and humans are essentially identical (except for one amino acid substitution in each). Also, zebrafish HDAC6 catalytic domain 2 generates crystals of better quality compared to human HDAC6; therefore, zebrafish HDAC6 is used for crystallographic studies to assess structure–affinity relationships of novel HDAC6 inhibitors [217, 218]. Moreover, several human metabolizing enzymes have counterparts in zebrafish, such as cytochrome P450 (CYP), sulphation, and glucuronidation enzymes. Human CYP3A4, the major detoxifying CYP in humans, shares zebrafish ortholog CYP3A65, which has a similar function, with 54% amino acid sequence identity [219-221].

Visualizing the spatial distribution of drugs and metabolites, simultaneously, in the zebrafish model has received widespread attention. Advances in matrix-assisted laser desorption/ionization mass spectrometry imaging (MALDI MSI) has made this possible and provided images of small molecules distributed in zebrafish larvae. However, the process is still technically challenging, and there is a need to improve imaging approaches in the zebrafish larvae model [222, 223]. In chapter 4, we develop an optimized MALDI MSI protocol to evaluate Sahaquine safety and examine its possible metabolites in the zebrafish larvae model.

## **1.5 Hypothesis and Objectives**

Based on the aforementioned information, the central hypothesis in this project is that single and dual inhibition of ERK1/2 signaling and HDAC6 activity will impair the survival of B cell NHL.

The main objectives of this thesis are as follows:

1. Test the efficacy of pharmacological inhibitors of ERK1/2 signaling and HDAC6 activity as single agents to prevent the proliferation and survival of several B cell NHL cell lines in vitro.
2. Evaluate the combined effect of dual ERK1/2 and HDAC6 inhibition in the cell culture model and characterize the combination mechanisms of action.
3. Assess Sahaquine (in-house HDAC6 inhibitor) safety and metabolism in the zebrafish larvae model using an optimized matrix-assisted laser desorption/ionization mass spectrometry imaging (MALDI MSI) approach.

## **Preface**

Mitogen-activated protein kinases (MAPKs) are essential signaling molecules that play a critical role in transmitting signals from the cell surface to the nucleus, where they regulate vital cellular processes. Due to their involvement in these processes, the dysregulation of MAPK signaling pathways can lead to various diseases, including cancer. Targeting the extracellular signal-regulated kinase 1 and 2 (ERK1/2) MAPK signaling pathway has received widespread attention since the discovery of ERK1/2 pathway oncogenic mutations leading to its constitutive activation. In B cells, the protein kinase Tumor Promoting Locus 2 (TPL2) is an essential activator of ERK1/2 in response to Toll-like-receptor (TLR) signals following immune stimulation. However, TLR signaling mediates parallel activation of both nuclear factor kappa B (NF- $\kappa$ B) and TPL2, leading to the overestimation of NF- $\kappa$ B roles and the underestimation of TPL2-ERK1/2 roles in the scientific literature. Therefore, at a very early stage of this thesis, we aimed to reach a deeper understanding of the impact of the TPL2-ERK1/2 signaling pathway on B-cell lymphoma proliferation. To this end, we performed several preliminary experiments in cell culture using different TPL2-ERK1/2 pharmacological inhibitors alone or in combinations.

## **Chapter 2: Inhibition of the TPL2-MKK1/2-ERK1/2 pathway in B-Cell Lymphomas**

Mariana Asslan<sup>1,2</sup>, Guy Martel<sup>1</sup>, and Simon Rousseau<sup>1,2,\*</sup>

<sup>1</sup>The Meakins-Christie Laboratories at the Research Institute of the McGill University Health Centre and <sup>2</sup> Department of Pharmacology, McGill University, Montreal, Quebec, Canada.

\*Correspondence: Simon Rousseau, Ph.D., The Meakins-Christie Laboratories at the RI-MUHC, 1001 Décarie Blvd, Montreal, QC, Canada, H4A 3J1. Phone: 514-934-1934 #76394, email: [simon.rousseau@mcgill.ca](mailto:simon.rousseau@mcgill.ca) <https://orcid.org/0000-0002-8773-575X>

To be submitted as a brief scientific report.

### Funding statement

This work was supported by Canadian Institute of Health Research (MOP#123496) and the Fonds de Recherche du Québec -Santé (FRQ-S salary award to S.R.). The Meakins-Christie Laboratories – RI-MUHC, are supported by a Centre Grant from FRQ-S.

## **Authors' contributions**

The main text of the article was prepared by Dr. Simon Rousseau and Mariana Asslan. Material preparation, data collection, and analysis were performed by Mariana Asslan. Guy Martel with help of Mariana Asslan performed Figure 4 and S1 experiments and prepared their figures with legends. All authors have reviewed and approved the final manuscript.

Keywords: TPL2 inhibitors, MKK1/2 inhibitors, Hematologic malignancies, B-lymphocytes.

## **2.1 Abstract**

A hallmark of many B-cell malignancies is the constitutive activation of the protein kinases extracellular signal-regulated kinase 1 and 2 (ERK1/2), resulting in uncontrolled cellular proliferation. ERK1/2 activation can occur either downstream of the classical MKK1/2-ERK1/2 cascade via RAF kinase or specifically in immune cells via the Tumor Promoting Locus 2 (TPL2) kinase in response to Toll-like-receptor (TLR) stimulation. We report here that the anti-lymphoma activity of TPL2 inhibitors is dependent on the presence of TLR activation in BCWM.1 cell line that harbors oncogenic mutations in the TLR adaptor molecule MYD88. These MYD88 gain-of-function mutations are found in 90% of Waldenström macroglobulinemia (WM), a rare incurable B-cell lymphoma. We then investigated the impact of ERK1/2 inhibition on the proliferation of OCI-Ly2 cells representing Diffuse Large B-Cell Lymphoma (DLBCL), the most common form of B-cell

lymphoma. We found that blocking the ERK1/2 signaling cascade using either MKK1/2 inhibitors (PD184352 and MEK162) or TPL2 inhibitors (Compound 1 and Compound 34) was mainly cytostatic. Finally, we showed that while TPL2-MKK1/2-ERK1/2 inhibition leads to cytostatic effect, Compound 1 has cytotoxic effect at high concentrations, mediated via targeting additional kinases. Taken together, this study demonstrates the involvement of TPL2 in oncogenic signaling of B-cell lymphoma and supports the idea that targeting multiple molecular pathways linked to cellular transformation is a superior avenue for future therapies.

## **2.2 Introduction**

Constitutive activation of the protein kinases extracellular signal-regulated kinase 1 and 2 (ERK1/2) is a hallmark of many B-cell malignancies (Platanias, 2003a), leading to uncontrolled cellular proliferation and growth. Activation of ERK1/2 in hematologic malignancies can occur downstream of the classical [rat sarcoma (RAS)- rapidly accelerated fibrosarcoma (RAF)- mitogen-activated protein kinase kinase 1 and 2 (MKK1/2)] pathway or alternatively downstream of the Tumor Promoting Locus 2 (TPL2) protein kinase following activation of the Toll-like-receptor (TLR) signaling pathway (Dumitru et al., 2000; Beinke et al., 2004; Rousseau and Martel, 2016). TLR pathways are normally associated with host defense responses and inflammation (Kawasaki and Kawai, 2014). Recently, this pathway was identified as the most frequently mutated signaling pathway in lymphoid neoplasms (Rousseau and Martel, 2016) which makes TPL2 an attractive target to treat hematologic malignancies.

The most commonly found mutated gene in lymphoid neoplasm is myeloid differentiation primary response protein 88 (MYD88) (>22%), a TLR signaling adapter molecule which can be affected by gain-of-function mutations, mainly the nucleotide substitution leucine to proline in codon 265 (MYD88 L265P) (Rousseau and Martel, 2016). This mutation leads to ERK1/2 activation in the absence of TLR cognate ligands such as lipopeptide and Flagellin (Rousseau et al., 2016). 90% of lymphoplasmacytic lymphoma/Waldenström macroglobulinemia (WM), an indolent incurable B cell non-Hodgkin Lymphoma, have MYD88 L265P mutations (Treon et al., 2015). MYD88 mutations can also be found in Chronic Lymphocytic Leukemia (CLL) or an activated B-cell-like (ABC) subgroup of Diffuse Large B Cell Lymphoma (DLBCL), the most common form of non-Hodgkin lymphoma.

DLBCL has a heterogeneous molecular origin, and future therapies will target the molecular defects responsible for oncogenic progression in specific subsets. Molecular heterogeneity means that tumor cells use different pathways to escape cell death signals and proliferate. The overexpression of the anti-apoptotic B-cell lymphoma 2 (BCL-2) protein is a common feature of DLBCL (Rosenwald et al., 2002) associated with poor prognosis (Hermine et al., 1996). BCL2 plays a key role in regulating intrinsic apoptosis via controlling cytochrome c release from the mitochondria (Yang et al., 1997). Venetoclax (ABT-199) is the first BCL-2 inhibitor approved by the FDA, alone or in combination, to treat several hematologic malignancies (Roberts, 2020). Previous studies showed that simultaneous inhibition of the MKK1/2 - ERK1/2 pathway and antiapoptotic Bcl-2 family members had superior anticancer effects against acute myeloid leukemia, colorectal, melanoma, and lung and pancreatic cancers (Sale and

Cook, 2013; Tan et al., 2013; Airiau et al., 2016). Therefore, we aimed to investigate the combined effect of BCL2-TPL2 dual inhibition in the DLBCL cell line.

In this report, we studied the effectiveness of inhibiting TPL2 and the classical MKK1/2 - ERK1/2 pathway, in the presence or absence of TLR ligands, on cell viability in non-Hodgkin lymphoma. In addition, we investigated whether the simultaneous inhibition of TPL2 and BCL2 is an efficient strategy to reduce DLBCL cell viability.

## **2.3 Methods**

### **2.3.1 Cell culture**

The immortalized BCWM.1 cell line from a MYD88[L265P] WM patient was obtained from Dr. Steve Treon (Bing Center for Waldenstrom's Macroglobulinemia, Harvard Medical School). Immortalized Human Diffuse Large B-Cell Lymphoma OCI-Ly2 cells were graciously provided by Prof. Minden (University of Toronto). RAMOS cells (Burkitt's B-cell lymphoma) were purchased from ATCC (Rockville, MD, USA). OCI-Ly2, RAMOS, and BCWM.1 cells were cultured in RPMI 1640 medium (#350-000-CL, Wisent) supplemented with 10% fetal bovine serum (#080-450, Wisent) and 1% penicillin/streptomycin (#450-201-EL, Wisent). All cells were maintained at 37°C in 5% CO<sub>2</sub> and 95% humidity. The medium was changed every 48–72 hours until cells were treated as described.

### **2.3.2 Trypan blue exclusion assay**

Cells were seeded in 12-well plates at a concentration of  $2.5 \times 10^5$  cells /mL. Cells were treated with increasing concentrations of inhibitors, including 5Z-7-Oxozeaenol (#HY-12686, MedChemExpress); BI605906 (#HY-13019, MedChemExpress); MEK162 (Binimetinib) (#HY-15202, MedChemExpress); PD184352 (CI-1040) (#HY-50295, MedChemExpress); Compound 1 (C1); and Compound 34 (C34), kindly provided by Professor Sir Philip Cohen (MRC PPU, University of Dundee, UK). The plates were incubated at 37°C in a humidified atmosphere containing 5% CO<sub>2</sub>. After incubation, cells were centrifuged and resuspended in phosphate-buffered saline (PBS) (#311-010-CL, Wisent). Then trypan blue (#609-130-EL, Wisent) was added (1:1), and viable cells were counted under a microscope using a hemocytometer.

### **2.3.3 Flow cytometry analysis of cell death by propidium iodide (PI) staining**

OCI-Ly2 and Ramos cells were seeded at  $2.5 \times 10^5$  cells/mL and treated with PD184352 at IC<sub>50</sub> (4 and 3 μM respectively) for 72 hours. As a positive control, cells were treated with 1.6mM H<sub>2</sub>O<sub>2</sub> for 24 hours. Prior to analysis by flow cytometry (BD LSRFortessa X-20), cells were washed and resuspended in 500 μL of Binding Buffer (#1006, BioVision) and incubated at dark with 1 μL of Propidium Iodide (PI, 250 μg/mL) (#1056, BioVision) staining for 5 minutes at room temperature. A total of 10,000 events were acquired and data were analyzed using FlowJo software.

### **2.3.4 MTT cell proliferation assay**

OCI-Ly2 and Ramos cells were seeded in 96-well plates and incubated with increasing concentrations of C1 and C34 (provided by Dr. Cohen Lab, Dundee University) alone or in combination with ABT199 (Venetoclax) (#HY-15531, MedChemExpress) and ABT263 (Navitoclax) (#HY-10087, MedChemExpress). In addition, OCI-Ly2 cells were treated with 625nM of Doxorubicin; 625nM of Vincristine; 10 $\mu$ M of Cyclophosphamide; or 1 $\mu$ g/mL of Rituximab. Cell numbers were assessed with the Vybrant MTT Cell Proliferation Assay Kit (#V-13154, Thermo Fisher Scientific Inc.), according to the manufacturer protocol. In short, cells were incubated with MTT solution (1mM) at 37°C for 2 hours, then centrifuged, and DMSO (200  $\mu$ L) was added. The plate was incubated at 37°C for 30 minutes and absorbance was measured with a Tecan Infinite M1000 microplate reader at 540 nm using “I-control 1.5” software. Optical density (OD) values were converted to cell numbers based on a standard curve equation generated using standard samples with known cell numbers (2-fold dilutions) and their correlated OD values.

## **2.4 Results**

### **2.4.1 The susceptibility of the BCWM.1 cell line to TAK1-IKK-TPL2-MKK1/2 pathway inhibitors is dependent on the presence of TLR activation.**

We have previously shown that the most common mutation found in hematologic malignancies, namely MYD88[L265P], leads to ERK1/2 activation via TPL2 in a heterologous expression system (Rousseau and Martel, 2016). We hypothesize that proliferative signals may be mediated by increased constitutive activation of ERK1/2 via

TPL2. Therefore, inhibition of key molecular effectors of ERK1/2 activation by MYD88[L265P] should decrease the proliferation of WM lymphoma cells. We exposed the BCWM.1 cell line from a MYD88[L265P] WM patient to 5Z-7-Oxozeaenol (TAK1 inhibitor) (Fig. 1A); BI605906 (IKK inhibitor) (Fig. 1B); Compound 1 (TPL2 inhibitor) (Fig. 1C); or MEK162 (MKK1/2 inhibitor) (Fig. 1D), all upstream activators of ERK1/2. The TAK1 inhibitor decreased cell viability at concentrations close to those required to prevent TAK1 protein kinase activity in cells, whereas both BI605906 and Compound 1 decreased cell viability, only at doses much higher than those required for maximal protein kinase inhibition. Finally, no impact was noted in the presence of the MKK1/2 inhibitor.

We then repeated the experience in the presence of agonists of Toll-Like Receptors (TLRs), namely PAM3CSK4, a TLR1/2 agonist; Flagellin, a TLR5 agonist; and Poly(I:C), a TLR3 agonist. Under the stimulated conditions, in contrast to the unstimulated ones, we noted a significant decrease in survival of the BCWM.1 cells in the presence of the TPL2 (Fig. 2A), IKK (Fig. 2B), and MEK1/2 (Fig. 2C) inhibitors.

Therefore, the impact of inhibition of the TPL2-MKK1/2 pathway on BCWM.1 cells is dependent on the environmental context. Next we focused on determining the impact of TPL2 inhibition on cells arising from other lymphomas.

**Fig.1**

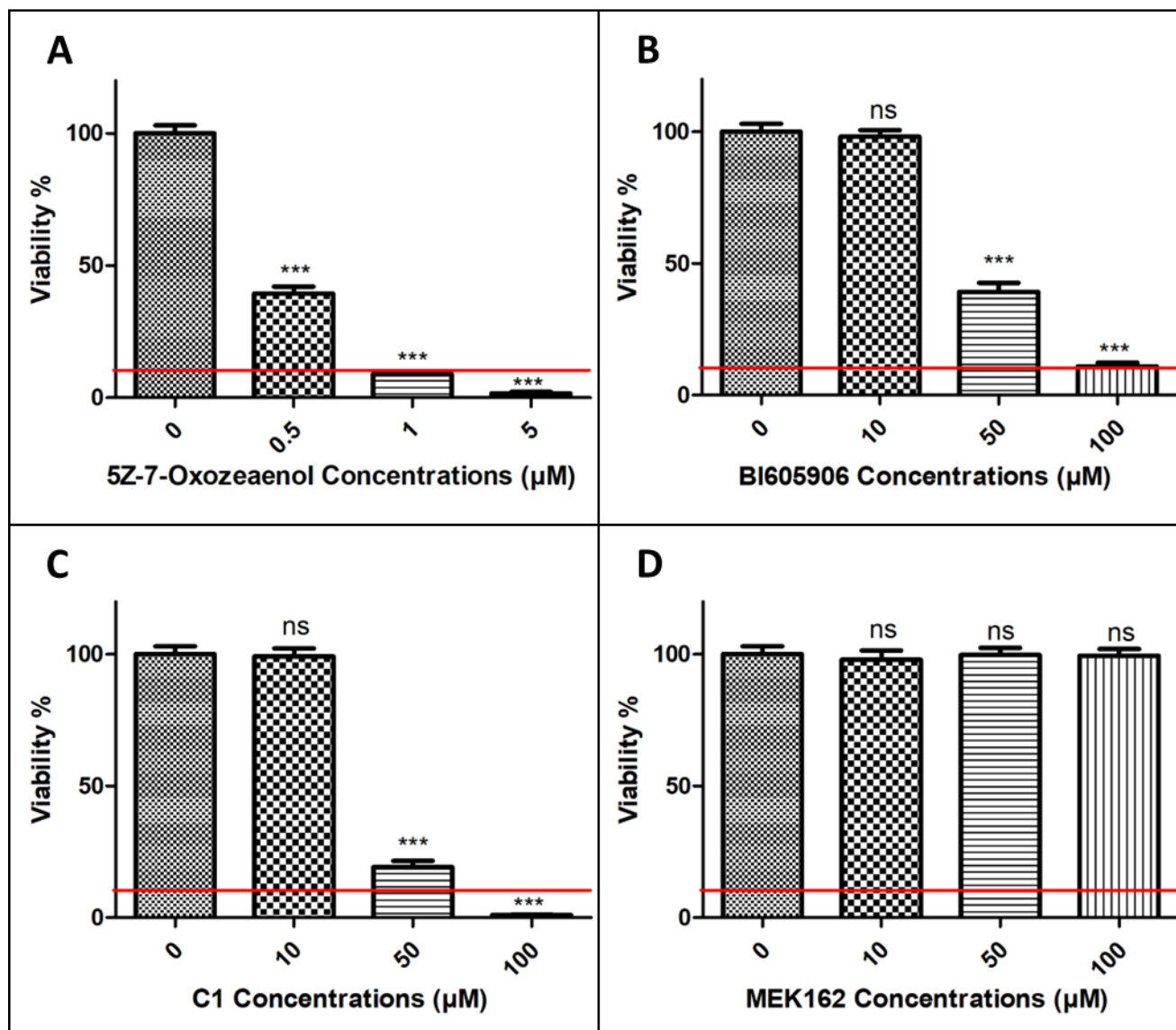


**Fig. 1 Susceptibility of the BCWM.1 cell line to MEK-ERK pathway inhibitors.**

Cell viability after treatment with (A) 5Z-7-Oxozeaenol; (B) BI605906; (C) Compound 1 (C1); and (D) MEK162 for 72 hours. Viability was measured using the Trypan Blue exclusion assay. Horizontal red lines represent the initial number of seeded cells.

Shown is the mean value (SD) from three experiments (n=6, one-way ANOVA with Dunnett's post hoc test, \*\*\*  $p < 0.001$ , \*\*  $p < 0.01$ , \*  $p < 0.05$ ).

**Fig.2**

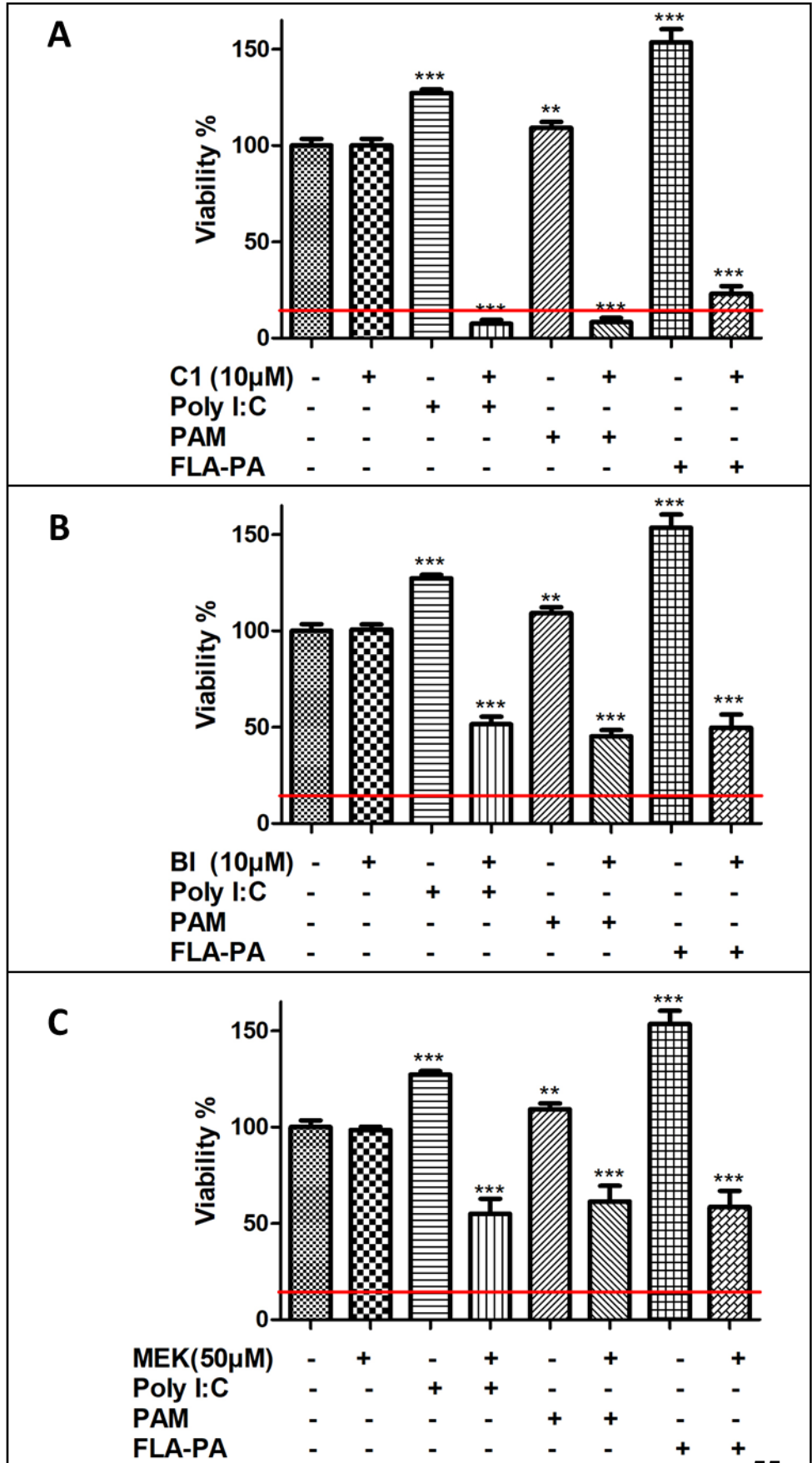


**Fig. 2 Effects of stimulating signals in the presence of MEK-ERK pathway inhibitors on BCWM.1 cell viability.**

BCWM.1 cells were stimulated with Polyinosinic-Polycytidylic acid (Poly I:C, 10 µg/mL, 75 minutes); Pam3CysSerLys4 (PAM, 1 µg/mL, 45 minutes); and Flagellin *Pseudomonas aeruginosa* (FLA-PA, 200 ng/mL, 30 minutes), then treated with (A) Compound 1 (C1, 10 µM), (B) BI605906 (BI, 10 µM), and (C) MEK162 (MEK, 50 µM) for 48 hours. Viability was measured using the Trypan Blue exclusion assay. Horizontal red lines represent the initial number of seeded cells. Shown is the mean value (SD) from three independent experiments (n=6, one-way ANOVA with Dunnett's post hoc test, \*\*\* p < 0.001, \*\* p < 0.01, \* p < 0.05).

**2.4.2 TPL2-MKK1/2 inhibition results in cytostatic effect on B-cells isolated from lymphomas.**

Next we studied the impact of MKK1/2 inhibition on B-cell lymphomas. OCI-Ly2 cells were treated with the MKK1/2 inhibitor PD184352 (CI-1040). Results showed that PD184352 reduced cell proliferation in a dose-dependent manner (Fig. 3A). Similar results were obtained with the Burkitt lymphoma cell line Ramos (Fig. 3B). In both cell lines, OCI-Ly2 and Ramos, PD184352 at IC<sub>50</sub> (4 and 3 µM, respectively) produced cytostatic effects but not cytotoxic (Fig. 3C). To test the involvement of TPL2 in the proliferation of OCI-Ly2 cells, they were exposed to either MEK162 or Compound 1, which efficiently decreased cellular proliferation (at IC<sub>50</sub> 5 µM) and induced death at higher doses (10 µM) (Fig. 4A). These concentrations are at least two-fold higher than the concentration required to achieve maximal TPL2 inhibition and prevent ERK1/2

phosphorylation. The effect of Compound 1 does not appear to be restricted to OCI-Ly2 cells, as a similar trend was also observed in the Burkitt lymphoma cell line Ramos (Fig. 4B). At the highest dose tested (10 $\mu$ M), Compound 1 was more effective than MEK162 in both cell lines. Moreover, Compound 1 was almost as efficacious as Rituximab, Doxorubicin, and Vincristine (standard DLBCL therapies) in decreasing OCI-Ly2 cell numbers (Fig. S1), not only preventing proliferation but also leading to cell death. Taken together these results indicate that while TPL2-MKK1/2 inhibition leads to cytostatic effect, Compound 1 has cytotoxic effect at high concentrations, suggesting that it acts via targeting additional kinases.

**Fig. 3**

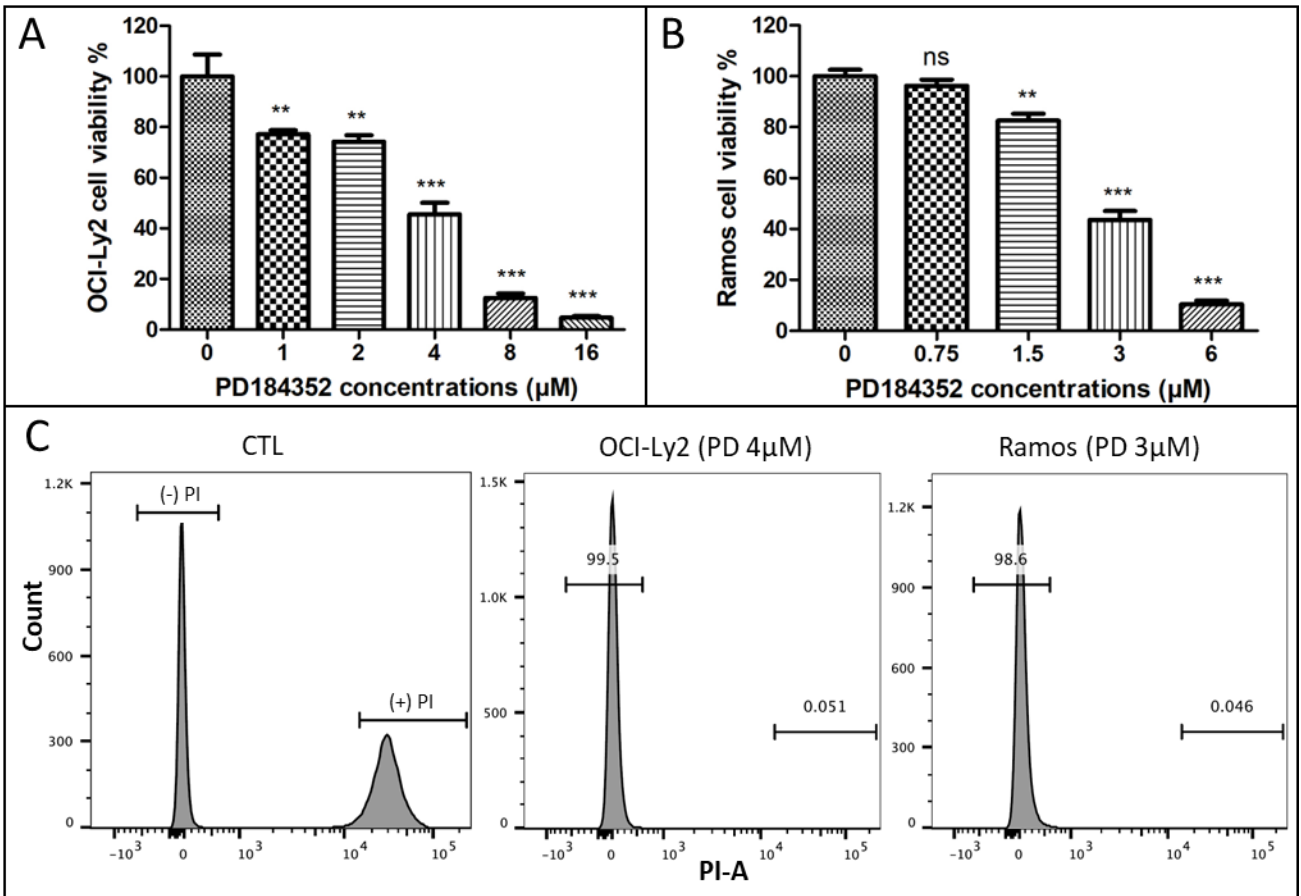


**Fig 3. Impact of MKK1/2 inhibition on B-cell viability.**

A. OCI-ly2 cells or B. Ramos cells were seeded in 12-well plates at  $2.5 \times 10^5$  cells/mL and treated with increasing concentration of PD184352 for 72 hours. Each treatment was done in duplicate, and the experiments were performed at least three times. Cell viability was measured with the Trypan Blue exclusion assay. Data presented as the mean  $\pm$  S.E.M. (one-way ANOVA with Dunnett test \*\*\*,  $p < 0.001$ ; \*\*,  $p < 0.01$ ; \*,  $p < 0.05$ ). C. Flow cytometry histograms showing propidium iodide (PI) staining after treatment with PD184352 at IC<sub>50</sub>. OCI-Ly2 cells (middle panel) or Ramos cells (right panel) were stained with PI after 72 hours of treatment, as in A and B.

**Fig. 4**

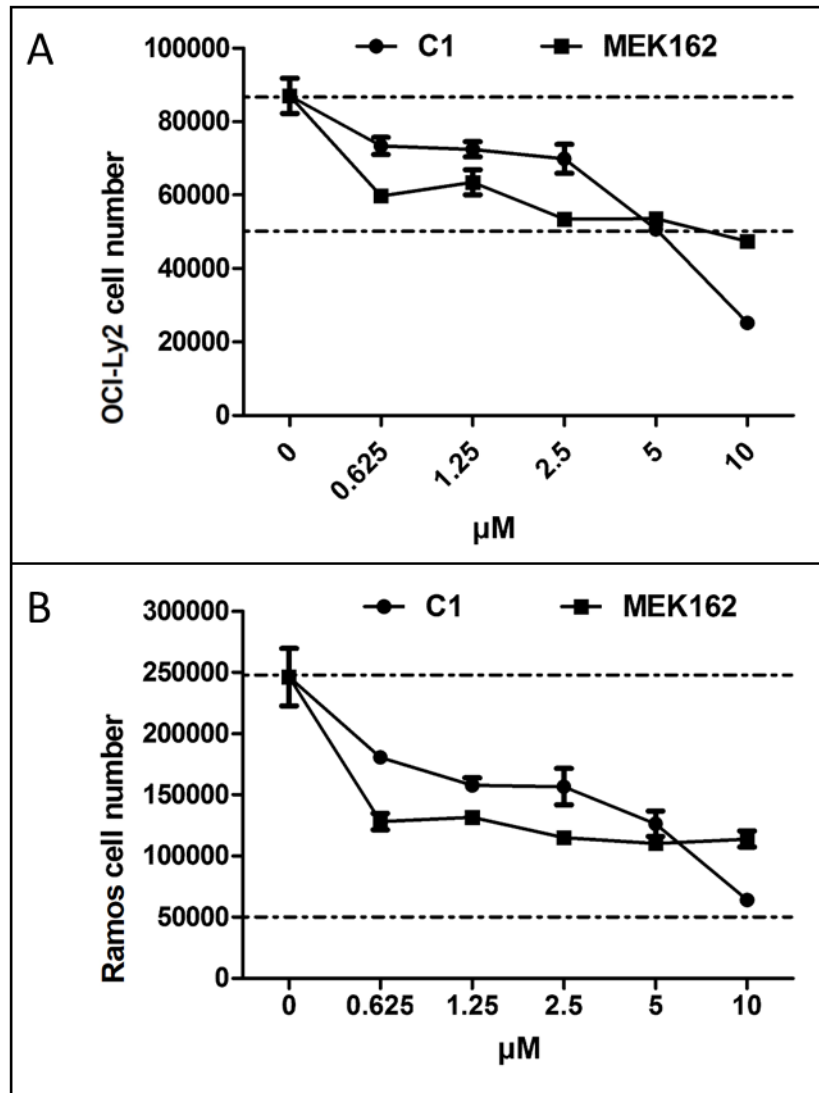


**Fig 4. Impact of TPL2 inhibition on B-cell viability.**

A. OCI-Ly2 cells were seeded in 96-well plates ( $5 \times 10^4$  cells/  $100 \mu\text{L}$ ) and incubated with an increasing concentration of Compound 1 (C1) or MEK162. The cell number was assayed at 72 hours with the Vybrant MTT Cell Proliferation Assay Kit. The lower

dashed lines represent the number of cells seeded, while the top line represents the end-of-experiment cell number. B. Ramos cells were treated with C1 or MEK162, and the cell number was measured after 48 hours of incubation, as in A. Each experiment included four replicates and was repeated three times. The results are expressed as the mean  $\pm$  S.E.M. of a single representative experiment.

### **2.4.3 Dual therapies using BCL2 and TPL2 inhibitors show no interaction towards decreasing OCI-LY2 cell viability.**

To explore the relationship between molecular defects and drug responsiveness, we delineated molecular pathways that are affected in a DLBCL cell line, namely OCI-Ly2 cells (Tweeddale et al., 1987). The cells were isolated from a 50-year-old male at relapse, with TP53 deletion; the isolated cells were MYC negative. They express low levels of the anti-apoptotic MCL1 protein but high levels of BCL-2, which correlates with their responsiveness to the BCL-2 inhibitors, namely ABT-199 (Klanova et al., 2016). Accordingly, we found a similar dose-dependent decrease in OCI-Ly2 cell viability as compared to ABT199 (Venetoclax) (Souers et al., 2013) (Fig. 5A) or to ABT263 (Navitoclax) (Tse et al., 2008) (Fig. 5B), two BCL-2 inhibitors. Therefore, BCL-2 provides necessary signals to OCI-Ly2 cells to escape cell death. In accordance with results presented in Fig.3, we observed a dose-dependent decrease in OCI-Ly2 cells correlated to increasing concentrations of two related TPL2 inhibitors, i.e. Compound 1 (Fig. 5C) and Compound 34 (Fig. 5D). Since BCL2 and TPL2 are associated with distinct cellular functions, survival, and proliferation, we hypothesize that dual inhibition may provide greater inhibitory potential in OCI-LY2 cells. Therefore, OCI-Ly2 cells were exposed to

TPL2 inhibitors with BCL2 inhibitors (Fig. S2), and drug interaction was assessed using two-way ANOVA (Fig. 6). No significant interactions were discovered between these two inhibitor families in OCI-Ly2 cells.

**Fig.5**

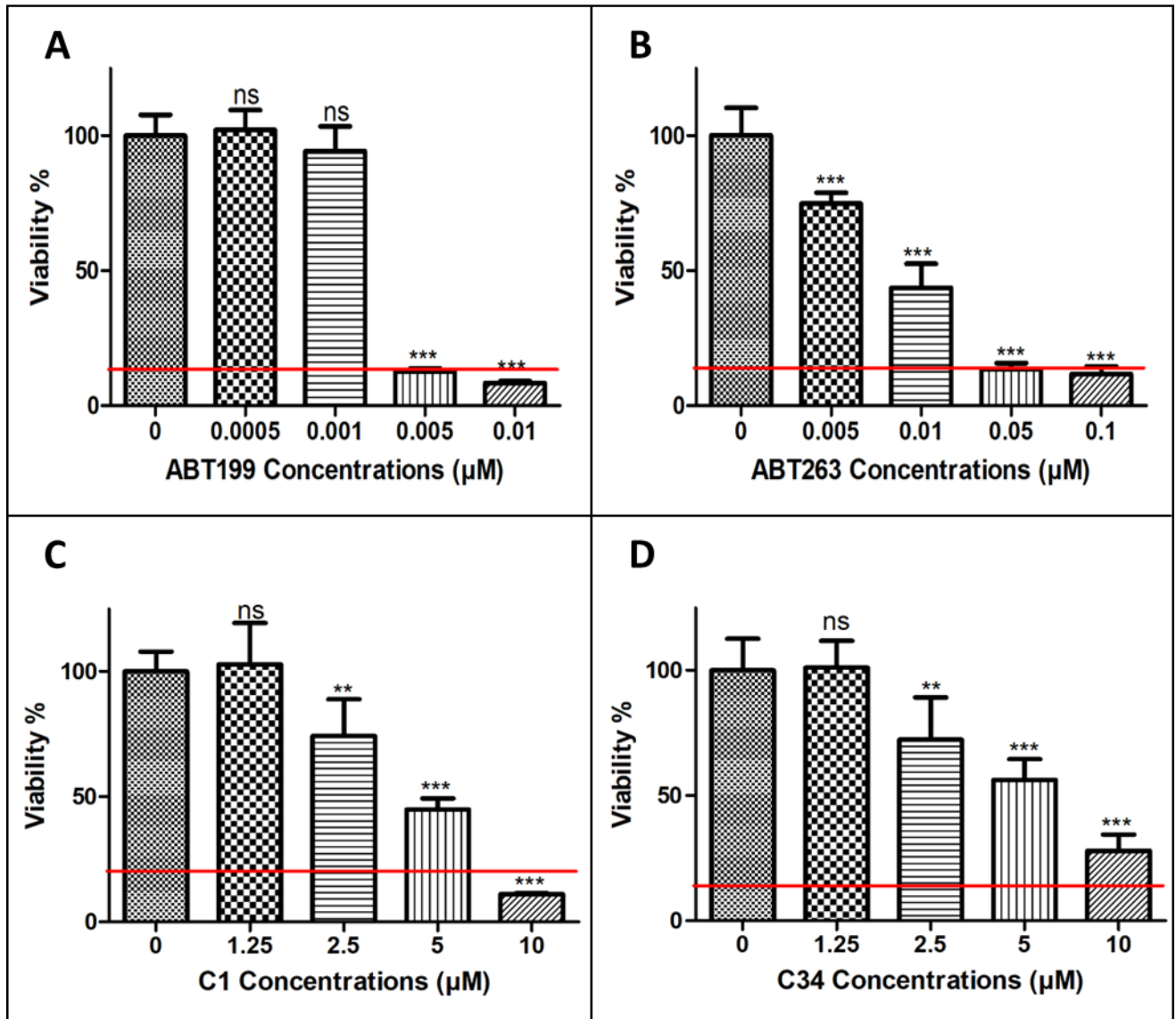


**Fig. 5** Single therapies reduced OCI-LY2 cell viability in a dose-dependent manner.

Herein presented are dose-viability plots of OCI-LY2 cell viability following treatment with (A) ABT199; (B) ABT263; (C) Compound 1 (C1); and (D) Compound 34 (C34) for 72 hours. Cells were seeded in 96-well plates ( $2.5 \times 10^4$  cells/ 100  $\mu$ L), and viability was measured using MTT assay. Horizontal red lines represent the initial number of seeded cells. Each bar represents a percentage value normalized to the mean value of the control group treated with a vehicle only (DMSO 0.1 %) with SD of three independent experiments (n=6, one-way ANOVA with Dunnett's post hoc test, \*\*\*  $p < 0.001$ , \*\*  $p < 0.01$ , \*  $p < 0.05$ ).

**Fig.6**

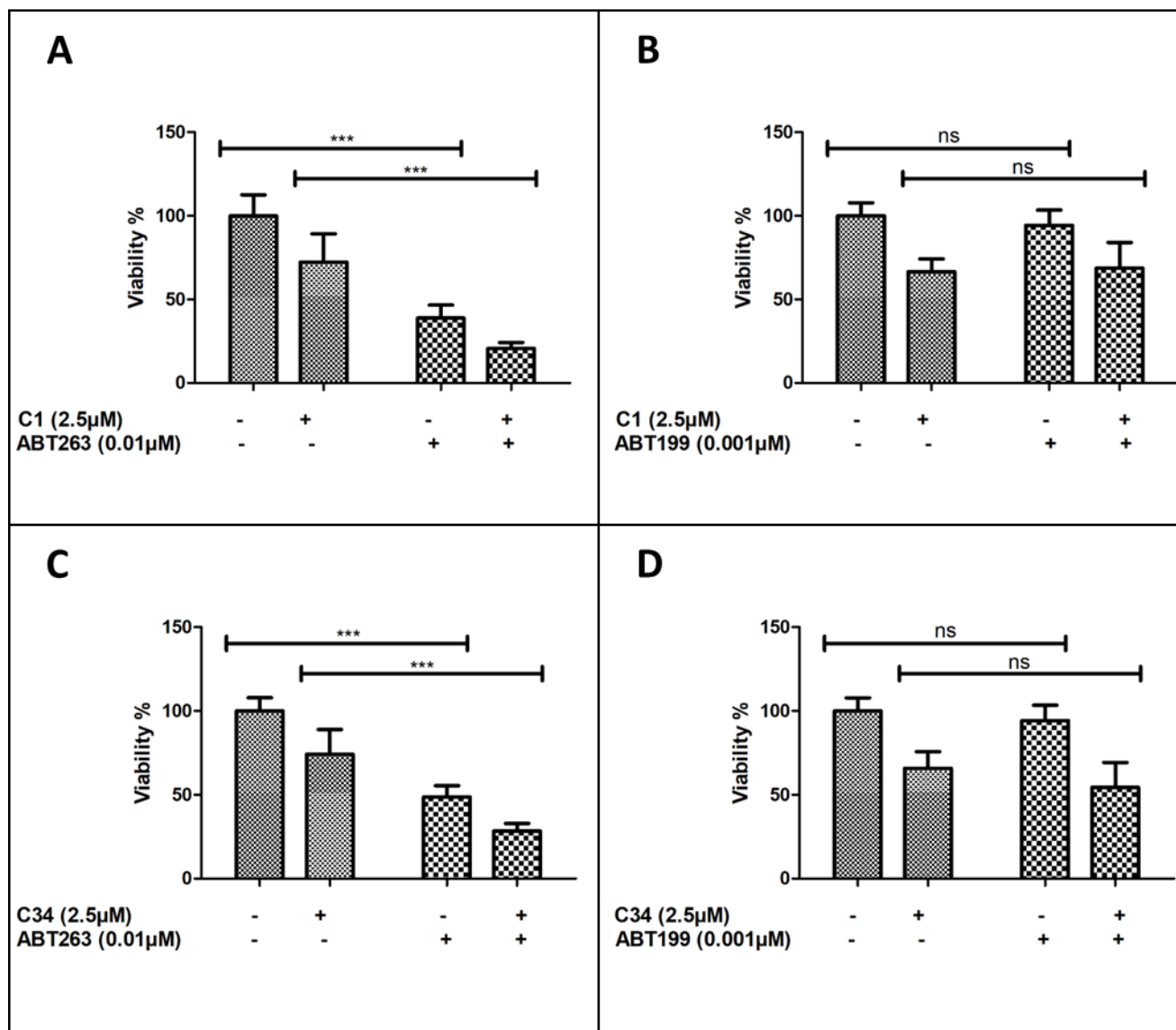


**Fig. 6 Dual therapies show no significant interaction in OCI-LY2 cells.**

Herein presented is OCI-LY2 cell viability following treatment with (A) Compound 1 (C1) and ABT263; (B) Compound 1 (C1) and ABT199; (C) Compound 34 (C34) and ABT263; and (D) Compound 34 (C34) and ABT199 for 72 hours. Viability was measured using MTT assay. Shown is the mean value (SD) from three independent experiments (n=6,

two-way ANOVA with Bonferroni post hoc test to compare means by row, \*\*\*  $p < 0.001$ , \*\*  $p < 0.01$ , \*  $p < 0.05$ ).

## 2.5 Discussion

In this report, we confirmed that blocking the ERK1/2 signaling cascade alone seems to be mainly cytostatic and that its antitumor activity may not necessarily lead to tumor regression (Montagut and Settleman, 2009). We noted that under basal conditions, no significant loss in cell viability could be discerned at concentrations known to completely prevent activation of the TPL2-MKK1/2 pathway in BCWM.1, OCI-Ly2, or RAMOS lymphoma cells. Interestingly, triggering TLR-signaling in BCWM.1 cells sensitizes these cells to TPL2-MKK1/2 pathway inhibition, leading to a significant loss in viability. This is not only true for TLR agonists activating MYD88 (PAM3CSK4 or Flagellin) but also agonists acting independently of MYD88 through the TRIF-signaling adaptor (Poly I:C), suggesting that the combination of TPL2-MKK1/2 signaling inhibitors in the presence of strong TLR activation triggers alternative cell death mechanisms not present under unstimulated conditions. This opens novel avenues of investigation with unconventional combination therapies.

An interesting result is the impact of Compound 1 at high concentrations on OCI-Ly2 cell viability. At the highest dose tested (10 $\mu$ M), Compound 1 was almost as efficacious as Rituximab, Doxorubicin, and Vincristine in decreasing OCI-Ly2 cell numbers, not only preventing proliferation but also leading to cell killing. This effect is likely mediated by inhibition of other targets in addition to TPL2 and ERK1/2. Whether this new target acts

in concert with or independent of ERK1/2 activation remains to be determined. The other target is likely another protein kinase, as Compound 1 is an ATP competitive inhibitor that came from a tyrosine kinase inhibitor collection (Green et al., 2007). Using the published profile of kinases affected by Compound 1 (Hall et al., 2007), the second most affected protein kinase is CAMKII. Interestingly, CAMKII $\gamma$  stabilizes the c-Myc protein (downstream effector of ERK1/2) through its phosphorylation, and this inhibition of CAMKII reduced tumor burden in T cell lymphomas (Gu et al., 2017), thus raising the possibility that Compound 1 serves to decrease CAMKII activity at the highest concentrations used, thus reducing MYC stability and being sufficient to induce killing. However, it is more likely that Compound 1 acts via the combined action of the kinases it targets, preventing ERK1/2 induced c-Myc gene expression via TPL2 and MYC protein destabilization via CAMKII (Yasuda et al., 2008).

Furthermore, ERK1/2 can phosphorylate the same residue as CAMKII (Ser62) on MYC (Pulverer et al., 1994), raising the possibility that inhibition of one kinase can be compensated by another, thus providing another pathway by which Compound 1 could be acting to induce cell killing. As Compound 1 was developed for its selectivity towards TPL2, it may be interesting to revisit the original series of compounds and those of the related quinoline-3-carbonitriles series for their potency in killing DLBCL cells (Green et al., 2007; Hall et al., 2007). These other compounds may have greater potency for lymphoma cell killing and enable the development of novel anti-lymphoma drugs that target lymphoma unresponsive to ERK1/2 cascade inhibition. Adding novel chemical families to the arsenal of drugs that can impact lymphomas will be an important element

in targeting the molecular heterogeneity of tumor cells and providing patient-specific therapies.

Alternative ways to enhance the effectiveness of TPL2-MKK1/2 pathway inhibitors include their combination with anti-survival inhibitors. It has been postulated that oncogenic kinase inhibitor efficacy may be boosted by the presence of BCL-2 inhibitors (Cragg et al., 2009). Furthermore, previous studies indicate that the therapeutic benefit of BCL-2 inhibitors alone, such as ABT-199 and ABT-263, is limited due to acute, dose-dependent thrombocytopenia (Itchaki and Brown, 2016). However, our data in OCI-Ly2 cells showed no significant interaction between these two families of inhibitors, with much greater efficacy belonging to the anti-BCL-2 family in this cell line. Therefore, future studies should consider other combination therapies with the TPL2-MKK12 pathway that may yield higher and more durable responses, while limiting detrimental effects.

## 2.6 References

Airiau, K., Prouzet-Mauléon, V., Rousseau, B., Pigneux, A., Jeanneteau, M., Giraudon, M., et al. (2016). Synergistic cooperation between ABT-263 and MEK1/2 inhibitor: effect on apoptosis and proliferation of acute myeloid leukemia cells. *Oncotarget* 7(1), 845-859. doi: 10.18632/oncotarget.6417.

Beinke, S., Robinson, M., Hugunin, M., and Ley, S. (2004). Lipopolysaccharide activation of the TPL-2/MEK/extracellular signal-regulated kinase mitogen-activated protein kinase cascade is regulated by I $\kappa$ B kinase-induced proteolysis of NF-

kappaB1 p105. *Molecular and cellular biology* 24, 9658–67. doi:  
10.1128/mcb.24.21.9658-9667.2004.

Cragg, M. S., Harris, C., Strasser, A., and Scott, C. L. (2009). Unleashing the power of inhibitors of oncogenic kinases through BH3 mimetics. *Nature Reviews Cancer* 9, 321–326. doi: 10.1038/nrc2615.

Dumitru, C., Ceci, J., Tsatsanis, C., Kontoyiannis, D., Stamatakis, K., Lin, J., et al. (2000). TNF-alpha induction by LPS is regulated posttranscriptionally via a Tpl2/ERK-dependent pathway. *Cell* 103, 1071–83.

Green, N., Hu, Y., Janz, K., Li, H.-Q., Kaila, N., Guler, S., et al. (2007). Inhibitors of tumor progression loci-2 (Tpl2) kinase and tumor necrosis factor alpha (TNF-alpha) production: selectivity and in vivo antiinflammatory activity of novel 8-substituted-4-anilino-6-aminoquinoline-3-carbonitriles. *Journal of medicinal chemistry* 50, 4728–45.

Gu, Y., Zhang, J., Ma, X., Kim, B., Wang, H., Li, J., et al. (2017). Stabilization of the c-Myc Protein by CAMKII $\gamma$  Promotes T Cell Lymphoma. *Cancer Cell* 32, 115-128.e7. doi: 10.1016/j.ccell.2017.06.001.

Hall, J., Kurdi, Y., Hsu, S., Cuozzo, J., Liu, J., Telliez, J.-B. B., et al. (2007). Pharmacologic inhibition of tpl2 blocks inflammatory responses in primary human monocytes, synoviocytes, and blood. *The Journal of biological chemistry* 282, 33295–304. doi: 10.1074/jbc.M703694200.

Hermine, O., Haioun, C., Lepage, E., d'Agay, M., Briere, J., Lavignac, C., et al. (1996). Prognostic significance of bcl-2 protein expression in aggressive non-Hodgkin's

lymphoma. Groupe d'Etude des Lymphomes de l'Adulte (GELA). *Blood* 87(1), 265-272.  
doi: 10.1182/blood.V87.1.265.265 %J Blood.

Itchaki, G., and Brown, J. R. (2016). The potential of venetoclax (ABT-199) in chronic lymphocytic leukemia. *Therapeutic advances in hematology* 7, 270–287. doi: 10.1177/2040620716655350.

Kawasaki, T., and Kawai, T. (2014). Toll-like receptor signaling pathways. *Front Immunol* 5, 461. doi: 10.3389/fimmu.2014.00461.

Klanova, M., Andera, L., Brazina, J., Svadlenka, J., Benesova, S., Soukup, J., et al. (2016). Targeting of BCL2 Family Proteins with ABT-199 and Homoharringtonine Reveals BCL2- and MCL1-Dependent Subgroups of Diffuse Large B-Cell Lymphoma. *Clinical cancer research : an official journal of the American Association for Cancer Research* 22, 1138–49. doi: 10.1158/1078-0432.CCR-15-1191.

Montagut, C., and Settleman, J. (2009). Targeting the RAF-MEK-ERK pathway in cancer therapy. *Cancer letters* 283, 125–34. doi: 10.1016/j.canlet.2009.01.022.

Platanias, L. C. (2003a). Map kinase signaling pathways and hematologic malignancies. *Blood* 101, 4667–79. doi: 10.1182/blood-2002-12-3647.

Platanias, L. C. (2003b). Map kinase signaling pathways and hematologic malignancies. *Blood* 101, 4667–79. doi: 10.1182/blood-2002-12-3647.

Pulverer, B., Fisher, C., Vousden, K., Littlewood, T., Evan, G., and Woodgett, J. (1994). Site-specific modulation of c-Myc cotransformation by residues phosphorylated in vivo. *Oncogene* 9, 59–70.

Roberts, A.W. (2020). Therapeutic development and current uses of BCL-2 inhibition. *Hematology* 2020(1), 1-9. doi: 10.1182/hematology.2020000154 %J Hematology.

Rosenwald, A., Wright, G., Chan, W.C., Connors, J.M., Campo, E., Fisher, R.I., et al. (2002). The Use of Molecular Profiling to Predict Survival after Chemotherapy for Diffuse Large-B-Cell Lymphoma. *346*(25), 1937-1947. doi: 10.1056/NEJMoa012914.

Rousseau, S., and Martel, G. (2016). Gain-of-Function Mutations in the Toll-Like Receptor Pathway: TPL2-Mediated ERK1/ERK2 MAPK Activation, a Path to Tumorigenesis in Lymphoid Neoplasms? *Frontiers in cell and developmental biology* 4, 50. doi: 10.3389/fcell.2016.00050.

Sale, Matthew J., and Cook, Simon J. (2013). The BH3 mimetic ABT-263 synergizes with the MEK1/2 inhibitor selumetinib/AZD6244 to promote BIM-dependent tumour cell death and inhibit acquired resistance. *Biochemical Journal* 450(2), 285-294. doi: 10.1042/BJ20121212 %J Biochemical Journal.

Souers, A.J., Levenson, J.D., Boghaert, E.R., Ackler, S.L., Catron, N.D., Chen, J., et al. (2013). ABT-199, a potent and selective BCL-2 inhibitor, achieves antitumor activity while sparing platelets. *Nat Med* 19(2), 202-208. doi: 10.1038/nm.3048.

Tan, N., Wong, M., Nannini, M.A., Hong, R., Lee, L.B., Price, S., et al. (2013). Bcl-2/Bcl-xL Inhibition Increases the Efficacy of MEK Inhibition Alone and in Combination with PI3 Kinase Inhibition in Lung and Pancreatic Tumor Models. *Molecular Cancer Therapeutics* 12(6), 853-864. doi: 10.1158/1535-7163.MCT-12-0949 %J Molecular Cancer Therapeutics.

Treon, S.P., Xu, L., and Hunter, Z. (2015). MYD88 Mutations and Response to Ibrutinib in Waldenström's Macroglobulinemia. *N Engl J Med* 373(6), 584-586. doi: 10.1056/NEJMc1506192.

Tse, C., Shoemaker, A.R., Adickes, J., Anderson, M.G., Chen, J., Jin, S., et al. (2008). ABT-263: a potent and orally bioavailable Bcl-2 family inhibitor. *Cancer Res* 68(9), 3421-3428. doi: 10.1158/0008-5472.Can-07-5836.

Tweeddale, M., Lim, B., Jamal, N., Robinson, J., Zalcborg, J., Lockwood, G., et al. (1987). The presence of clonogenic cells in high-grade malignant lymphoma: a prognostic factor. *Blood* 69, 1307–14.

Yang, J., Liu, X., Bhalla, K., Kim, C.N., Ibrado, A.M., Cai, J., et al. (1997). Prevention of Apoptosis by Bcl-2: Release of Cytochrome c from Mitochondria Blocked. *Science* 275(5303), 1129-1132. doi: doi:10.1126/science.275.5303.1129.

Yasuda, T., Sanjo, H., Pagès, G., Kawano, Y., Karasuyama, H., Pouyssegur, J., et al. (2008). Erk kinases link pre-B cell receptor signaling to transcriptional events required for early B cell expansion. *Immunity* 28, 499–508. doi: 10.1016/j.immuni.2008.02.015.

## 2.7 Supplementary data

**Fig.S1**

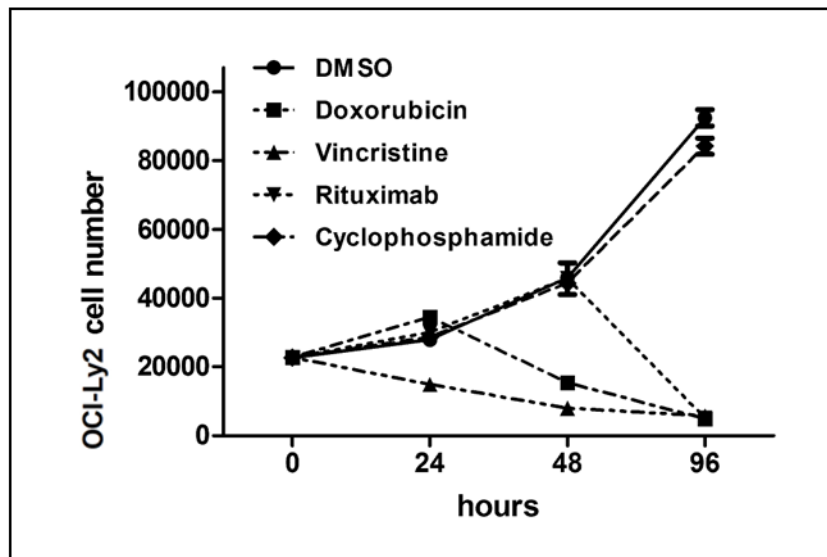


**Fig. S1 Impact of standard immunochemotherapies on B-cell viability.**

OCI-Ly2 was seeded in 96-well plates ( $2.5 \times 10^4$  cells/ 100  $\mu$ L) and incubated with 625nM of Doxorubicin, 625nM of Vincristine, 10 $\mu$ M of Cyclophosphamide, or 1 $\mu$ g/mL of Rituximab, and the cell number was assessed using the Vybrant MTT Cell Proliferation Assay Kit. Each experiment contained four replicates and was repeated three times. The results are expressed as the mean  $\pm$  S.E.M. of a single representative experiment.

**Fig.S2**

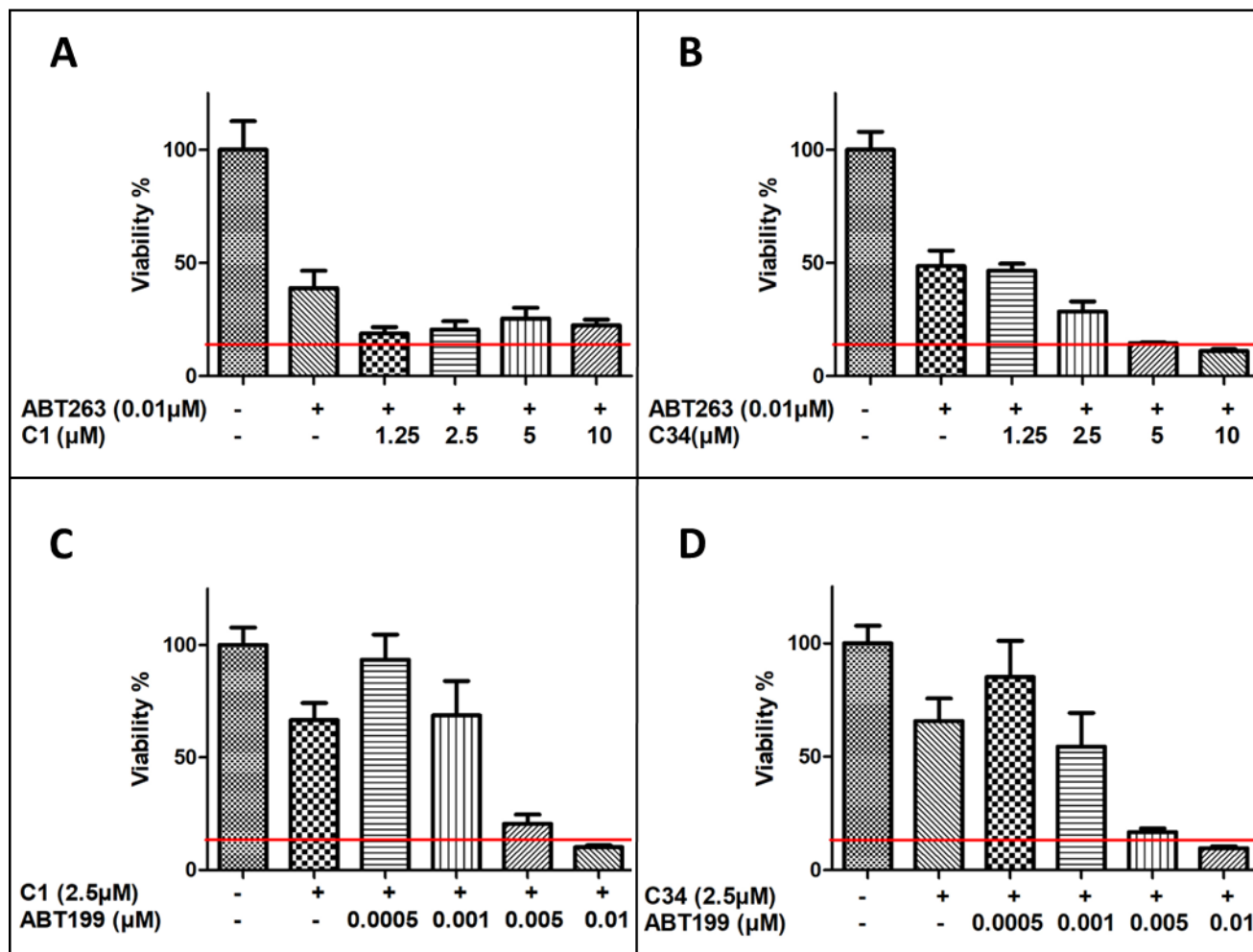


**Fig. S2 The effect of dual therapies on OCI-LY2 cell viability.**

Dose-viability plots of OCI-LY2 cells following treatment with (A) Compound 1 (C1) and ABT263; (B) Compound 34 (C34) and ABT263; (C) Compound 1 (C1) and ABT199; and (D) Compound 34 (C34) and ABT199 for 72 hours. Cells were seeded in 96-well plates (2.5x10<sup>4</sup> cells/ 100  $\mu$ L) and viability was measured using MTT assay. Horizontal red lines represent the initial number of seeded cells. Shown is the mean value (SD) from three independent experiments (n=6).

## **Preface**

Results from chapter 2 showed that inhibition of ERK1/2 signaling via targeting either TPL2 or MKK1/2 mainly reduced cell proliferation in B cell NHL cell lines, namely OCI-LY2 cells, representing DLBCL (the most common type of NHL) and RAMOS cells representing Burkitt lymphoma (a rare type of B cell NHL). Interestingly, Compound 1 at higher concentrations than those required to inhibit TPL2 activity induced killing effects, probably due to inhibiting other off targets. These findings indicate that inhibiting multiple oncogenic targets can produce cytotoxic effects. Therefore, in this chapter we have focused on combined therapies instead of single therapies.

# **Chapter 3: Single and Dual Inhibition of Extracellular Signal Regulated Kinases 1/2 and Histone Deacetylase 6 as Potential Therapies for Diffuse Large B-Cell Lymphoma**

Mariana Asslan<sup>1,2</sup>, Lorne Taylor<sup>1</sup>, Maja Beus<sup>3</sup>, Dusica Maysinger<sup>2</sup>, Simon Rousseau<sup>1,2</sup>

1. Research Institute of the McGill University Health Centre, Montreal, Canada.
2. Pharmacology Department, McGill University, Montreal, Canada.
3. Faculty of Pharmacy and Biochemistry, University of Zagreb, Zagreb, Croatia.

Under review in Biomedicine & Pharmacotherapy journal.

Corresponding author

Simon Rousseau, The Meakins-Christie Laboratories at the RI-MUHC, 1001 Boul. Décarie, Montréal, H4A 3J1, Canada, Phone: +1-514-934-1934 (76394), Email: [simon.rousseau@mcgill.ca](mailto:simon.rousseau@mcgill.ca)

Funding sources

This work was supported by NSERC Discovery grant RGPIN-2015-06768 (SR) and RGPIN-2020-07011 (DM). SR is supported by a Chercheur-Boursier Senior Salary Award from the Fonds de Recherche du Québec – Santé. MA has been supported by awards from the Department Of Pharmacology and Experimental Therapeutics - McGill University; the Faculty of Medicine - McGill University; and the Research Institute of the McGill University Health Centre (RI-MUHC).

### **Authors' contributions**

The main text of the manuscript was written by Mariana Asslan. Material preparation, data collection, and analysis were performed by Mariana Asslan. Lorne Taylor and Mariana Asslan performed the proteomic analysis. Maja Beus prepared Sahaquine. All authors have reviewed and approved the final manuscript.

Keywords: Lymphomas, ERK1/2 inhibition, HDAC6 inhibition, Sahaquine, drug combination.

### **3.1 Abstract:**

Diffuse large B-cell lymphoma (DLBCL) is the most common type of lymphoma in adults. Even though immunochemotherapy leads to significant improvements in the overall survival of DLBCL patients, as the disease progresses, more than half of the patients relapse due to disease heterogeneity. Thus, novel targeted therapeutics are

needed to replace the current frontline therapies. In subtypes of DLBCL overexpression of extracellular signal-regulated kinases, 1/2 (ERK1/2) and histone deacetylase 6 (HDAC6) have been reported, making them valuable targets for therapeutic interventions. In this study, we have investigated the effectiveness of the mitogen-activated protein kinase kinase 1/2 (MKK1/2) inhibitor - PD184352 (CI-1040) - and HDAC6 inhibitors - ACY1215 (ricolinostat) and Sahaquine- both as single anti-lymphoma agents and in combination, in preclinical models. Monotherapies generally suppressed the growth of B-cell lymphoma cell lines by disrupting cell cycle progression. To enhance the anti-lymphoma therapeutic efficacy, we combined MKK1/2 and HDAC6 inhibitors in a cell culture model. Promising cytocidal results were obtained from both combinations, with apoptosis induction observed in the Sahaquine with PD184352 group but not in the PD184352 with ACY1215 group. Proteomic analysis was carried out to identify the molecular targets of the experimental therapies. This study provides insight into innovative strategy and suggests that dual MKK1/2 and HDAC6 inhibition acts additively in DLBCL. Therefore, our study results show promise as a more efficacious clinical strategy for the improvement of lymphoma treatment in the future than a single therapy.

### **3.2 Introduction**

Diffuse large B-cell lymphoma (DLBCL), the most common type of adult lymphoma, is an aggressive malignancy affecting mature B lymphocytes. Clinical, genetic, and molecular heterogeneities are defining characteristics of DLBCL [1]. Although most patients initially respond to immunochemotherapy (R-CHOP), less than half of them

achieve durable remission [2-7]. Thus, development of novel targeted therapies is particularly attractive as an alternative to standard chemotherapy associated with adverse effects. Deregulation of ERK signaling is a prominent feature of B-cell lymphomas [8, 9] including DLBCL [10, 11]. Moreover, histone-modifying gene mutations are common in DLBCL and are likely to result in reduced acetylation and enhanced methylation which can promote malignant transformation [12, 13].

Extracellular signal-regulated kinases 1/2 (ERK1/2) are activated by mitogen-activated protein kinase kinase 1/2 (MKK1/2) via signals from variant receptors including Toll-like receptors via MYD88 [14]; B-cell receptor [15, 16]; and Receptor tyrosine kinases [17, 18]. Activation of ERK1/2 leads to their phosphorylation and the initiation of cellular responses [19], such as controlling c-MYC expression [20-22] and regulating NF- $\kappa$ B activity [23].

Inhibitors targeting the ERK1/2 signaling pathway have received widespread attention based on their central role in regulating the growth and survival of cells [24, 25]. However, several ERK signaling inhibitors failed clinical trials as monotherapies, including the MKK1/2 inhibitor PD184352 [26]. PD184352 was well-tolerated, but it did not show sufficient anti-cancer activity when used alone [27]. Other FDA-approved inhibitors of the ERK1/2 pathway are usually used in combinations in order to improve the clinical outcome [28-30]. In pre-clinical models, they were tested in combination with pan-histone deacetylase (HDAC) inhibitors, and the results suggested that this combination provides a promising therapeutic strategy for various cancers such as leukemia [31, 32], colon and lung adenocarcinoma [33], pancreatic cancer [34], multiple myeloma [35], ovarian cancer [36], and brain tumor [37, 38].

HDAC inhibitors emerged as promising therapeutics due to their ability to induce growth arrest and apoptosis [39]. Several pan-HDAC inhibitors have been FDA-approved, including SAHA, a hydroxamic acid derivative used for the treatment of T cell lymphoma [40]. However, the clinical efficacy of pan-HDAC inhibitors is limited due to their profound side effects [41, 42]. To overcome this obstacle, selective HDAC inhibitors have been developed, including ACY1215, an HDAC6 inhibitor.

Recent evidence showed that one of the most frequently altered HDACs in DLBCL is histone deacetylase 6 (HDAC6), a class IIb member of HDACs [43, 44]. HDAC6 is a deacetylase present mainly in the cytoplasm and it controls the activity of various non-histone proteins by catalyzing the removal of acetyl groups from lysine residues. HDAC6 mediates reversible deacetylation of  $\alpha$ -tubulin [45]; heat shock protein 90 (HSP90) [46]; MYD88 [47]; ERK1 [48]; peroxiredoxin I and II [49]; p65 [50, 51]; and p53 [52]. Additionally, it regulates c-Myc expression [53] and NF- $\kappa$ B activity [54, 55]. Moreover, HDAC6 plays a protective role in damaged cells by promoting DNA repair [56], regulating cell viability in response to misfolded protein stress [57] and preventing apoptotic signaling proteins from translocation to the mitochondria [58-60].

Although ACY1215 had a good safety profile in lymphoma patients [61], it failed clinical trials due to the lack of significant response [62]. One of the reasons is the concentration plateau, i.e. its blood concentrations cannot be increased to achieve the therapeutic range. To enhance its effectiveness at physiological concentrations, ACY1215 has been tested in combinations [62, 63].

Another HDAC6-selective inhibitor, Sahaquine, was developed with high selectivity towards HDAC6 at nanomolar concentrations. It is a new hydroxamic acid hybrid

molecule that has shown antitumor activity against glioblastoma [64], as well as breast, bone, and liver human cancer cell types [65]. Sahaquine safety and metabolism were evaluated in the Zebrafish model, showing a good safety profile [66]. Sahaquine anti-lymphoma effectiveness has not been investigated as a single therapy or in the combination with a MKK1/2 inhibitor.

In this study, we tested the susceptibility of human-derived B-cell lymphoma cell lines (OCI-LY2, Ramos, BCWM.1) to Sahaquine, ACY1215, and PD184352 as monotherapies. This was followed by the assessment and quantification of the combination of PD184352 with Sahaquine or ACY1215 to evaluate the dual therapies' combined effect in a cell culture model. The interaction between Sahaquine and PD184352 was compared to ACY1215 with PD184352 in the OCI-LY2 DLBCL cell line. Broad-approach proteomic analysis was used to identify the molecular targets of the Sahaquine and PD184352 combination.

### **3.3 Methods and Materials**

#### **3.3.1 Cell culture**

OCI-LY2 human DLBCL cells were graciously provided by Prof. Minden (University of Toronto, Ontario Cancer Institute). BCWM.1 human Waldenstrom Macroglobulinemia cells were obtained from Prof. S.P. Treon (Bing Center for Waldenström's Macroglobulinemia, Dana-Farber Cancer Institute, Boston, Massachusetts, USA). RAMOS human Burkitt Lymphoma cells were purchased from ATCC (Rockville, MD, USA). Cells were grown in RPMI 1640 medium (#350-000-CL, Wisent) supplemented

with 10% fetal bovine serum (#080-450, Wisent) and 1% penicillin/streptomycin (#450-201-EL, Wisent), incubated at 37°C with 5% CO<sub>2</sub> and 95% relative humidity. Cells were passaged every 2–3 days.

### **3.3.2 Cell counting assay**

For mono- and dual-therapies, cells were treated with MKK1/2 inhibitor PD184352 (CI-1040) (#HY-50295, MedChemExpress); HDAC6 inhibitor ACY1215 (Ricolinostat) (#HY-16026, MedChemExpress); and HDAC6 inhibitor Sahaquine (synthesized as previously described) [64] alone or in combination. For OCI-LY2 and RAMOS cell lines, 2-fold serial dilutions were prepared, whereas for the BCWM.1 cell line, 1.5-fold serial dilutions of inhibitors were prepared. For dual therapies, both inhibitors were combined at the approximate same effect level (IC<sub>50</sub> of drug A with IC<sub>50</sub> of drug B) with a fixed combination ratio. After 72 hours of treatment, cells were washed with phosphate-buffered saline (PBS) and incubated with propidium iodide (PI) (#1056, BioVision) in the dark for 5 minutes (to exclude dead cells). Viable cells were counted using a BD LSRFortessa X-20 flow cytometer. To quantify the drug interaction, data were analyzed using CompuSyn (V 1.0) software based on the method described by Chou and Talalay (Chou and Talalay, 1984) for dose-effect analysis. Combination index (CI) values were classified as follows: CI < 0.3 = highly synergistic; 0.3–0.7 = synergistic; 0.7–0.9 = moderate to slight synergistic; 0.9–1.1 = nearly additive; 1.1–1.45 = slight to moderate antagonistic; 1.45–3.3 = antagonistic; and >3.3 = strong antagonistic.

### **3.3.3 Cell cycle assay**

OCI-LY2 cells (1x10<sup>6</sup> cells for single therapies and 2x10<sup>6</sup> for dual therapies) were collected at different time points after treatments and washed with PBS. Cells were fixed

and permeabilized in 70% cold ethanol for 30 minutes at 4°C. Following fixation, samples were washed with PBS and incubated in the dark with 20 µl Propidium Iodide (PI; 1 mg/mL) (#1056, BioVision) and 5 µL RNase A 10 mg/mL (#EN0531, ThermoFisher Scientific) in 480 µL PBS for 30 minutes at room temperature. Samples were analyzed using a BD LSRFortessa X-20 flow cytometer. The effect on cell cycle progression based on the DNA content of stained cells was determined using the FlowJo software.

### **3.3.4 Apoptosis and necrosis assay**

Treated OCI-LY2 cells (1x10<sup>6</sup> cells for single therapies and 2x10<sup>6</sup> for dual therapies) were harvested at different time points. Early apoptosis was assessed using the Annexin V-EGFP reagent (#1004, BioVision). Late apoptosis and necrosis were assessed using PI (#1056, BioVision). After treatment, cells were washed and resuspended in 500 µL of Binding Buffer (# 1006, BioVision), then incubated with 1 µL of Annexin V-EGFP and 1 µL of PI for 5 minutes in the dark at room temperature. Cells were analyzed by a BD LSRFortessa X-20 flow cytometer. Based on staining, cells were classified as viable (annexin V-negative, PI-negative); early apoptotic (annexin V-positive, PI-negative); and late apoptotic/necrotic cells (annexin V-positive, PI-positive). The percentage of cells in each quadrant was quantified using the FlowJo software.

### **3.3.5 Nuclear staining**

After treatment, OCI-LY2 cells were washed with PBS and incubated with Hoechst 33342 staining solution (1/2000, #H1399, Invitrogen) in the dark for 10 minutes. Following incubation, the staining solution was removed and the cells were washed with PBS. Cells were placed on imaging slides and covered with Carl Zeiss cover glasses

(#474030-9000). Slides were imaged with a confocal microscope (Zeiss Axio Observer Z1 LSM700) using a 405 nm laser.

### **3.3.6 Immunostaining for flow cytometry analysis**

#### **3.3.6.1 Cytoplasmic proteins**

Following treatment, OCI-LY2 human DLBCL cells ( $1 \times 10^6$  cells for single therapies and  $2 \times 10^6$  for dual therapies) were washed with PBS (#311-010-CL, Wisent) and fixed with 4% paraformaldehyde (PFA) (10 minutes at room temperature, #252549, Sigma-Aldrich). Following fixation, cells were washed with PBS and then permeabilized using 0.1% Triton X-100 (10 min, #BP151-100, Fisher Scientific). Blocking was performed with 10% Bovine Serum Albumin (BSA) (30 minutes, #A7906-50G, Sigma-Aldrich) in PBS and then incubated with primary antibodies (acetyl- $\alpha$ -tubulin K40, 1/200; Cell Signaling, #5335; phospho-p44/42 ERK1/2 Thr202/Tyr204, 1/200; Cell Signaling, #4370) in 10% BSA/PBS overnight at 4°C. Samples were incubated (5 minutes) and washed three times with PBS. Secondary antibodies (anti-rabbit Alexa Fluor 488, 1/500; Cell Signaling, #4412) in 10% BSA/PBS were incubated with samples for 1 hour in the dark at room temperature, then washed three times with PBS. Cells were then resuspended in PBS for flow cytometry acquisition.

#### **3.3.6.2 Nuclear proteins**

After treatment, OCI-LY2 cells ( $1 \times 10^6$  cells for single therapies and  $2 \times 10^6$  for dual therapies) were washed with PBS then fixed and permeabilized with 1% PFA in Permeabilization Buffer (20 minutes at 4°C, #00-8333-56, Invitrogen). Samples were washed with Permeabilization Buffer and then blocked with 10% BSA in

Permeabilization Buffer for 30 minutes. Samples were incubated overnight at 4°C with primary antibody (acetyl-histone H3 K14, 1/200; Cell Signaling, #7627) in 10% BSA/Permeabilization Buffer. Following incubation, samples were incubated (5 minutes) and then washed three times with Permeabilization Buffer. Samples were incubated with a secondary antibody (anti-rabbit Alexa Fluor 488, 1/500; Cell Signaling, #4412) in 10% BSA/Permeabilization Buffer for 1 hour in the dark at room temperature. Following incubation, cells were washed three times with Permeabilization Buffer. Cells were then resuspended in PBS for flow cytometry acquisition.

### **3.3.7 Proteomic analysis**

Following the indicated treatments, OCI-LY2 cells (1x10<sup>8</sup> for single therapies and 1.5x10<sup>8</sup> for dual therapies) were lysed using urea lysis buffer. The lysate from each sample was divided into two parts, the first part used for whole lysate proteomic analysis and the second for acetylpeptide enrichment analysis.

#### **3.3.7.1 Whole lysate analysis**

Samples were digested using an in-gel digestion technique. In short, samples were loaded onto a single stacking gel band to remove lipids, detergents, and salts. The single gel band containing all proteins was reduced with dithiothreitol (DTT), alkylated with iodoacetic acid, and digested with trypsin. 2 µg of extracted peptides were resolubilized in 0.1% aqueous formic acid and loaded onto a Thermo Acclaim Pepmap (Thermo, 75 µm ID X 2 cm C18 3 µm beads) precolumn and then onto an Acclaim Pepmap Easyspray (Thermo, 75 µm X 15 cm with 2 µm C18 beads) analytical column separation using a Dionex Ultimate 3000 µHPLC at 250 nL/min with a gradient of 2–35% organic (0.1% formic acid in acetonitrile) over a period of three hours. Peptides

were analyzed using a Thermo Orbitrap Fusion mass spectrometer operating at 120,000 resolution (FWHM in MS1) with HCD sequencing (15,000 resolution) at top speed for all peptides with a charge of 2+ or greater. The raw data were converted into \*.mgf format (Mascot generic format) for search purposes, using the Mascot 2.6.2 search engine (Matrix Science) against Human Uniprot sequences (2020). The database search results were loaded onto Scaffold v5.0 (Proteome Sciences) for statistical treatment and data visualization.

### **3.3.7.2 Acetylpeptide enrichment analysis**

For enrichment experimentation, samples were digested and enriched for acetylated peptides by immunoaffinity purification using the PTMScan Acetyl-Lysine Motif [Ac-K] Kit (#13416, Cell Signaling) as recommended by the manufacturer. Acetylpeptides were analyzed using a Thermo Orbitrap Fusion mass spectrometer operating at 120,000 resolution (FWHM in MS1) with HCD sequencing (15,000 resolution) at top speed for all peptides with a charge of 2+ or greater. The raw data were converted into \*.mgf format (Mascot generic format) for search purposes using the Mascot 2.6.2 search engine (Matrix Science) against Human Uniprot sequences (2020). The database search results were loaded onto Scaffold v5.0 (Proteome Sciences) for statistical treatment and data visualization. Label free quantification on MS1 parent ion signals of acetylated peptides were generated, integrated, and compared using Pinnacle v1.1.103 (Optys Tech).

### **3.3.8 Statistical analysis**

All data were analyzed and plotted as mean  $\pm$  SD using GraphPad Prism, unless otherwise indicated. Experiments were performed independently at least three times. To compare the control group (n=6) to each of the treated groups (n=6), a two-tailed one-way analysis of variance (ANOVA) with Dunnett's post hoc test was used. An unpaired two-tailed Student's t-test was performed to compare two groups. The level of significance for all analyses was  $p < 0.05$ . (\*\*\*) indicating statistical significance  $p < 0.001$ , (\*\*)  $p < 0.01$ , (\*)  $p < 0.05$ .

## **3.4 Results**

### **3.4.1 Monotherapies reduce B-cell lymphoma cell line growth in a concentration-dependent manner.**

The anti-lymphoma activity of the MKK1/2 inhibitor (PD184352) and two HDAC6-selective inhibitors (Sahaquine and ACY1215) was tested in different B-cell lymphoma cell lines, including OCI-LY2, RAMOS, and BCWM.1 cell lines. Concentration ranges and approximate effect levels for each inhibitor in all of the cell lines were selected based on preliminary screens using the Trypan Blue exclusion assay.

Each of the single inhibitors induced growth inhibition in a concentration-dependent manner in OCI-LY2 (Figure 1a, b, d); RAMOS (Figure S1a, b, d); and BCWM.1 (Figure S2a, b, d) cell lines, based on flow cytometry cell counting assay. The half maximal inhibitory concentration (IC50) values for PD184352, Sahaquine, and ACY1215 were

calculated in OCI-LY2 (4  $\mu\text{M}$ , 5  $\mu\text{M}$ , 1.5  $\mu\text{M}$ ), RAMOS (3  $\mu\text{M}$ , 3  $\mu\text{M}$ , 1  $\mu\text{M}$ ) and BCWM.1 (6  $\mu\text{M}$ , 7  $\mu\text{M}$ , 2.5  $\mu\text{M}$ ), respectively, using CompuSyn (V 1.0) software and rounded to the next integer, except for ACY1215.

Fig.1

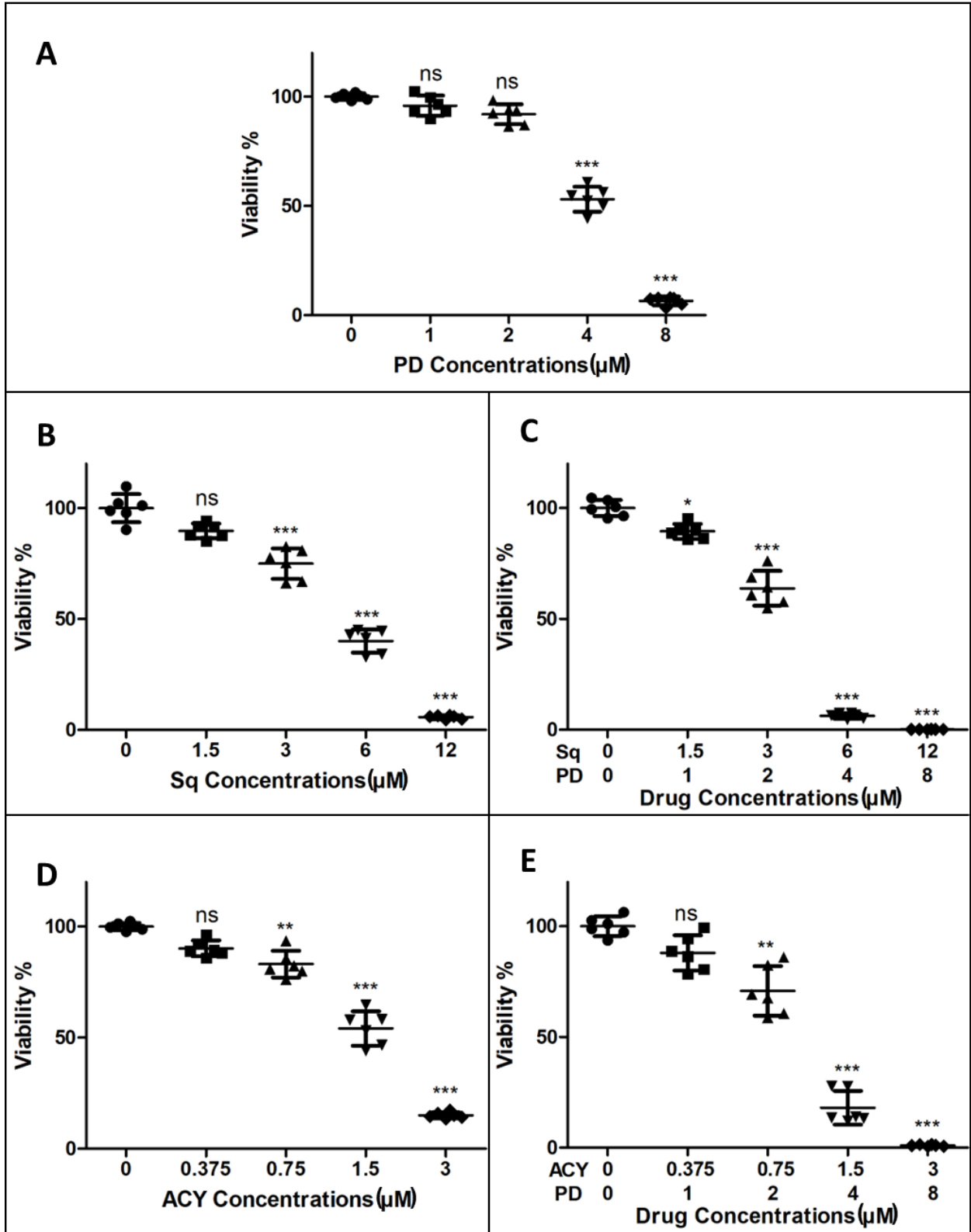


**Fig. 1 Single and dual therapies reduced OCI-LY2 cell viability in a dose-dependent manner.**

Dose-response plots of OCI-LY2 cell viability following treatment with (A) PD184352 (PD), (B) Sahaquine (Sq), (C) PD and Sq, (D) ACY1215 (ACY), and (E) PD and ACY for 72 hours. Each point represents a percentage value normalized to the mean value of the control group treated with vehicle only (DMSO 0.2 %). Horizontal bars represent the average values (SD) of at least three independent experiments (n=6, one-way ANOVA with Dunnett's post hoc test; \*\*\* p < 0.001; \*\* p < 0.01; \* p < 0.05). Cell viability was measured using flow cytometry cell counting and data were analyzed using FlowJo software.

**3.4.2 MKK1/2-HDAC6 inhibitor combinations show additivity in OCI-LY2 and RAMOS cells, but antagonism in BCWM.1 cells.**

The interactions between the MKK1/2 inhibitor (PD184352) and either of the HDAC6 inhibitors (Sahaquine or ACY1215) were studied in OCI-LY2, RAMOS, and BCWM.1 B-cell lymphoma cell lines. Both combination of inhibitors (PD184352 and Sahaquine, or PD184352 and ACY1215) were added at increasing concentrations, maintaining a constant ratio between both inhibitors within an individual experiment. Cells were stained with PI and counted using flow cytometry to measure cell growth and generate the combination dose-response plots in OCI-LY2 (Figure 1c, e); RAMOS (Figure S1c, e); and BCWM.1 (Figure S2c, e) cell lines.

To visualize drug interactions, the median-effect isobolograms were created using CompuSyn (V 1.0) software. In both combinations, the iso-effect points to different effect levels (IC50, IC75, IC90) being very close or on the corresponding additive line,

indicating an additive effect in OCI-LY2 (Figure 2a, b) and RAMOS cells (Figure 2c, d). However, in the BCWM.1 cell line, the iso-effect pointing across the effect levels in both combinations was above the corresponding additive line indicating antagonism in BCWM.1 cells (Figure 2e, f).

To quantify these drug interactions, combination index (CI) values were calculated in the 3 cell lines for both combinations. The interaction in OCI-LY2 cells between PD184352 and Sahaquine [1:1.5 ratio] or PD184352 and ACY1215 [1:0.375 ratio] at different inhibitory levels (IC<sub>50</sub> to IC<sub>95</sub>) showed decreasing CI values from (1.16 to 0.71) and (1.30 to 0.78), respectively (Table 1). Lower CI values were obtained in the first combination (PD184352 and Sahaquine) in comparison to the second combination (PD184352 and ACY1215) at all effect levels. Similar trends were observed in the RAMOS cell line with higher CI values at IC<sub>95</sub> in certain combinations, namely PD184352 and Sahaquine (0.74) and PD184352 and ACY1215 (0.98) (Table 1). In contrast, CI values for both combinations in the BCWM.1 cell line showed predominantly antagonistic interactions at all inhibitory levels, with CI values higher than 1.44 (Table 1).

**Fig.2**

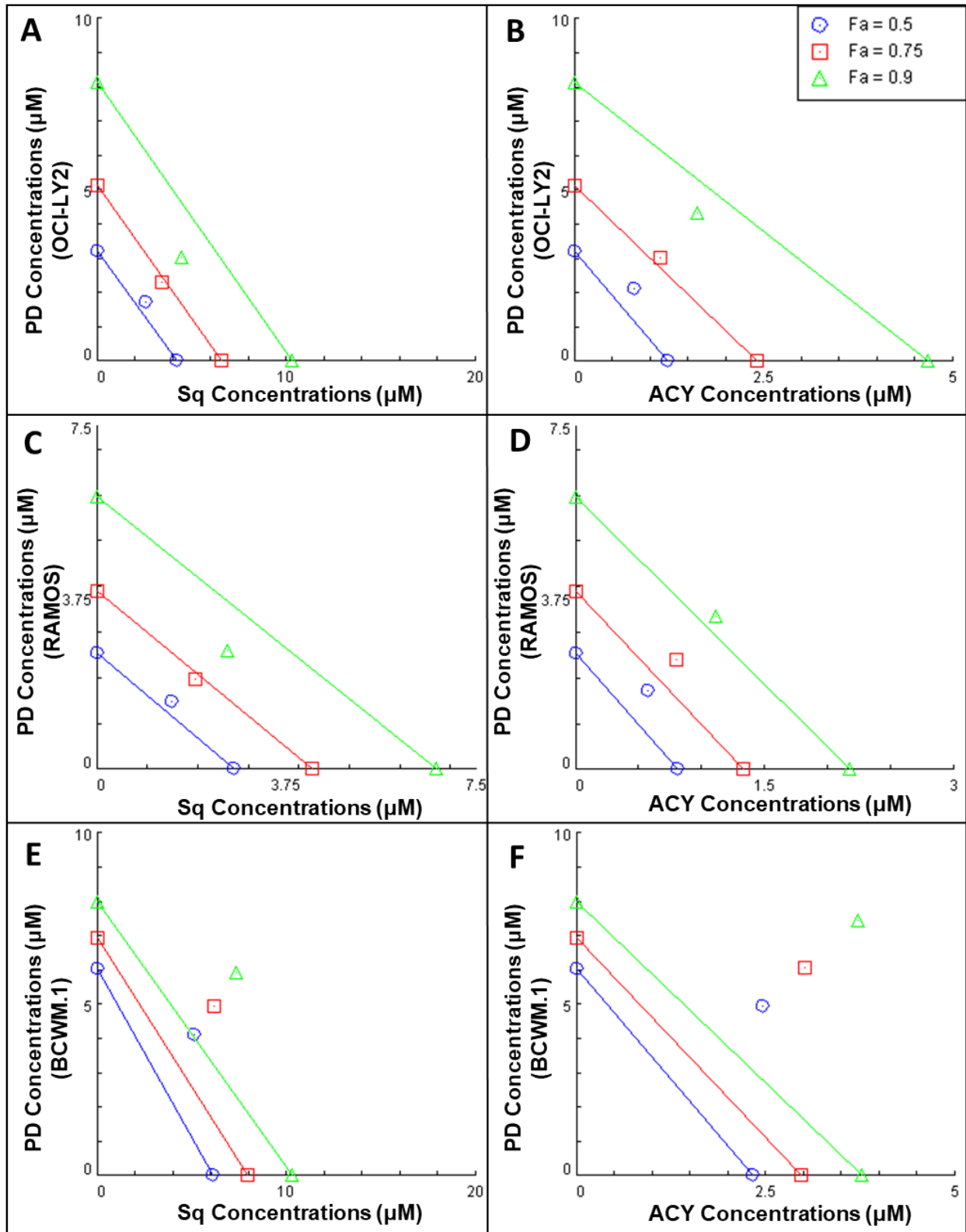


**Fig. 2 Isobolograms for the combination of MKK1/2-HDAC6 inhibitors in B-cell lymphoma human cell lines.**

The isobolograms illustrate the interactivity classifications for drug combinations of PD184352 and Sahaquine (A,C,E) or PD184352 and ACY1215 (B,D,F) at the ED50, ED75, and ED90 effect levels with a fixed combination ratio (within the same experiment) in OCI-LY2 (A,B); RAMOS (C,D); and BCWM.1 (E,F) cell lines. X and Y axes represent inhibitor concentrations ( $\mu\text{M}$ ). If the iso-effect point (the point producing the same efficacy in combination, as in a single treatment) is located above, below, or on (very close to) the additive line, then the interaction is antagonistic, synergistic, or additive, respectively. Isobolograms were generated using CompuSyn (V 1.0) software.

Cell line	Combo	CI values at:			
		IC50	IC75	IC90	IC95
OCI-LY2	Sq+PD [1.5:1]	1.16	0.97	0.81	0.71
	ACY+PD [0.375:1]	1.30	1.07	0.88	0.78
RAMOS	Sq+PD [1:1]	1.13	0.96	0.82	0.74
	ACY+PD [0.33:1]	1.38	1.22	1.07	0.98
BCWM.1	Sq+PD [1.25:1]	1.53	1.49	1.45	1.44
	ACY+PD [0.5:1]	1.88	1.90	1.92	1.94

**Table 1 Combination Index (CI) values at different effect levels showed additivity in OCI-LY2 and RAMOS cells, but antagonism in BCWM.1 cells.**

CI values were scrutinized after 72 hours of exposure to PD184352 and Sahaquine or PD184352 and ACY1215 with a constant combination ratio. CompuSyn (V 1.0) software was used to calculate CI values at different effect levels.

**3.4.3 Dual therapies increased the percentage of cells at the sub-G1/G1 phase while decreasing the percentage at the S and G2 phases in the OCI-LY2 cell line.**

To determine the effect of single therapies and both combinations (PD184352 and Sahaquine or PD184352 and ACY1215) on cell cycle phase distribution in the OCI-LY2 cell line, the DNA content of PI-stained cells was evaluated.

The cell cycle profile after exposure to PD184352 (4  $\mu$ M) for 24 hours exhibited a decrease in the proportion of cells in the sub-G1/G1 phase (Figure 3a) with a concomitant increase in S phase cells (Figure 3b). However, these responses were attenuated over time, in comparison to control cells treated with DMSO 0.2%.

In the presence of Sahaquine (5  $\mu$ M) or ACY1215 (1.5  $\mu$ M), gradual accumulation of cells at sub-G1/G1 (Figure 3a) was observed over time, compared to control cells. No sub-G1 peak was detected in the case of Sahaquine (Figure S3a) or ACY1215 (Figure S3b) single treatment.

Both combinations showed an increase in the fraction of sub-G1/G1 phase cells (Figure 3a) and a decrease in the number of cells in S (Figure 3b) and G2 (Figure 3c) phases, compared to single therapies, with clear sub-G1 peaks in PD184352 and Sahaquine (Figure S3c) and PD184352 and ACY1215 (Figure S3d) groups. The effects of

PD184352 (4  $\mu$ M) and Sahaquine (5  $\mu$ M) dual treatment were more pronounced than the PD184352 (4  $\mu$ M) and ACY1215 (1.5  $\mu$ M) combination in all cell phases.

**Fig.3**

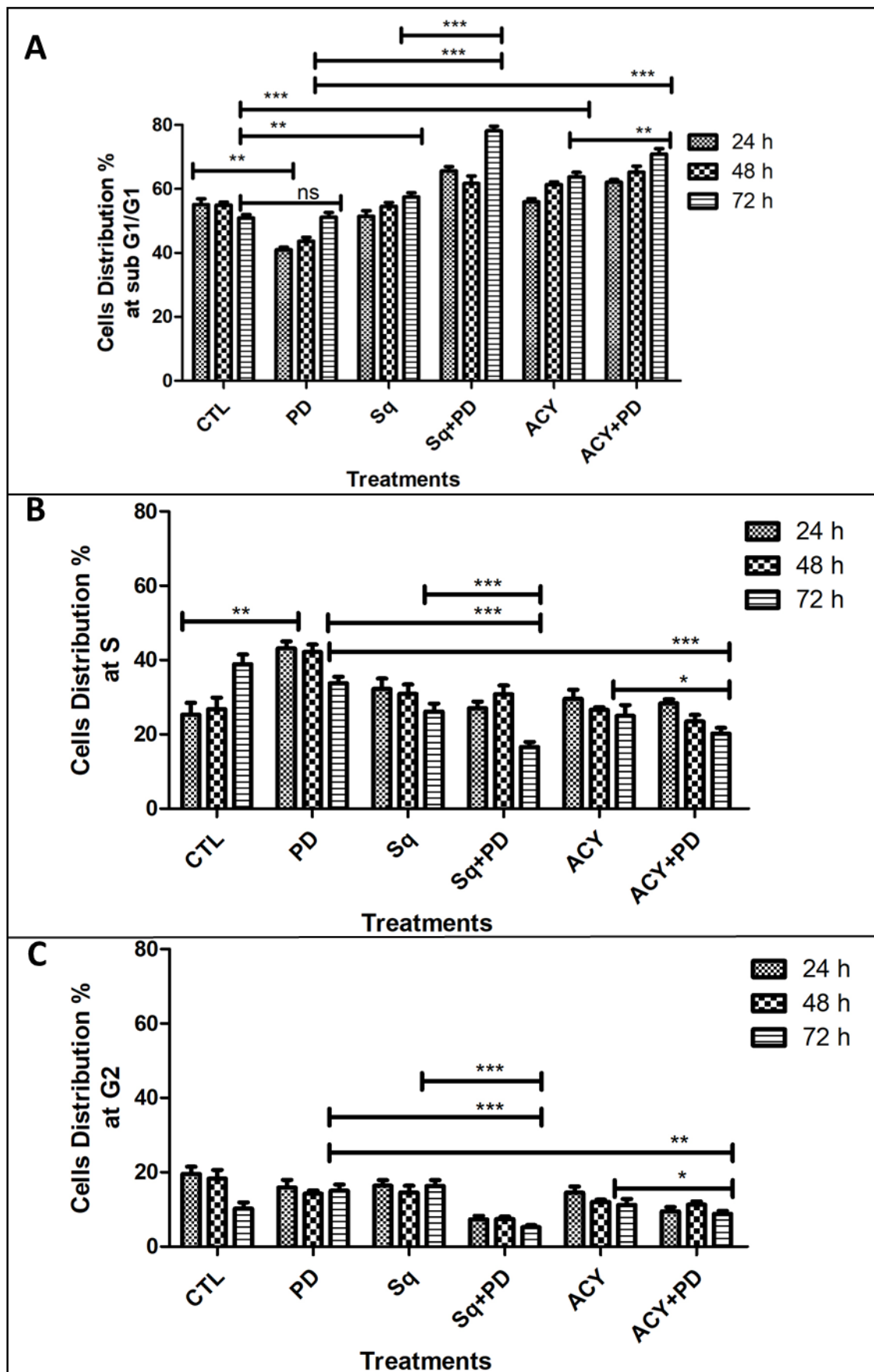


**Fig. 3 Dual therapies increased the percentage of cells at sub G1/G1 and decreased the percentage at S and G2 phases compared to single therapies.**

Cell cycle distribution was scrutinized at 3 different time points (24, 48, 72 hours) in OCI-LY2 cells, for PD184352 (PD; 4  $\mu$ M); Sahaquine (Sq; 5  $\mu$ M); and ACY1215 (ACY; 1.5  $\mu$ M) treatments alone or in combination at IC50 concentrations. DNA content was labeled with propidium iodide solution and cells were subjected to FACS analysis. Three phases were identified: (A) sub G1/G1 phase; (B) S phase; and (C) G2 phase. Data were analyzed using FlowJo's automated Dean-Jett-Fox algorithm. The percentage of cells in each phase is presented as the mean value (SD) from at least three independent experiments (n=6, unpaired two-tailed student t-test, \*\*\* p < 0.001, \*\* p < 0.01, \* p < 0.05).

**3.4.4 Combined therapies exert cytotoxic effects, whereas monotherapies show cytostatic effects.**

Based on previous results, we further investigated the cytotoxic effects of both combinations (PD184352 with either Sahaquine or ACY1215) at their IC50 values, compared to single therapies in the OCI-LY2 cell line. To assess whether the cytotoxic effects of both combinations were mediated by the induction of apoptosis or necrosis, Annexin V/ PI binding assay was performed.

Flow cytometry analysis showed that the single therapy groups had mainly cytostatic effects after 72 hours of treatment, with 89%, 95%, and 93% viable cells in PD184352, Sahaquine, and ACY1215 groups, respectively (Figure 4a), compared to the control

group (95% viability). However, both combinations produced cytotoxic effects, with 44% and 79% viable cells in PD184352 with Sahaquine, and PD184352 with ACY1215 groups, respectively (Figure 4a).

The PD184352 and Sahaquine combination showed the continuous presence of early apoptotic cells making up 12%, 18%, and 11% of the population at 24, 48, and 72 hours, respectively (Figure S4a,c,e), with a concomitant increase in the percentage of late apoptotic and necrotic cells over treatment time from 12% to 46% (Figure S4a,c,e). This was not the case in the PD184352 and ACY1215 combination (Figure S4b,d,f).

To confirm these results, apoptotic cells were visualized by DNA fragmentation assay using Hoechst 33342 nuclear staining. After 24 hours of treatment, confocal imaging showed that fragmented DNA and apoptotic bodies were mainly detected in the PD184352 and Sahaquine group (Figure 4b), and not in the single therapies or PD184352 and ACY1215 groups (Figure 4b).

**Fig.4**

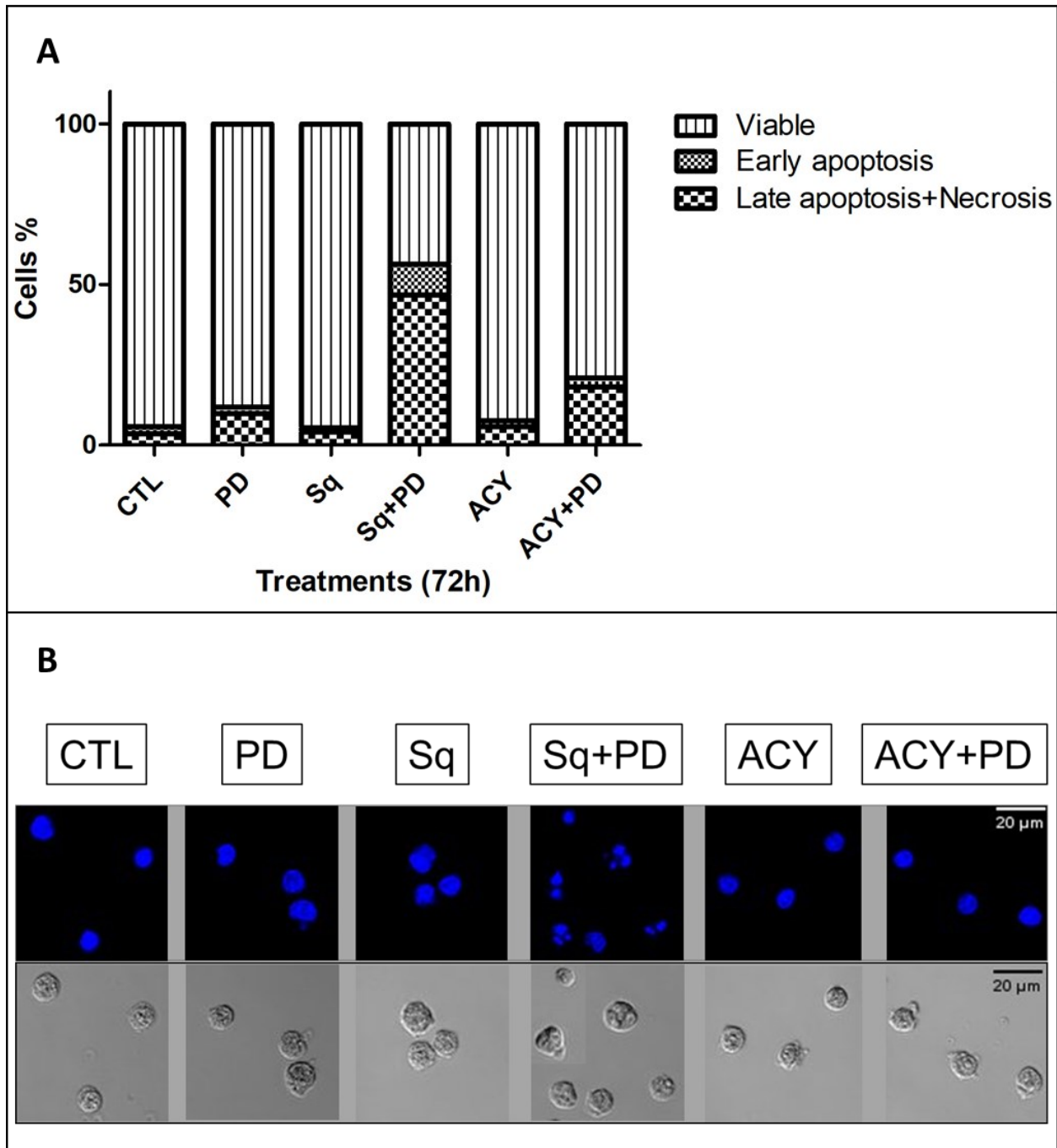


**Fig. 4 Monotherapies had cytostatic effects while combined therapies showed cytotoxic effects with apoptosis induction in PD184352 with the Sahaquine group only.**

(A) Quantification of annexin V and propidium iodide staining, showing the percentage of OCI-LY2 cells in different quadrants, analyzed using FlowJo software. Shown is the mean value from three experiments (n=6). (B) Representative micrographs of OCI-LY2 cells' nuclei that were labeled with Hoechst 33342 staining after 24 hours of treatment. Cells were imaged using a confocal microscope and stained DNA was visualized using ImageJ. Cells in (A) and (B) were treated with IC50 concentrations of PD184352 (PD 4  $\mu$ M), Sahaquine (Sq; 5  $\mu$ M), and ACY1215 (ACY; 1.5  $\mu$ M) inhibitors alone or in combination.

### **3.4.5 Single and dual therapies affect ERK phosphorylation and ( $\alpha$ -tubulin/H3K14) acetylation.**

To explore the inhibitory activity of the single treatments and both combinations on MKK1/2, HDAC6, and global histone 3 (H3) deacetylation, we assessed ERK phosphorylation,  $\alpha$ -tubulin, and H3K14 acetylation, respectively, using flow cytometric immunofluorescence analysis.

OCI-LY2 cells were stimulated with phorbol 12-myristate 13-acetate (PMA, 100 nM) for 30 minutes after a 2-hour treatment with PD184352 (4  $\mu$ M), Sahaquine (5  $\mu$ M), ACY1215 (1.5  $\mu$ M), and their combinations. PMA-induced phosphorylation of ERK was completely blocked in PD184352 alone and PD184352 combined with either Sahaquine

or ACY1215 groups (Figure 5a). Also, phosphorylated ERK levels were decreased in Sahaquine and ACY1215 groups by 15% and 23%, respectively (Figure 5a), compared to the PMA group.

The acetylation of  $\alpha$ -tubulin was not affected after 24-hour exposure to PD184352 (4  $\mu$ M) treatment (Figure 5b), whereas treatments with Sahaquine (5  $\mu$ M) or ACY1215 (1.5  $\mu$ M) significantly increased  $\alpha$ -tubulin acetylation by 5- and 48-fold, respectively (Figure 5b), compared to the control. However, the increase in  $\alpha$ -tubulin acetylation after Sahaquine or ACY1215 treatments was not changed after the addition of PD184352 to Sahaquine or ACY1215 treatments (Figure 5b).

The level of acetylated H3K14 was not affected by PD184352 (4  $\mu$ M) treatment (Figure 5c). The acetylation was increased after Sahaquine (5  $\mu$ M) and ACY1215 (1.5  $\mu$ M) exposure by 3.2-fold and 3.5-fold, respectively (Figure 5c), compared to the control following 24-hour treatment. Notably, the addition of PD184352 to Sahaquine or ACY1215 groups resulted in a further increase in H3K14 acetylation levels to reach a 4-fold increase in comparison to the control (Figure 5c).

Fig.5

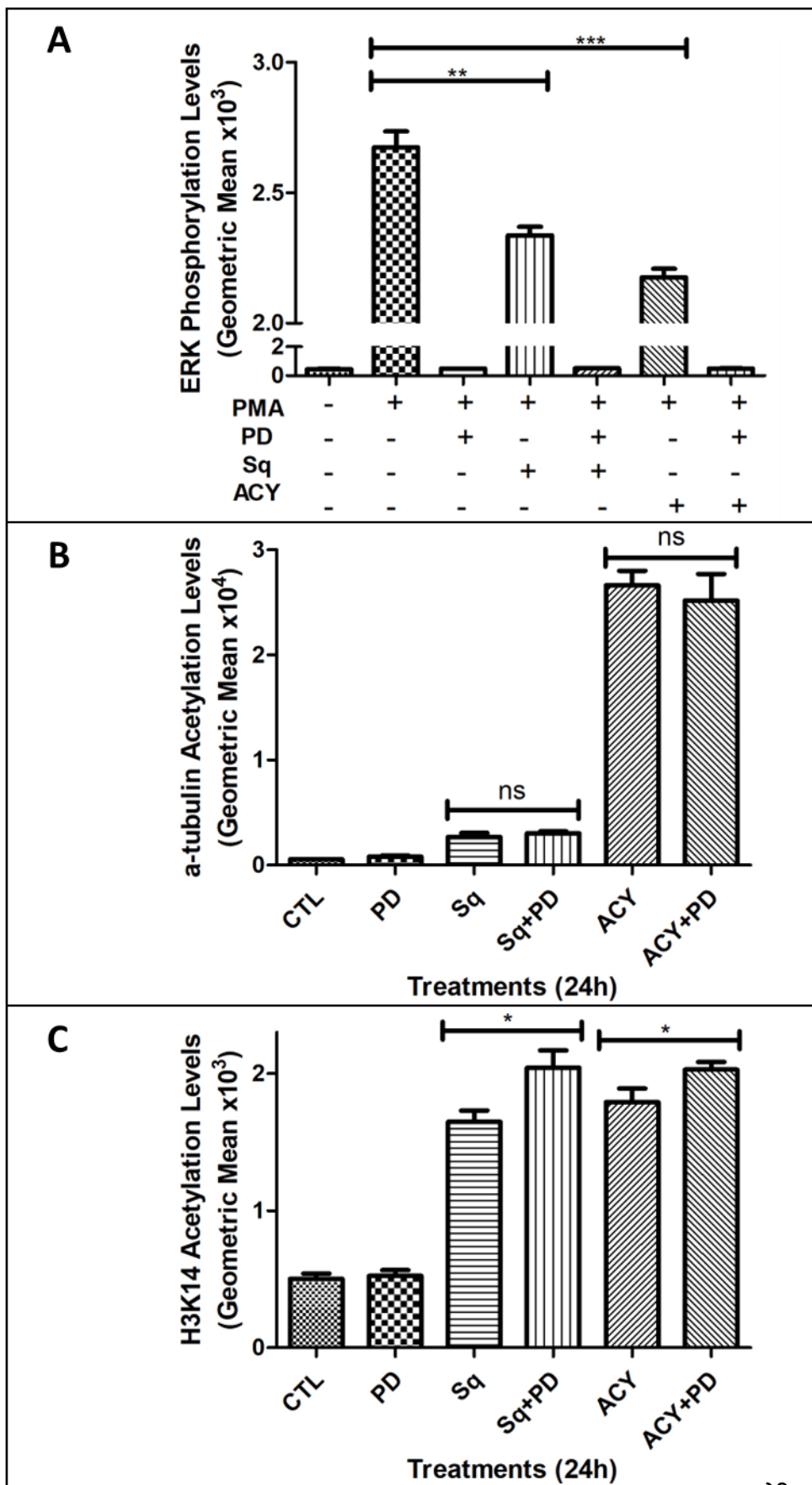


**Fig. 5 Effects of single and dual therapies on ERK phosphorylation and ( $\alpha$ -tubulin/H3K14) acetylation.**

(A) Levels of phosphorylated ERK after phorbol 12-myristate 13-acetate (PMA, 100 nM, 30 min) stimulation in samples treated for 2 hours. Acetylation of (B)  $\alpha$ -tubulin and (C) H3K14 following 24-hour exposure. OCI-LY2 cells were treated with PD184352 (PD; 4  $\mu$ M), Sahaquine (Sq; 5  $\mu$ M), ACY1215 (ACY; 1.5  $\mu$ M), and their combination, then subjected to FACS analysis. Data was analyzed using FlowJo software. Shown is the mean value (SD) of three experiments (n=6, unpaired two-tailed student t-test, \*\*\* p < 0.001, \*\* p < 0.01, \* p < 0.05).

**3.4.6 Proteomic analyses after treatment with PD184352 and Sahaquine alone or in combination.**

To identify the molecular targets associated with the effectiveness of PD184352 and Sahaquine combination, proteomic analysis with acetylation enrichment was performed using acetylation immunoaffinity purification beads.

LC-MS/MS-based proteomic analysis was carried out after 24-hour treatment with either PD184352 (4  $\mu$ M) or Sahaquine (5  $\mu$ M), in addition to the combination of PD184352 with Sahaquine, in OCI-LY2 cell line. In the whole lysate, 1804 proteins were identified (Table S1), whereas, 229 proteins were identified in the enriched lysate (Table S2).

To analyze the enriched proteomes, top hits were defined as the proteins that were mainly found acetylated in the combination group, with very low to absent acetylation levels in single treatment groups (0-1%), compared to the combination group, and completely absent (not acetylated) in the control group (0.2% DMSO).

Based on these criteria, eight proteins were identified and manually examined for MS/MS spectral quality, with careful examination of the relative quantities using the MS1 parent ion integration from Pinnacle, confirming the lack of trypsin cleavage of the acetylated lysine site after trypsin digestion. Four proteins were excluded after manual examination. The top four proteins included (from top to bottom) Actin-related protein 2/3 complex subunit 2 (ARPC2); Delta(3,5)-Delta(2,4)-dienoyl-CoA isomerase mitochondrial (ECH1); Cathepsin D (CATD/CTSD; and Strawberry notch homolog 1 (SBNO1) (Table 2). The abundance of these proteins (whole lysate) did not vary significantly between the single and dual treatment groups (Table 2).

Protein Hits & Roles	Top Hits	ARPC2	ECH1	CATD	SBNO1
	Roles	Repair DNA damage/ cell motility	Fatty acid $\beta$ -oxidation	Aspartic protease	Helicase-like protein
Enriched Lysate	CTL	0	0	0	0
	PD	$5 \times 10^3$	0	$2 \times 10^5$	0
	PD+Sq	$2 \times 10^8$	$3 \times 10^7$	$3 \times 10^7$	$3 \times 10^6$
	Sq	$8 \times 10^5$	0	0	$2 \times 10^4$
Whole Lysate	CTL	33	28	0	0
	PD	32	30	0	0
	PD+Sq	35	28	2	0
	Sq	35	25	2	0

**Table 2 Top hit proteins that were mainly acetylated in PD184352 and Sahaquine combination group but not in the single treatment or control groups.**

OCI-LY2 cells were treated for 24 hours with PD184352 (4  $\mu$ M) and Sahaquine (5  $\mu$ M), alone or in combination, then lysed for proteomic analysis. For the whole lysate experiment, data were loaded onto Scaffold and expressed as normalized total spectra. For the acetylation enrichment experiment, data were loaded first onto Scaffold then Pinnacle to compare MS1 peptide peak areas (integrated MS counts across the LC peaks for each peptide) for relative comparisons.

### **3.5 Discussion**

In this study, we demonstrated that the MKK1/2 inhibitor (PD184352) and HDAC6 inhibitors (Sahaquine and ACY1215) alone reduced cell growth of B cell lymphoma cell lines, specifically OCI-LY2, RAMOS, and BCWM.1 cells. The combination of MKK1/2 and HDAC6 inhibitors produced additivity in OCI-LY2 and RAMOS, but antagonism in BCWM.1. Monotherapies induced cytostatic effects by interfering with cell cycle progression in OCI-LY2. However, dual therapies showed cytocidal effects. The combination of PD184352 and Sahaquine induced apoptosis and showed superior effects compared to PD184352 and ACY1215 combination.

Additivity was most apparent in the OCI-LY2 DLBCL cell line after treatments with PD184352 (MKK1/2 inhibitor) and either Sahaquine (in-house HDAC6 inhibitor) or ACY1215 (commercial HDAC6 inhibitor). Similarly, additivity was observed in another

tested B-cell lymphoma cell line (RAMOS). The patterns of CI values at different effect levels were similar to that observed previously in the OCI-LY2 cell line. However, the values of CI were lower in OCI-LY2, indicating that the interaction in the OCI-LY2 cell line is more favorable than in the RAMOS cell line. Conversely, antagonistic effects emerged in the BCWM.1 cell line after dual treatments.

These findings can be explained in part by the presence of mutated MYD88 [L265P] in BCWM.1 cells, resulting in upregulated NF- $\kappa$ B activity [67] leading to antagonism, as signaling downstream of MYD88 activates both ERK1/2 and NF- $\kappa$ B pathways [9], whereas OCI-LY2 and RAMOS [68] cell lines have wild-type MYD88. Moreover, the RAMOS cell line harbors mutations in c-MYC [69], leading to c-MYC overexpression [70], while the OCI-LY2 cell line has wild-type c-MYC [71]. This could partially explain a higher sensitivity to the combinations in the OCI-LY2 cell line. Thus, we focused only on this cell line in further experiments. The OCI-LY2 cell line carries mutant p53 [71] which is a negative prognostic factor for DLBCL patients [72-76]. Therefore, dual MKK1/2 and HDAC6 inhibition can be considered as a potential alternative strategy to treat DLBCL with p53 aberrations, but not those with high NF- $\kappa$ B activity. Future studies will have to assess these combinations in DLBCL primary cells harboring mutant p53 with normal NF- $\kappa$ B activity.

Single treatments induced growth inhibition rather than killing effects in B-cell lymphoma cell lines. The inhibition of MKK1/2 by PD184352 in the OCI-LY2 cell line mainly disrupted the cell cycle. However, cells can compensate for MKK-ERK pathway inhibition through regulatory loops and compensatory signaling to assure cellular

balance and stability [77, 78], thus leading to cell cycle perturbation attenuation over time.

Treatment with both of the HDAC6 inhibitors resulted in cell cycle arrest with similar response patterns. At the same effect level (IC50), Sahaquine produced mild HDAC6 inhibition, in comparison to ACY1215 which induced very strong HDAC6 inhibition, measured by  $\alpha$ -tubulin acetylation. However, at IC50, the inhibitory effects were not limited to HDAC6 activity. Both Sahaquine and ACY1215 also inhibited ERK1/2 enzymatic activity and triggered H3 hyperacetylation to the same extent.

A previous study showed that Sahaquine can inhibit ERK1/2 activity in U251N human glioblastoma cells [64]. In this study, we obtained similar results in the OCI-LY2 lymphoma cell line and showed that the levels of phosphorylated ERK1/2 were reduced after Sahaquine, as well as after ACY1215 treatment. Since HDAC6 can directly deacetylate ERK1 (K72), thereby promoting its activity, HDAC6 inhibition leads to an increase in ERK1 acetylation and a reduction of its activity [48]. However, that reduction in activity does not lead to the same impact on cultured cells as dual-therapy, suggesting that this decreased activity is not sufficient to achieve cytotoxic effect and that the targeted ERK1/2 inhibitor is still required.

The effects of Sahaquine and ACY1215 single treatments on H3 acetylation (H3K14) can be explained by the cross-inhibition of class I HDACs due to similarities in catalytic sites, as class I and class IIb HDACs possess catalytic tyrosine residue in the HDAC binding pocket [79].

Combining MKK1/2 and HDAC6 inhibitors induced cell death, as shown in B-cell lymphomas in vitro studies. Enhanced cytotoxic effects were achieved by combining PD184352 with Sahaquine compared to the combination with ACY1215 based on cell cycle and apoptosis/necrosis studies. This data reflects the combination index values obtained. The lower CI values in the first combination refer to greater interaction between PD184352 and Sahaquine than PD184352 and ACY1215. This interaction led to apoptosis induction in the PD184352 with Sahaquine group. However, in the second group (PD184352 with ACY1215) apoptosis was halted. These findings can be explained by the fact that Sahaquine produced a milder increase in acetylated  $\alpha$ -tubulin levels, whereas ACY1215 treatment resulted in dramatically increased levels of  $\alpha$ -tubulin acetylation. A recent study linked the acetylation levels of  $\alpha$ -tubulin with the apoptotic process, suggesting the presence of threshold acetylation value that can trigger or attenuate apoptosis [80].

Another study showed that high levels of  $\alpha$ -tubulin acetylation can stabilize antiapoptotic protein (Mcl-1) and therefore inhibit apoptosis [81]. We obtained consistent results and showed that high acetylation levels of  $\alpha$ -tubulin in Sahaquine or ACY1215 single treatment groups masked apoptotic cell death. Nevertheless, the additive effects resulting from combining PD184352 with Sahaquine abolished this effect and induced apoptosis. However, due to extremely high  $\alpha$ -tubulin acetylation levels in the PD184352 with ACY1215 group, this combination failed to produce apoptosis, but still induced apoptotic-independent cell death.

The combination effects on phosphorylated ERK1/2 and acetylated  $\alpha$ -tubulin were comparable to that of single treatments. However, both combinations resulted in higher levels of H3 acetylation compared to Sahaquine or ACY1215 alone. The presence of enhanced H3 hyperacetylation can be explained as a cellular attempt to facilitate DNA-repairing mechanisms [82, 83], after the DNA damage caused by dual therapies related to cell death.

Proteomic analysis confirmed these findings and showed that the acetylation of ARPC2 protein (K275, K295) [84] was mainly enhanced in the PD184352 with Sahaquine combination. ARPC2 belongs to the ARP2/3 protein complex that mediates actin polymerization in the cytoplasm and nucleus; therefore, it plays certain roles in cell motility [85] and DNA double-strand break repair via a homology-directed repair mechanism [86], respectively. Previous studies showed that the ARP2/3 complex can be affected by ERK [87] and HDAC6 activities [88]. Moreover, the ARP2/3 complex amplifies BCR signaling and maximizes B cell activation [89].

ECH1 protein (K327) [84], another important hit, is a target of SIRT3 protein that is the main mitochondrial deacetylase [90]. This finding suggests the possibility of crosstalk between HDAC6 (cytoplasmic) and SIRT3 (mitochondrial) deacetylases. A previous study found positive correlation between the expression of HDAC6 and SIRT3 in a subgroup of primary brain tumors [91].

Another hit was SBNO1 protein (K149, K413, K1222) [84], which was previously identified as a target of Myc-associated protein with JmjC domain (MAPJD) that is commonly activated in lung cancer [92]. A SBNO1 reported acetylation site was

detected in the enriched samples; however, ARPC2 and ECH1 acetylation site were digested in these samples.

CATD that is highly expressed in NHL [93] was among the top four hits. In contrast to the other hits, CATD has no reported acetylation sites and therefore was probably conjugated to other acetylated proteins. Previous studies showed CATD playing a role in ERK1/2 and p38 MAPK phosphorylation [94, 95]; therefore, ERK1/2 inhibition may well affect CATD activity. Further targeted validation of Sahaquine and PD184352 combination effects on the identified top four hits is needed.

Taken together, these results suggest that the combination of MKK1/2 and HDAC6 inhibitors in vitro presents a predominant strategy to induce death in B-cell lymphoma cell lines. High NF- $\kappa$ B activity created resistance, whereas c-MYC overexpression reduced sensitivity to MKK1/2 and HDAC6 dual inhibition. In combination with PD184352, Sahaquine showed superior effects via promoting apoptosis, when compared to the ACY1215 combination. Excessive  $\alpha$ -tubulin acetylation has adverse effects in the PD184352 with ACY1215 combination leading to apoptosis inhibition in B-cell lymphomas. Future animal studies are required to assess the safety and anti-lymphoma activity of dual MKK1/2 and HDAC6 inhibition in vivo.

#### Conflict of interest

The authors declare no conflict of interest.

#### Data availability

All data generated or analyzed during this study are included in this article and in supplementary electronic information files.

### 3.6 References

1. Abramson JS, Shipp MA. Advances in the biology and therapy of diffuse large B-cell lymphoma: moving towards a molecularly targeted approach. *Blood*. 2005;106(4):1164-74.
2. Zhang J, Grubor V, Love CL, Banerjee A, Richards KL, Mieczkowski PA, et al. Genetic heterogeneity of diffuse large B-cell lymphoma. 2013;110(4):1398-403.
3. Miao Y, Medeiros LJ, Xu-Monette ZY, Li J, Young KH. Dysregulation of Cell Survival in Diffuse Large B Cell Lymphoma: Mechanisms and Therapeutic Targets. 2019;9.
4. Friedberg JW. Relapsed/Refractory Diffuse Large B-Cell Lymphoma. *Hematology*. 2011;2011(1):498-505.
5. Gisselbrecht C, Glass B, Mounier N, Gill DS, Linch DC, Trneny M, et al. Salvage Regimens With Autologous Transplantation for Relapsed Large B-Cell Lymphoma in the Rituximab Era. 2010;28(27):4184-90.
6. Van Den Neste E, Schmitz N, Mounier N, Gill D, Linch D, Trneny M, et al. Outcome of patients with relapsed diffuse large B-cell lymphoma who fail second-line salvage regimens in the International CORAL study. *Bone Marrow Transplantation*. 2016;51(1):51-7.

7. Pasqualucci L, Trifonov V, Fabbri G, Ma J, Rossi D, Chiarenza A, et al. Analysis of the coding genome of diffuse large B-cell lymphoma. *Nature Genetics*. 2011;43(9):830-7.
8. Vendramini E, Bomben R, Pozzo F, Bittolo T, Tissino E, Gattei V, et al. KRAS and RAS-MAPK Pathway Deregulation in Mature B Cell Lymphoproliferative Disorders. *Cancers*. 2022;14(3).
9. Rousseau S, Martel G. Gain-of-Function Mutations in the Toll-Like Receptor Pathway: TPL2-Mediated ERK1/ERK2 MAPK Activation, a Path to Tumorigenesis in Lymphoid Neoplasms? 2016;4.
10. Dai B, Zhao XF, Mazan-Mamczarz K, Hagner P, Corl S, Bahassi el M, et al. Functional and molecular interactions between ERK and CHK2 in diffuse large B-cell lymphoma. *Nature communications*. 2011;2:402.
11. Shaffer AL, 3rd, Young RM, Staudt LM. Pathogenesis of human B cell lymphomas. *Annual review of immunology*. 2012;30:565-610.
12. Morin RD, Mendez-Lago M, Mungall AJ, Goya R, Mungall KL, Corbett RD, et al. Frequent mutation of histone-modifying genes in non-Hodgkin lymphoma. *Nature*. 2011;476(7360):298-303.
13. Jiang Y, Melnick A. The epigenetic basis of diffuse large B-cell lymphoma. *Seminars in hematology*. 2015;52(2):86-96.
14. Kawai T, Akira S. TLR signaling. *Cell Death & Differentiation*. 2006;13(5):816-25.

15. Seda V, Mraz M. B-cell receptor signaling and its crosstalk with other pathways in normal and malignant cells. 2015;94(3):193-205.
16. Woyach JA, Johnson AJ, Byrd JC. The B-cell receptor signaling pathway as a therapeutic target in CLL. *Blood*. 2012;120(6):1175-84.
17. McKay MM, Morrison DK. Integrating signals from RTKs to ERK/MAPK. *Oncogene*. 2007;26(22):3113-21.
18. Du Z, Lovly CM. Mechanisms of receptor tyrosine kinase activation in cancer. *Molecular Cancer*. 2018;17(1):58.
19. Yoon S, Seger R. The extracellular signal-regulated kinase: Multiple substrates regulate diverse cellular functions. *Growth Factors*. 2006;24(1):21-44.
20. Yasuda T, Sanjo H, Pagès G, Kawano Y, Karasuyama H, Pouyssegur J, et al. Erk Kinases Link Pre-B Cell Receptor Signaling to Transcriptional Events Required for Early B Cell Expansion. *Immunity*. 2008;28(4):499-508.
21. Gramling MW, Eischen CM. Suppression of Ras/Mapk pathway signaling inhibits Myc-induced lymphomagenesis. *Cell Death & Differentiation*. 2012;19(7):1220-7.
22. Kerkhoff E, Houben R, Löffler S, Troppmair J, Lee J-E, Rapp UR. Regulation of c-myc expression by Ras/Raf signaling. *Oncogene*. 1998;16(2):211-6.
23. Zhang W, Liu HT. MAPK signal pathways in the regulation of cell proliferation in mammalian cells. *Cell Research*. 2002;12(1):9-18.
24. Roberts PJ, Der CJ. Targeting the Raf-MEK-ERK mitogen-activated protein kinase cascade for the treatment of cancer. *Oncogene*. 2007;26(22):3291-310.

25. Roskoski R. Targeting ERK1/2 protein-serine/threonine kinases in human cancers. *Pharmacological Research*. 2019;142:151-68.
26. Cheng Y, Tian H. Current Development Status of MEK Inhibitors. *Molecules*. 2017;22(10).
27. Frémin C, Meloche S. From basic research to clinical development of MEK1/2 inhibitors for cancer therapy. *Journal of Hematology & Oncology*. 2010;3(1):8.
28. Chin HM, Lai DK, Falchook GS. Extracellular Signal-Regulated Kinase (ERK) Inhibitors in Oncology Clinical Trials. *Journal of Immunotherapy and Precision Oncology*. 2020;2(1):10-6.
29. García-Gómez R, Bustelo XR, Crespo P. Protein–Protein Interactions: Emerging Oncotargets in the RAS-ERK Pathway. *Trends in Cancer*. 2018;4(9):616-33.
30. Han J, Liu Y, Yang S, Wu X, Li H, Wang Q. MEK inhibitors for the treatment of non-small cell lung cancer. *J Hematol Oncol*. 2021;14(1):1.
31. Yu C, Dasmahapatra G, Dent P, Grant S. Synergistic interactions between MEK1/2 and histone deacetylase inhibitors in BCR/ABL+ human leukemia cells. *Leukemia*. 2005;19(9):1579-89.
32. Nishioka C, Ikezoe T, Yang J, Koeffler HP, Yokoyama A. Inhibition of MEK/ERK signaling synergistically potentiates histone deacetylase inhibitor-induced growth arrest, apoptosis and acetylation of histone H3 on p21waf1 promoter in acute myelogenous leukemia cell. *Leukemia*. 2008;22(7):1449-52.

33. Ozaki K-i, Minoda A, Kishikawa F, Kohno M. Blockade of the ERK pathway markedly sensitizes tumor cells to HDAC inhibitor-induced cell death. *Biochemical and Biophysical Research Communications*. 2006;339(4):1171-7.
34. Chao M-W, Chang L-H, Tu H-J, Chang C-D, Lai M-J, Chen Y-Y, et al. Combination treatment strategy for pancreatic cancer involving the novel HDAC inhibitor MPT0E028 with a MEK inhibitor beyond K-Ras status. *Clinical Epigenetics*. 2019;11(1):85.
35. Ramakrishnan VG, Miller KC, Macon EP, Kimlinger TK, Haug J, Kumar S, et al. Histone deacetylase inhibition in combination with MEK or BCL-2 inhibition in multiple myeloma. *Haematologica*. 2019;104(10):2061-74.
36. Liu S, Zou Q, Chen J-P, Yao X, Guan P, Liang W, et al. Targeting enhancer reprogramming to mitigate MEK inhibitor resistance in preclinical models of advanced ovarian cancer. *The Journal of Clinical Investigation*. 2021;131(20).
37. da Cunha Jaeger M, Ghisleni EC, Cardoso PS, Siniglaglia M, Falcon T, Brunetto AT, et al. HDAC and MAPK/ERK Inhibitors Cooperate To Reduce Viability and Stemness in Medulloblastoma. *Journal of Molecular Neuroscience*. 2020;70(6):981-92.
38. Essien EI, Hofer TP, Atkinson MJ, Anastasov N. Combining HDAC and MEK Inhibitors with Radiation against Glioblastoma-Derived Spheres. *Cells*. 2022;11(5).
39. Cosenza M, Pozzi S. The Therapeutic Strategy of HDAC6 Inhibitors in Lymphoproliferative Disease. *Int J Mol Sci*. 2018;19(8).

40. Stimson L, Wood V, Khan O, Fotheringham S, La Thangue NB. HDAC inhibitor-based therapies and haematological malignancy. *Annals of Oncology*. 2009;20(8):1293-302.
41. Subramanian S, Bates SE, Wright JJ, Espinoza-Delgado I, Piekarz RL. Clinical Toxicities of Histone Deacetylase Inhibitors. 2010;3(9):2751-67.
42. Duvic M, Zhang C. Clinical and laboratory experience of vorinostat (suberoylanilide hydroxamic acid) in the treatment of cutaneous T-cell lymphoma. *British Journal of Cancer*. 2006;95(1):S13-S9.
43. Marquard L, Poulsen CB, Gjerdrum LM, De Nully Brown P, Christensen IJ, Jensen PB, et al. Histone deacetylase 1, 2, 6 and acetylated histone H4 in B- and T-cell lymphomas. 2009;54(6):688-98.
44. Gloghini A, Buglio D, Khaskhely NM, Georgakis G, Orłowski RZ, Neelapu SS, et al. Expression of histone deacetylases in lymphoma: implication for the development of selective inhibitors. 2009;147(4):515-25.
45. Hubbert C, Guardiola A, Shao R, Kawaguchi Y, Ito A, Nixon A, et al. HDAC6 is a microtubule-associated deacetylase. *Nature*. 2002;417(6887):455-8.
46. Bali P, Pranpat M, Bradner J, Balasis M, Fiskus W, Guo F, et al. Inhibition of Histone Deacetylase 6 Acetylates and Disrupts the Chaperone Function of Heat Shock Protein 90: A NOVEL BASIS FOR ANTILEUKEMIA ACTIVITY OF HISTONE DEACETYLASE INHIBITORS\*. *Journal of Biological Chemistry*. 2005;280(29):26729-34.

47. New M, Sheikh S, Bekheet M, Olzscha H, Thezenas M-L, Care MA, et al. TLR Adaptor Protein MYD88 Mediates Sensitivity to HDAC Inhibitors via a Cytokine-Dependent Mechanism. *Cancer Res.* 2016;76(23):6975-87.
48. Wu JY, Xiang S, Zhang M, Fang B, Huang H, Kwon OK, et al. Histone deacetylase 6 (HDAC6) deacetylates extracellular signal-regulated kinase 1 (ERK1) and thereby stimulates ERK1 activity. *The Journal of biological chemistry.* 2018;293(6):1976-93.
49. Parmigiani RB, Xu WS, Venta-Perez G, Erdjument-Bromage H, Yaneva M, Tempst P, et al. HDAC6 is a specific deacetylase of peroxiredoxins and is involved in redox regulation. 2008;105(28):9633-8.
50. Jia YJ, Liu ZB, Wang WG, Sun CB, Wei P, Yang YL, et al. HDAC6 regulates microRNA-27b that suppresses proliferation, promotes apoptosis and target MET in diffuse large B-cell lymphoma. *Leukemia.* 2018;32(3):703-11.
51. Yang CJ, Liu YP, Dai HY, Shiue YL, Tsai CJ, Huang MS, et al. Nuclear HDAC6 inhibits invasion by suppressing NF- $\kappa$ B/MMP2 and is inversely correlated with metastasis of non-small cell lung cancer. *Oncotarget.* 2015;6(30):30263-76.
52. Ryu H-W, Shin D-H, Lee DH, Choi J, Han G, Lee KY, et al. HDAC6 deacetylates p53 at lysines 381/382 and differentially coordinates p53-induced apoptosis. *Cancer Letters.* 2017;391:162-71.
53. Li Y, Zhang X, Polakiewicz RD, Yao TP, Comb MJ. HDAC6 is required for epidermal growth factor-induced beta-catenin nuclear localization. *The Journal of biological chemistry.* 2008;283(19):12686-90.

54. Zhang W, Kone BC. NF- $\kappa$ B inhibits transcription of the H<sup>+</sup>-K<sup>+</sup>-ATPase  $\alpha$ 2-subunit gene: role of histone deacetylases. 2002;283(5):F904-F11.
55. Barter MJ, Butcher A, Wang H, Tsompani D, Galler M, Rumsby EL, et al. HDAC6 regulates NF- $\kappa$ B signaling to control chondrocyte IL-1-induced MMP and inflammatory gene expression. Scientific Reports. 2022;12(1):6640.
56. Namdar M, Perez G, Ngo L, Marks PA. Selective inhibition of histone deacetylase 6 (HDAC6) induces DNA damage and sensitizes transformed cells to anticancer agents. 2010;107(46):20003-8.
57. Kawaguchi Y, Kovacs JJ, McLaurin A, Vance JM, Ito A, Yao T-P. The Deacetylase HDAC6 Regulates Aggresome Formation and Cell Viability in Response to Misfolded Protein Stress. Cell. 2003;115(6):727-38.
58. Boucherat O, Chabot S, Paulin R, Trinh I, Bourgeois A, Potus F, et al. HDAC6: A Novel Histone Deacetylase Implicated in Pulmonary Arterial Hypertension. Scientific Reports. 2017;7(1):4546.
59. Subramanian C, Jarzembowski JA, Opirari AW, Castle VP, Kwok RPS. HDAC6 Deacetylates Ku70 and Regulates Ku70-Bax Binding in Neuroblastoma. Neoplasia. 2011;13(8):726-34.
60. Chaudhary N, Nakka KK, Chavali PL, Bhat J, Chatterjee S, Chattopadhyay S. SMAR1 coordinates HDAC6-induced deacetylation of Ku70 and dictates cell fate upon irradiation. Cell Death & Disease. 2014;5(10):e1447-e.

61. Amengual JE, Lue JK, Ma H, Lichtenstein R, Shah B, Cremers S, et al. First-in-Class Selective HDAC6 Inhibitor (ACY-1215) Has a Highly Favorable Safety Profile in Patients with Relapsed and Refractory Lymphoma. 2021;26(3):184-e366.
62. Vogl DT, Raje N, Jagannath S, Richardson P, Hari P, Orlowski R, et al. Ricolinostat, the First Selective Histone Deacetylase 6 Inhibitor, in Combination with Bortezomib and Dexamethasone for Relapsed or Refractory Multiple Myeloma. *Clinical cancer research : an official journal of the American Association for Cancer Research*. 2017;23(13):3307-15.
63. Yee AJ, Bensinger WI, Supko JG, Voorhees PM, Berdeja JG, Richardson PG, et al. Ricolinostat plus lenalidomide, and dexamethasone in relapsed or refractory multiple myeloma: a multicentre phase 1b trial. *The Lancet Oncology*. 2016;17(11):1569-78.
64. Zhang I, Beus M, Stochaj U, Le PU, Zorc B, Rajić Z, et al. Inhibition of glioblastoma cell proliferation, invasion, and mechanism of action of a novel hydroxamic acid hybrid molecule. *Cell Death Discov*. 2018;4(1):41.
65. Beus M, Rajić Z, Maysinger D, Mlinarić Z, Antunović M, Marijanović I, et al. SAHAquines, Novel Hybrids Based on SAHA and Primaquine Motifs, as Potential Cytostatic and Antiplasmodial Agents. 2018;7(8):624-38.
66. Asslan M, Lauzon N, Beus M, Maysinger D, Rousseau S. Mass spectrometry imaging in zebrafish larvae for assessing drug safety and metabolism. *Analytical and Bioanalytical Chemistry*. 2021;413(20):5135-46.
67. Treon SP, Xu L, Yang G, Zhou Y, Liu X, Cao Y, et al. MYD88 L265P Somatic Mutation in Waldenström's Macroglobulinemia. 2012;367(9):826-33.

68. Liu X, Chen JG, Munshi M, Hunter ZR, Xu L, Kofides A, et al. Expression of the prosurvival kinase HCK requires PAX5 and mutated MYD88 signaling in MYD88-driven B-cell lymphomas. *Blood advances*. 2020;4(1):141-53.
69. Pham LV, Tamayo AT, Li C, Bueso-Ramos C, Ford RJ. An epigenetic chromatin remodeling role for NFATc1 in transcriptional regulation of growth and survival genes in diffuse large B-cell lymphomas. *Blood*. 2010;116(19):3899-906.
70. Habel M-E, Jung D. c-Myc over-expression in Ramos Burkitt's lymphoma cell line predisposes to iron homeostasis disruption in vitro. *Biochemical and Biophysical Research Communications*. 2006;341(4):1309-16.
71. Chang H, Blondal JA, Benchimol S, Minden MD, Messner HA. p53 Mutations, c-myc and bcl-2 Rearrangements in Human Non-Hodgkin's Lymphoma Cell Lines. *Leukemia & Lymphoma*. 1995;19(1-2):165-71.
72. Xu-Monette ZY, Wu L, Visco C, Tai YC, Tzankov A, Liu WM, et al. Mutational profile and prognostic significance of TP53 in diffuse large B-cell lymphoma patients treated with R-CHOP: report from an International DLBCL Rituximab-CHOP Consortium Program Study. *Blood*. 2012;120(19):3986-96.
73. Xu-Monette ZY, Medeiros LJ, Li Y, Orlowski RZ, Andreeff M, Bueso-Ramos CE, et al. Dysfunction of the TP53 tumor suppressor gene in lymphoid malignancies. *Blood*. 2012;119(16):3668-83.
74. Zenz T, Kreuz M, Fuge M, Klapper W, Horn H, Staiger AM, et al. TP53 mutation and survival in aggressive B cell lymphoma. 2017;141(7):1381-8.

75. Jiang S, Qin Y, Jiang H, Liu B, Shi J, Meng F, et al. Molecular profiling of Chinese R-CHOP treated DLBCL patients: Identifying a high-risk subgroup. 2020;147(9):2611-20.
76. Qin Y, Jiang S, Liu P, Yang J, Yang S, He X, et al. Characteristics and Management of TP53-Mutated Diffuse Large B-Cell Lymphoma Patients. Cancer management and research. 2020;12:11515-22.
77. von Manstein V, Yang CM, Richter D, Delis N, Vafaizadeh V, Groner B. Resistance of Cancer Cells to Targeted Therapies Through the Activation of Compensating Signaling Loops. Current signal transduction therapy. 2013;8(3):193-202.
78. Sturm OE, Orton R, Grindlay J, Birtwistle M, Vyshemirsky V, Gilbert D, et al. The Mammalian MAPK/ERK Pathway Exhibits Properties of a Negative Feedback Amplifier. 2010;3(153):ra90-ra.
79. Melesina J, Simoben CV, Praetorius L, Bülbül EF, Robaa D, Sippl W. Strategies To Design Selective Histone Deacetylase Inhibitors. 2021;16(9):1336-59.
80. Wang Q, Liu X. The dual functions of  $\alpha$ -tubulin acetylation in cellular apoptosis and autophagy induced by tanespimycin in lung cancer cells. Cancer cell international. 2020;20:369.
81. Wattanathamsan O, Thararattanobon R, Rodsiri R, Chanvorachote P, Vinayanuwattikun C, Pongrakhananon V. Tubulin acetylation enhances lung cancer resistance to paclitaxel-induced cell death through Mcl-1 stabilization. Cell Death Discov. 2021;7(1):67.

82. Duan MR, Smerdon MJ. Histone H3 lysine 14 (H3K14) acetylation facilitates DNA repair in a positioned nucleosome by stabilizing the binding of the chromatin Remodeler RSC (Remodels Structure of Chromatin). *The Journal of biological chemistry*. 2014;289(12):8353-63.
83. Wang Y, Kallgren SP, Reddy BD, Kuntz K, López-Maury L, Thompson J, et al. Histone H3 lysine 14 acetylation is required for activation of a DNA damage checkpoint in fission yeast. *The Journal of biological chemistry*. 2012;287(6):4386-93.
84. Choudhary C, Kumar C, Gnad F, Nielsen ML, Rehman M, Walther TC, et al. Lysine Acetylation Targets Protein Complexes and Co-Regulates Major Cellular Functions. 2009;325(5942):834-40.
85. Welch MD, DePace AH, Verma S, Iwamatsu A, Mitchison TJ. The human Arp2/3 complex is composed of evolutionarily conserved subunits and is localized to cellular regions of dynamic actin filament assembly. *The Journal of cell biology*. 1997;138(2):375-84.
86. Schrank BR, Aparicio T, Li Y, Chang W, Chait BT, Gundersen GG, et al. Nuclear ARP2/3 drives DNA break clustering for homology-directed repair. *Nature*. 2018;559(7712):61-6.
87. Mendoza MC, Vilela M, Juarez JE, Blenis J, Danuser G. ERK reinforces actin polymerization to power persistent edge protrusion during motility. *Science signaling*. 2015;8(377):ra47.

88. Shi P, Wang Y, Huang Y, Zhang C, Li Y, Liu Y, et al. Arp2/3-branched actin regulates microtubule acetylation levels and affects mitochondrial distribution. *Journal of Cell Science*. 2019;132(6).
89. Bolger-Munro M, Choi K, Scurll JM, Abraham L, Chappell RS, Sheen D, et al. Arp2/3 complex-driven spatial patterning of the BCR enhances immune synapse formation, BCR signaling and B cell activation. *eLife*. 2019;8.
90. Hebert AS, Dittenhafer-Reed KE, Yu W, Bailey DJ, Selen ES, Boersma MD, et al. Calorie restriction and SIRT3 trigger global reprogramming of the mitochondrial protein acetylome. *Molecular cell*. 2013;49(1):186-99.
91. Dali-Youcef N, Froelich S, Moussallieh F-M, Chibbaro S, Noël G, Namer IJ, et al. Gene Expression Mapping of Histone Deacetylases and Co-factors and Correlation with Survival Time and 1H-HRMAS Metabolomic Profile in Human Gliomas. *Scientific Reports*. 2015;5(1):9087.
92. Suzuki C, Takahashi K, Hayama S, Ishikawa N, Kato T, Ito T, et al. Identification of Myc-associated protein with JmjC domain as a novel therapeutic target oncogene for lung cancer. *Molecular Cancer Therapeutics*. 2007;6(2):542-51.
93. Nicotra G, Manfroi F, Follo C, Castino R, Fusco N, Peracchio C, et al. High expression of cathepsin D in non-Hodgkin's lymphomas negatively impacts on clinical outcome. *Disease markers*. 2010;28(3):167-83.
94. Laurent-Matha V, Maruani-Herrmann S, Prébois C, Beaujouin M, Glondu M, Noël A, et al. Catalytically inactive human cathepsin D triggers fibroblast invasive growth. *The Journal of cell biology*. 2005;168(3):489-99.

95. Ketterer S, Mitschke J, Ketscher A, Schlimpert M, Reichardt W, Baeuerle N, et al. Cathepsin D deficiency in mammary epithelium transiently stalls breast cancer by interference with mTORC1 signaling. *Nature communications*. 2020;11(1):5133.

### **3.7 Supplementary data**

Fig. S1

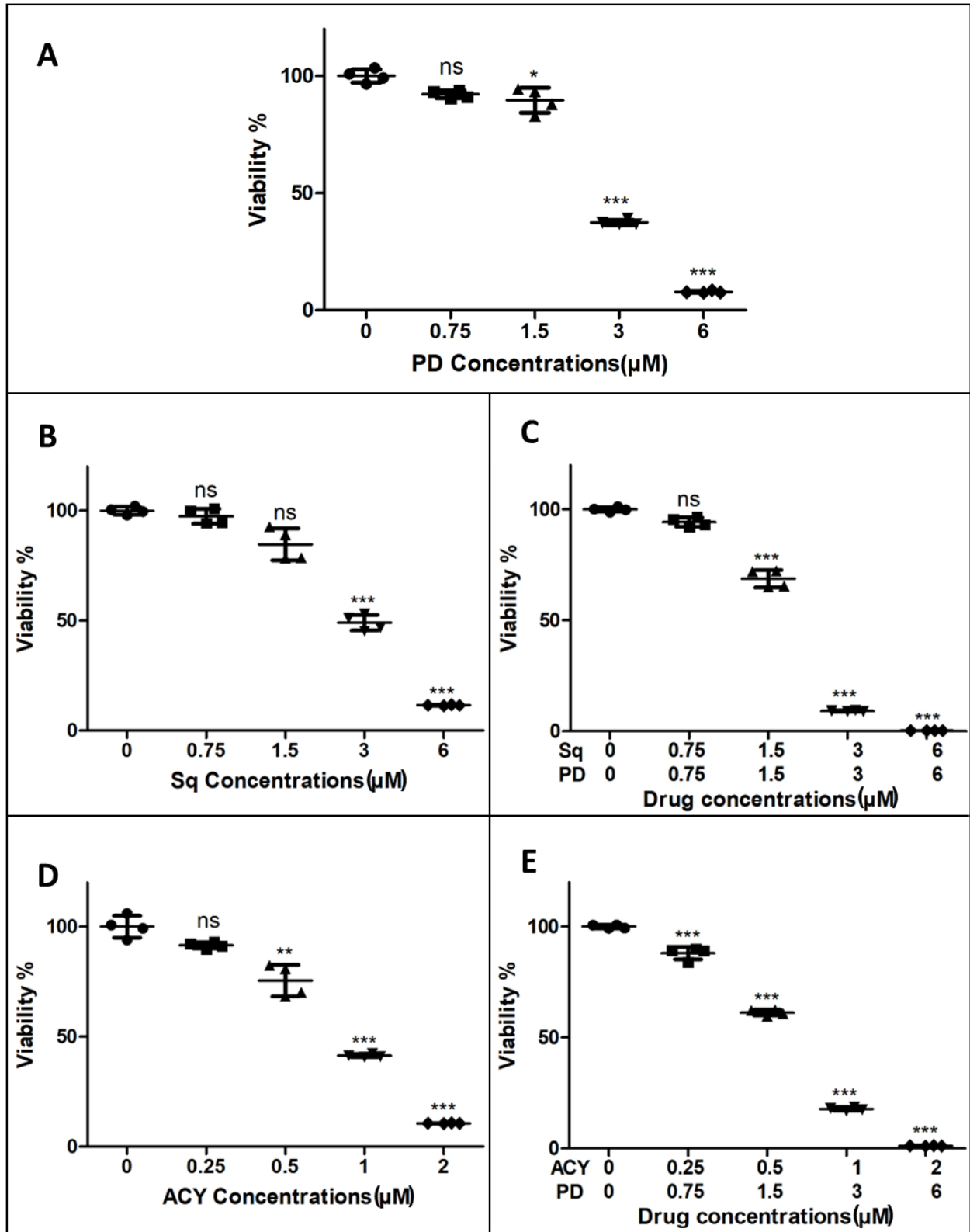


**Fig. S1 Single and dual therapies reduced RAMOS cell viability in a dose-dependent manner.**

Dose-response plots of RAMOS cell viability following treatment with (A) PD184352, (B) Sahaquine (Sq), (C) PD184352 and Sahaquine, (D) ACY1215 (ACY), and (E) PD184352 and ACY1215 for 72 h. Each point represents a percentage value normalized to the mean value of control group treated with vehicle only (DMSO 0.2 %). Horizontal bars represent the average values (SD) of at least two independent experiments (n=4, one-way ANOVA with Dunnett's post hoc test, \*\*\*  $p < 0.001$ , \*\*  $p < 0.01$ , \*  $p < 0.05$ ). Cell viability was measured using flow cytometry cell counting, and data was analyzed using FlowJo software.

Fig. S2

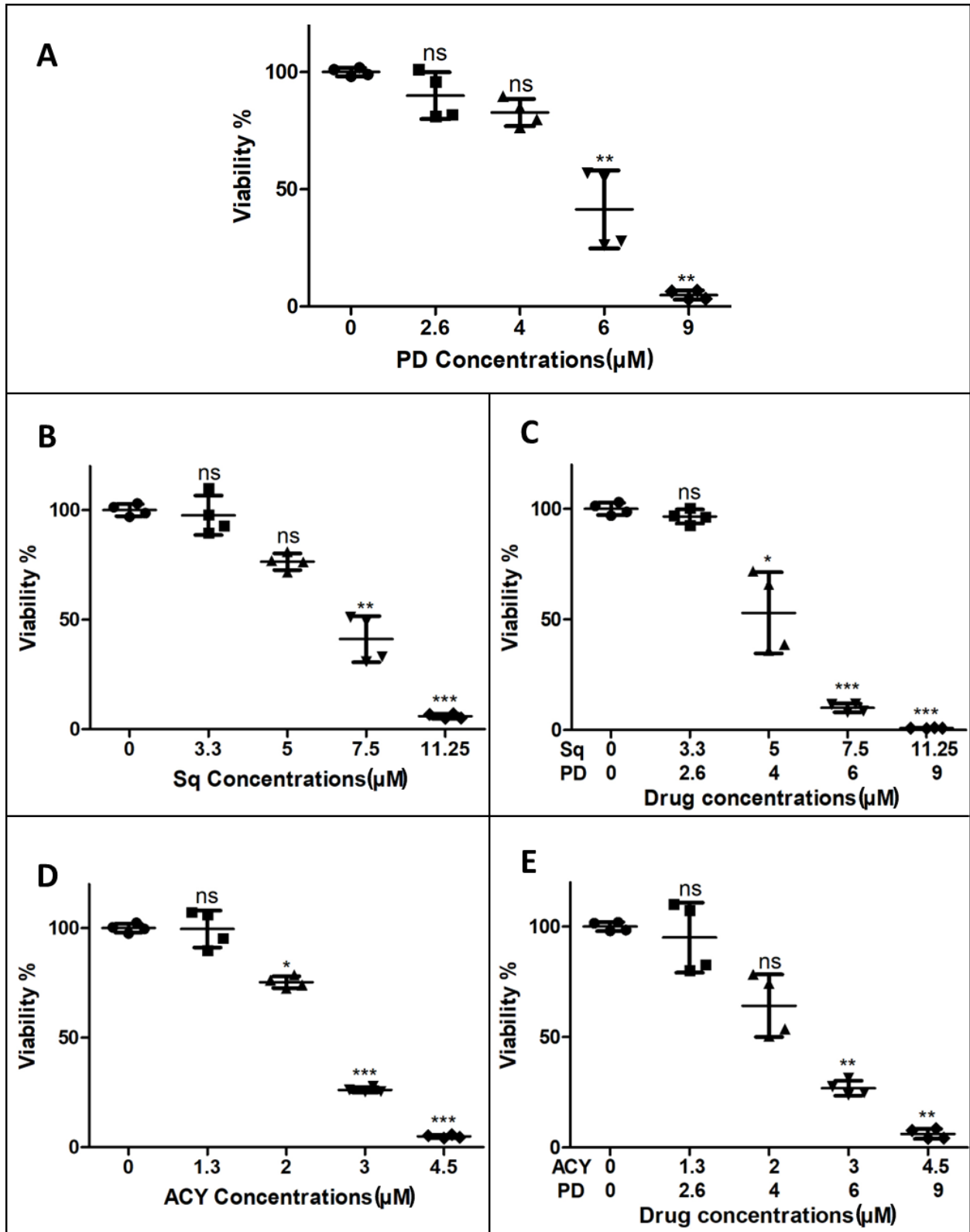


**Fig. S2 Single and dual therapies reduced BCWM.1 cell viability in a dose-dependent manner.**

Dose-response plots of BCWM.1 cell viability following treatment with (A) PD184352, (B) Sahaquine (Sq), (C) PD184352 and Sahaquine, (D) ACY1215 (ACY), and (E) PD184352 and ACY1215 for 72 h. Each point represents a percentage value normalized to the mean value of control group treated with vehicle only (DMSO 0.2 %). Horizontal bars represent the average values (SD) of at least two independent experiments (n=4, one-way ANOVA with Dunnett's post hoc test, \*\*\*  $p < 0.001$ , \*\*  $p < 0.01$ , \*  $p < 0.05$ ). Cell viability was measured using flow cytometry cell counting, and data was analyzed using FlowJo software.

**Fig.S3**

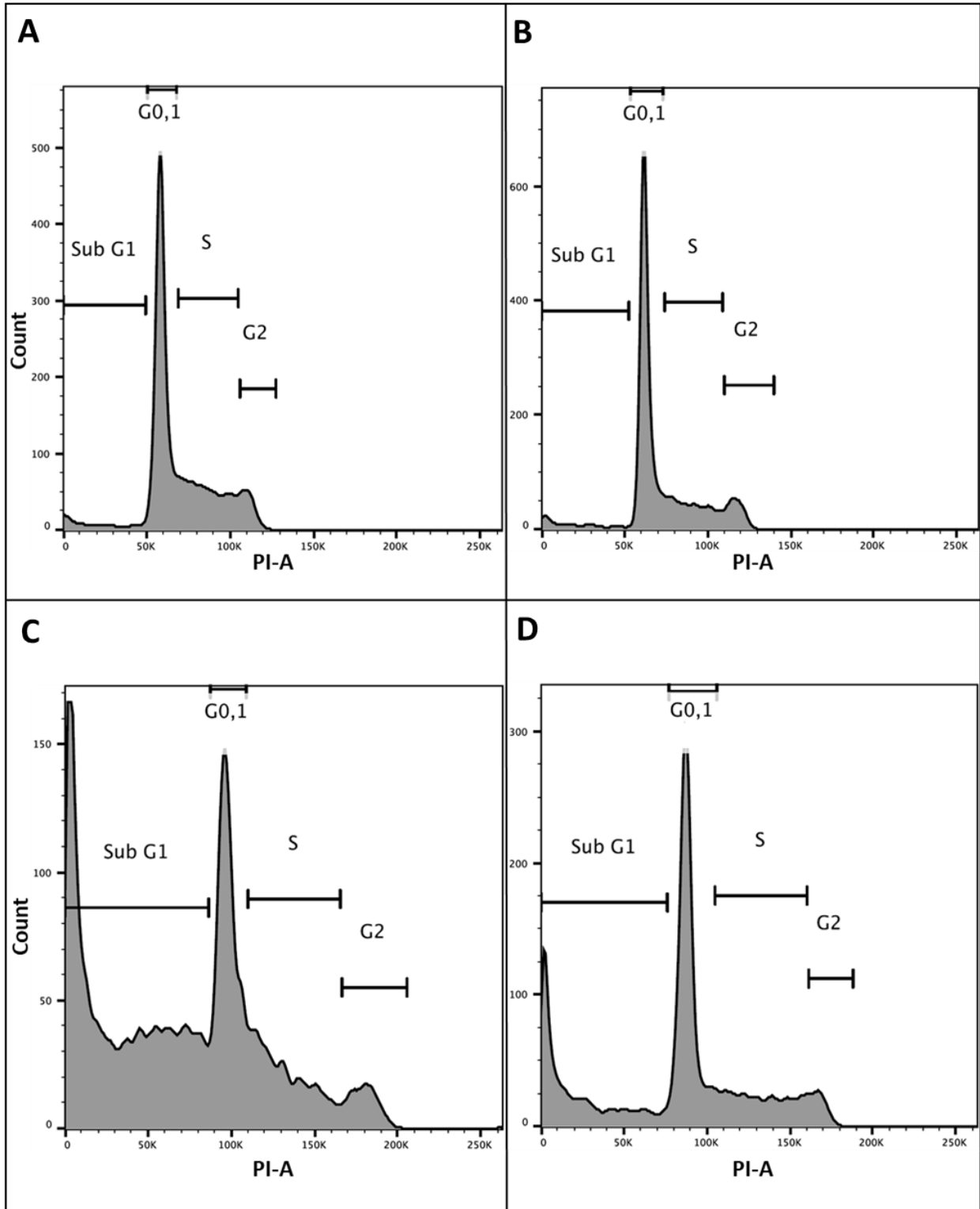


**Fig. S3 The combination of PD184352 with either Sahaquine or ACY1215 produced Sub G1 pick that was absent in Sahaquine or ACY1215 single therapy groups.**

Representative cell-cycle histograms of propidium iodide fluorescence profiles in samples treated with (A) Sahaquine (5  $\mu$ M), (B) ACY1215 (1.5  $\mu$ M) (C) PD184352 (4  $\mu$ M) and Sahaquine (5  $\mu$ M), and (D) PD184352 (4  $\mu$ M) and ACY1215 (1.5  $\mu$ M) for 72 h. X-axis represents propidium iodide staining area, y-axis represents OCI-LY2 cells count. Data were analyzed using FlowJo software.

**Fig. S4**

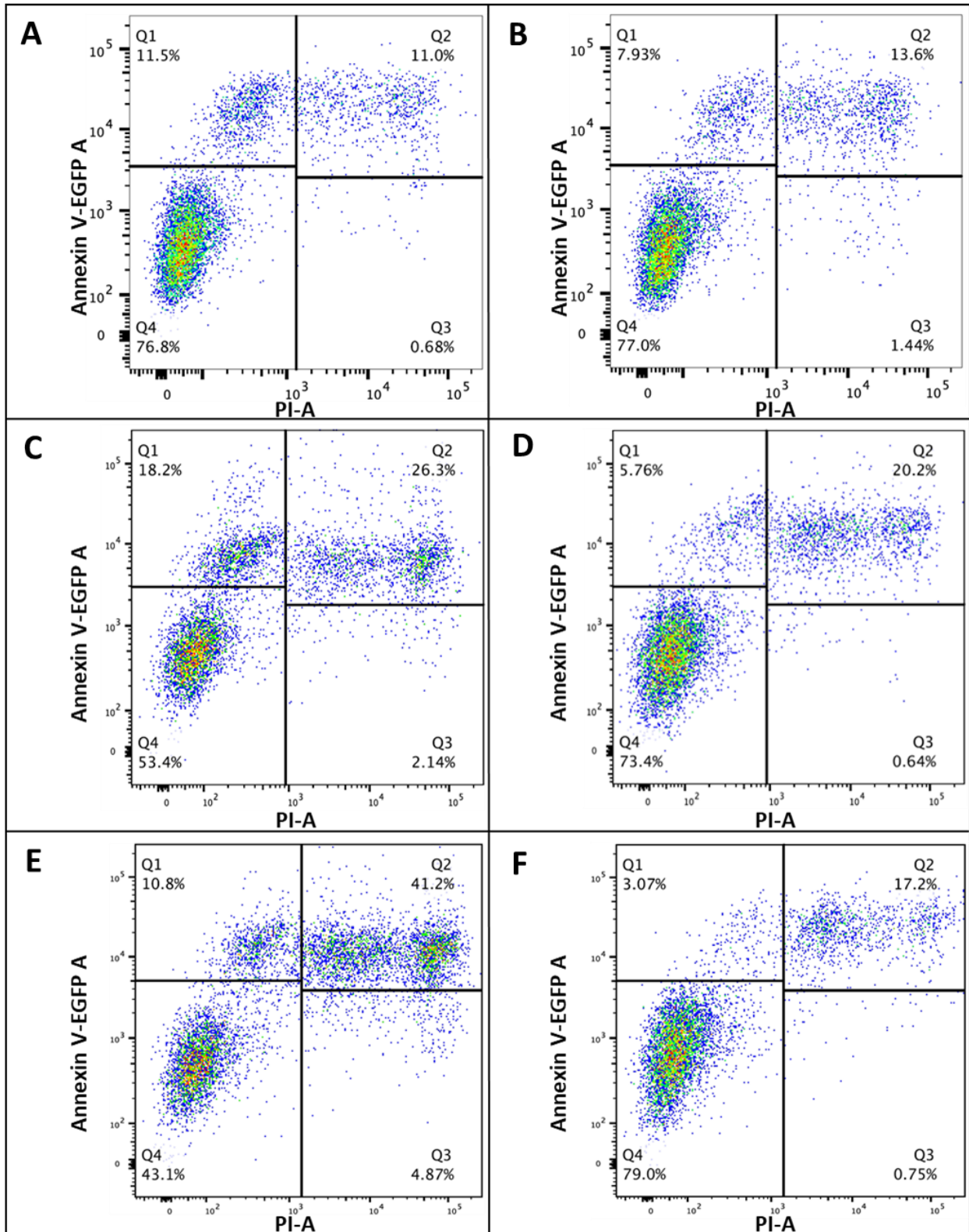


**Fig. S4 PD184352 and Sahaquine combination induced mainly apoptotic cell death in contrast to PD184352 and ACY1215 combination.**

Scatter plots demonstrate the presence or absence of apoptotic cells in PD184352 (4  $\mu$ M) and Sahaquine (5  $\mu$ M) combination group (A,C,E), or PD184352 (4  $\mu$ M) and ACY1215 (1.5  $\mu$ M) group (B,D,F), in OCI-LY2 cell line at different time points including 24 h (A,B), 48 h (C,D), and 72 h (E,F). The forward scatter represents propidium iodide staining area. The side scatter represents Annexin V-EGFP staining area. Data were analyzed using FlowJo software. Each experiment was repeated 3 times (n=6), and one representative experiment is shown.

## **Preface**

Results obtained from chapter 3 show that the combination of PD184352 (MKK1/2 inhibitor) with either ACY1215 or Sahaquine (HDAC6 inhibitors) induced cytotoxic effect which is preferable to cytostatic effect in cancer treatments. To translate these pre-clinical findings to clinical research, inhibitors safety information is initial requirement. Safety studies are available for PD184352 and ACY1215 (both are safe in humans) but no safety data is available for Sahaquine yet. Therefore, we decided to evaluate Sahaquine safety and metabolism in vivo model to increase the potential clinical usefulness of Sahaquine and PD184352 combination.

## **Chapter 4: Mass spectrometry imaging in zebrafish larvae for assessing drug safety and metabolism**

Mariana Asslan<sup>1,2</sup>, Nidia Lauzon<sup>1</sup>, Maja Beus<sup>3</sup>, Dusica Maysinger<sup>2</sup>, Simon Rousseau<sup>1,2</sup>

1. Research Institute of the McGill University Health Centre, Montreal, Canada.
2. Pharmacology Department, McGill University, Montreal, Canada.
3. Faculty of Pharmacy and Biochemistry, University of Zagreb, Zagreb, Croatia.

Published in *Analytical and Bioanalytical Chemistry* (2021), 413(20), 5135-5146. DOI: 10.1007/s00216-021-03476-4

Corresponding author

Simon Rousseau, The Meakins-Christie Laboratories at the RI-MUHC, 1001 Boul. Décarie, Montréal, H4A 3J1, Canada, Phone: +1-514-934-1934 (76394), Email: [simon.rousseau@mcgill.ca](mailto:simon.rousseau@mcgill.ca)

## **Authors' contributions**

The main text of the manuscript was written by Mariana Asslan with contributions from Nidia Lauzon. Zebrafish experiments material preparation, data collection and analysis were performed by Mariana Asslan. Nidia Lauzon and Mariana Asslan performed MALDI experiments. Maja Beus prepared Sahaquine. Editing prior to submission was performed by all authors. All authors approved the final manuscript.

## **Acknowledgements**

The authors would like to acknowledge Dr. Hugh Clarke and his research associate Dr. Qin Yang (CHHD Program, RI-MUHC) for initial technical assistance in performing microinjections, Drs. Sanjoy Kumar Das and Bertrand Jean-Claude (Drug Discovery Platform, RI-MUHC) for their scientific insights about potential Sq metabolites, Dr. Pierre Chaurand (Université de Montréal) for his precious advice on the manuscript and Joseph Leger (Concordia University) for his assistance in editing the text.

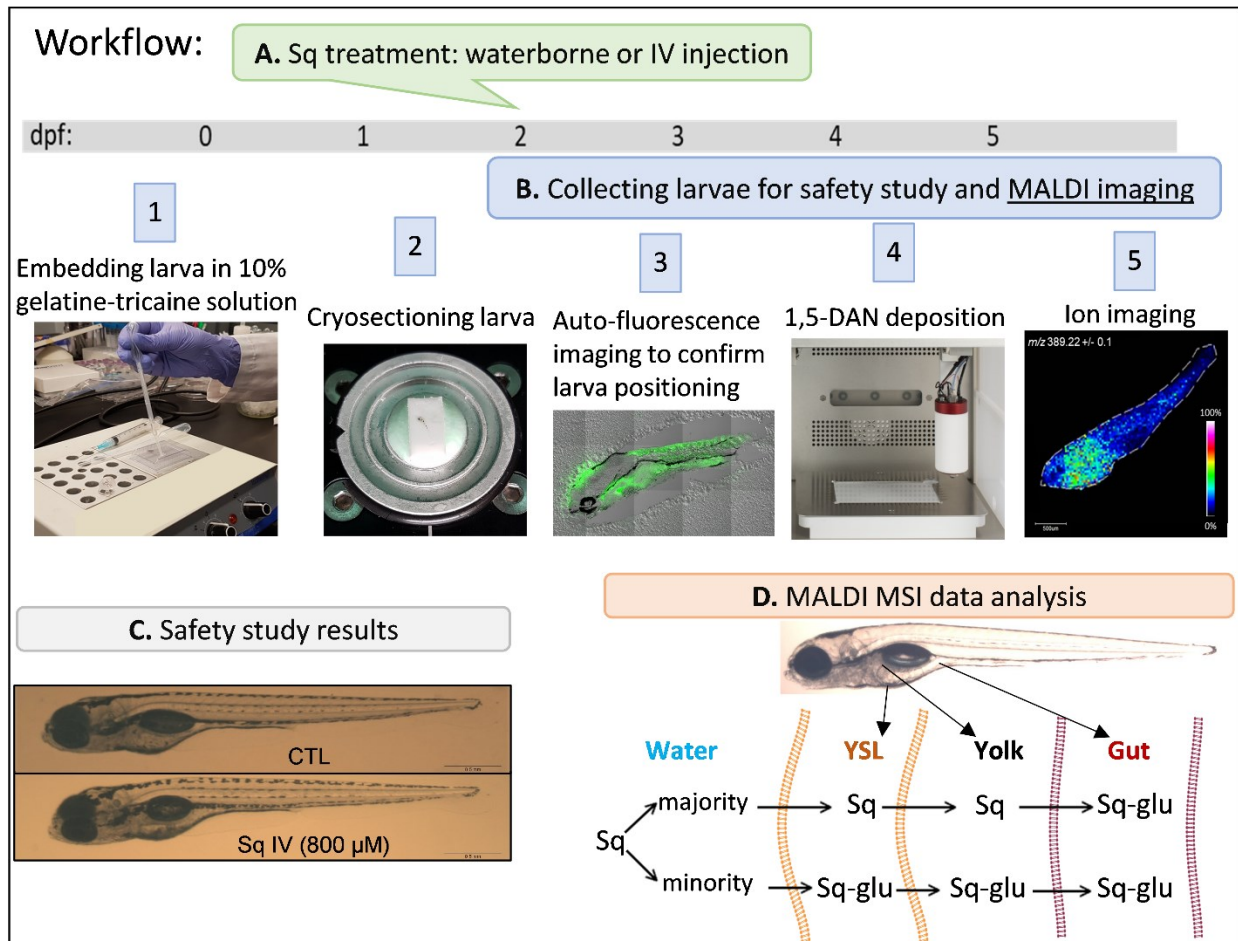
## **Keywords**

Drug safety, metabolism, Sahaquine, zebrafish, mass spectrometry imaging.

## **4.1 Abstract**

Drug safety assessment in the early phases of drug discovery is critical to facilitate the rapid development of novel therapeutics. Recently, teleost zebrafish (*Danio rerio*) has emerged as a promising vertebrate model for the assessment of drug safety. Zebrafish is a convenient model because of its small size, high fecundity, embryo transparency and ex utero development. In this study, we developed a matrix-assisted laser desorption/ionization mass spectrometry imaging (MALDI MSI) method applied to zebrafish larvae to investigate safety and metabolism of Sahaquine (Sq), an anticancer agent inhibiting histone deacetylase 6. This technique improves on prior studies using liquid chromatography-mass spectrometry (LC-MS) by adding analysis of the drug spatial distribution. Using this method, it was determined that Sq dissolved in fish water (1 – 2000  $\mu\text{M}$ ) did not reach the larval body and was mainly distributed throughout the yolk. High Sq concentration (800  $\mu\text{M}$ ) administered intravenously allowed the compound to reach the larval body but did not induce phenotypic abnormalities. Sq was metabolized into its glucuronidated form within 24 h and was excreted within 72 h. MALDI MSI was instrumental in showing that Sq-glucuronide was mainly formed in the gut and slightly in yolk syncytial layer; and provided valuable insights into xenobiotics elimination in zebrafish larvae. This study indicate that Sq has a good safety profile and merits further investigations in other disease models. In addition, the optimized MALDI MSI protocol provided here can be widely applied to study distribution and metabolic fate of other structurally related molecules.

## Graphical abstract



## 4.2 Introduction

Drug toxicity is one of the main issues limiting the therapeutic benefits of novel drugs in clinical trials [1]. Therefore, more predictive preclinical models are needed to provide accurate toxicity assessments at the early stages of drug discovery [2, 3]. This will save effort, time and money when developing these novel therapeutics [4, 5]. Recently, teleost

zebrafish (*Danio rerio*) have emerged as a powerful vertebrate model for many fields such as physiology [6], microbiology [7], genetics [8], toxicology [9], and drug discovery [10], due to its unique features. Zebrafish have relatively high genetic similarity (70%) to humans which supports the translational value of this model [11]. Moreover, the optical clarity of zebrafish embryos and their rapid development allow the real-time testing of biological processes and make visible malformations easily detectable [12]. The high fecundity and small size of zebrafish lead to a significant improvement in high-throughput chemical screens using vertebrate model [13]. Zebrafish is amenable to genetic manipulation, which facilitate target identification and validation, using transgenic and mutated fish [14]. Zebrafish models also provide a unique opportunity to xenograft human tumors into zebrafish larvae to investigate tumor sensitivity to treatment, as the biological intercommunication between these two species is conserved [15-18]. Furthermore, zebrafish xenobiotic metabolism, including drugs, is comparable to human metabolism [19, 20]. Zebrafish are lecithotrophic organisms relying on nutrients from maternally deposited yolks over the first five days of life. The yolk consists mainly of lipids and proteins and is separated from the developing embryo by the yolk syncytial layer (YSL) [21]. The YSL is a cytoplasmic layer surrounding the yolk and plays crucial roles during embryonic and larval stages by controlling morphogenesis and metabolism [22]. Zebrafish have proved to be valuable models to estimate toxicity in humans due to their similar responses to toxicants [12, 23-25]. Experiments with zebrafish larvae are less invasive, can sometimes replace mammals use at early stages of drug discovery, and bridge the gap between in vitro and in vivo models leading to a reduction in the number of research animals. Therefore, they are aligned with the 3R principle (Refinement,

Replacement, Reduction) [26]. For these reasons, zebrafish are becoming a model of choice for studies aimed at rapid and cost-effective screens [27, 28]. However, zebrafish model has some drawbacks due to the distinct physiology of the fish resulting from adaptation to aquatic environment, such as absence of lungs, presence of swimming bladder and lipid-rich yolk [10].

The utility of zebrafish model in drug discovery relies on understanding the distribution profile of the investigated compounds [29-32]. Adapting approaches that ignore distribution pattern, such as LC-MS, sometimes can result in misleading information as shown previously by Kirla et al. [33]. Hence, there is a need to develop and improve imaging approaches for zebrafish model. Advances in MALDI MSI have allowed researchers to image small molecules in zebrafish larvae, but it is still challenging [33-36]. MALDI MSI is a rapidly growing bioanalytical technology that allows for the simultaneous mapping of drugs and their metabolites in biological tissue sections, unlike the autoradiographic standard method – whole-body autoradiography – that lacks MALDI MSI specificity and LC-MS that lacks the spatial information [29, 37, 38]. MALDI MSI relies on the deposition of a UV-absorbing matrix on a thin tissue section to aid in the desorption/ionization process [39]. The matrix solution, uniformly sprayed onto the tissue section, selectively extracts the analytes and co-crystallizes them, conserving the molecular spatial distribution. Upon laser irradiation, the matrix molecules induce the desorption of the co-crystallized analytes and ionize them. The ions are then analyzed by time-of-flight (TOF) MS [40]. In this manuscript, we have adapted MALDI MSI to

investigate safety and metabolism of Sahaquine (Sq), an anticancer agent, in zebrafish larvae.

Sahaquine (Sq) is a novel hybrid compound that inhibits histone deacetylase 6. Several of our earlier studies showed that Sq has anticancer activity in different human tumor cell types including glioblastoma [41], breast, bone and liver cancers [42]. in micromolar concentrations (1 - 20  $\mu$ M). Sq safety and metabolism have not been evaluated in in vivo models. Hence, we assessed if Sq is non-selectively cytotoxic in zebrafish if provided in equimolar and higher concentrations than those killing tumor cells. In addition, we studied Sq and its metabolites distributions in zebrafish models.

We show here Sq safety, distribution and metabolism in zebrafish larvae model and provide an optimized MALDI-TOF MSI protocol that can be widely applied to study metabolic fate and distribution of other structurally related molecules.

## **4.3 Materials and Methods**

### **4.3.1 Materials**

Sahaquine was synthesized as previously described [41]. CellTracker™ CM-Dil dye C7001 was purchased from Invitrogen. Pronase (10165921001) was purchased from Roche. Gelatin G1890, Tricaine (MS-222) E10521, Methylene blue M9140, N-Phenylthiourea (PTU) P7629, 5Z-7-Oxozeaenol (O9890) and MALDI matrices 1,5-

diaminonaphthalene (DAN),  $\alpha$ -cyano-4-hydroxycinnamic acid (CHCA), 2,5-dihydroxybenzoic acid (DHB), 2-mercaptobenzothiazole (MBT) and trifluoroacetic acid (TFA) were purchased from Sigma-Aldrich (St-Louis, MO, USA). Liquid chromatography grade solvents were purchased from VWR (Radnor, PA, USA).

#### **4.3.2 Zebrafish husbandry**

AB strain zebrafish (*Danio rerio*) were raised according to standard experimental conditions [43, 44]. Adult fish were kept at the ratio of 1:1 male to female at 28.5°C under 14 h light/10 h dark cycles. Adults (9 pairs) between 6-12 months old were crossed in mating tanks. Embryos were collected within 30 mins of the beginning of light cycle and washed with E3 medium (5 mM NaCl, 0.17 mM KCl, 0.33 mM CaCl<sub>2</sub>, 0.33 mM MgSO<sub>4</sub>).

Embryos were maintained in E3 medium containing 3\*10<sup>-5</sup> % methylene blue at 28.5 °C until they reached the required embryonic stage. All experimental protocols in this study were approved by the McGill University animal compliance office (protocol #7438).

#### **4.3.3 Waterborne exposure toxicity assay**

Embryos obtained by natural spawning were cultured in petri dishes at 28.5°C and E3 medium was changed daily. Sq treatment was applied at two days post fertilization (dpf), with a final concentration of DMSO at 1 %. Larvae were cultured in 12-well plates, with three larvae per well, in 2 ml of Sq (1 - 2000  $\mu$ M) diluted in E3 medium. The lowest used concentrations represent the physiologically active concentrations (1 – 20  $\mu$ M) in cell culture [41, 42]. The highest used concentrations were limited by the solvent

(DMSO) toxicity in waterborne and microinjection experiments [45]. Larval viability, morphology and length were analyzed using an inverted microscope at two time points - 1-day post-treatment (dpt) and 3 dpt. Brightfield images of each larva were captured using Motic Images Plus 2.0 software and length was measured. The heartbeats of unanesthetized larvae were assessed visually under microscope only at 1 dpt. The heartbeats were not measured at 3dpt to avoid tricaine usage to anesthetize the larvae as they can swim freely at this stage.

#### **4.3.4 Sq intravenous (IV) microinjection toxicity assay**

Injection needles were made using glass capillaries (BF100-78-10, Sutter Instrument) and pulled with a vertical needle puller (P-97, Sutter Instrument). Using a microforge (MF-900, Narishige), injection needles were cut at 10  $\mu\text{m}$  tip diameter. Holding pipettes were prepared using glass capillaries (601000, A-M SYSTEMS). After pulling the holding pipettes, these were manually broken with a forceps, opening the tip at 350  $\mu\text{m}$ , polished with sandpaper and then fired. Larvae were placed into tricaine solution (0.016 %) and held from the yolk. Compounds were injected into 2 dpf zebrafish larvae using a microinjection system (PLI-100A; Harvard Apparatus, Harvard Biosciences, Inc.) and TransferMan 4r micromanipulator (Eppendorf) connected to an inverted microscope (Zeiss Axio Observer Z1). Either DMSO alone or Sq dissolved in DMSO (0.1 M) were injected in the common cardinal vein (duct of Cuvier) at 2 or 4 nl to obtain a final Sq concentrations of 800 or 1600  $\mu\text{M}$  inside the larvae, assuming the compound is equally distributed in the larvae volume (250 nl). After injection, larvae were washed of tricaine

and healthy larvae were cultured in E3 at 28.5°C. Toxicity was studied as previously described above in waterborne exposure toxicity assay.

#### **4.3.5 Larvae embedding, sectioning and confocal microscopy imaging**

Larvae were collected from the toxicity studies at different time points (1 for each time point) and anesthetized with tricaine. To facilitate cryosectioning, larvae were embedded in 10 % gelatine dissolved in larvae tricaine solution. This embedding medium was preferable to other low melting mediums (HPMC/PVP) [46] in terms of ease of larva positioning. Gelatine solution was heated to 50°C and poured into pre-heated disposable molds (FIS22363552, Fisherbrand). Larvae were then transferred to the molds with their lateral side parallel to the bottom of the mold and stored at -80°C until analyzed. Sections from larvae blocks were cut at 20 µm thickness using a cryostat (Leica CM1950 Microsystems GmbH, Wetzlar, Germany) and sections were thaw-mounted on an Indium-Tin-Oxide-coated microscope glass slide (Delta Technologies Ltd, Loveland, CO). Slides were then imaged with a confocal microscope (Zeiss Axio Observer Z1 LSM700) using 488 nm laser to confirm larvae positioning prior to MSI analyses.

#### **4.3.6 MALDI Mass Spectrometry Imaging**

##### **4.3.6.1 Sample preparation**

Upon desiccation, larvae sections were washed with hexane (30 s in a slide container) and dried under vacuum for 30 minutes. The MALDI matrix DAN was then uniformly

sprayed on the zebrafish larvae sections using a M3 TM-sprayer (HTX Technologies, Chapel Hill, NC, USA) connected to an isocratic LC pump using the following parameters: DAN solution (5 mg/ml) in 67 % acetonitrile; nozzle temperature 65 °C; nozzle height 40 mm; nitrogen pressure 10 psi; flow rate 75 µl/min; z-arm velocity 1200 mm/min; moving pattern VV; track spacing 3 mm; number of passes 26; and drying time 0 s.

#### **4.3.6.2 Mass Spectrometry Imaging**

MSI of the tissue sections were performed on a MALDI TOF/TOF ultrafleXtreme mass spectrometer equipped with a SmartBeam II Nd:YAG 355 nm laser operating at 2000 Hz, using the small laser focus setting (Bruker Daltonics, Billerica, MA, USA). MSI data were acquired in the positive ion mode using 500 shots per pixel with a spatial resolution of 20 µm in the 100-700 Da mass range. External calibration was carried out on zebrafish larvae homogenate using a homemade mix of small molecules. Post-MSI internal calibration was also performed using matrix and known signals. The MALDI MSI data were visualized using FlexImaging 4.1 software (Bruker Daltonics) and SCiLS software (2019b Premium 3D, Bruker Daltonics).

#### **4.3.7 Xenograft model**

#### **4.3.7.1 Cells preparation**

Xenotransplantation was performed using the OCI-LY2 lymphoma cell line. For in vitro labeling using CellTracker CM-Dil dye, cells were grown and collected at  $5 \times 10^6$  cells for each condition. Cells were washed with PBS and incubated with CM-Dil at 37 °C for 5 minutes, then at 4°C for 20 minutes. Afterwards, cells were washed again with PBS and resuspended in 50  $\mu$ l RPMI. The lymphoma cell suspension was loaded into injection needles using a micro-loader tip (930001007, Eppendorf).

#### **4.3.7.2 Larvae preparation**

At 20 hours post fertilization (hpf), PTU was added to a final concentration of 0.003 % to prevent pigmentation of the embryos. At 48 hpf, embryos were dechorionated using Pronase (1 mg/ml) followed by extensive washes with E3. Then, larvae were anesthetized in 0.016 % tricaine. Using injection needles with a 20  $\mu$ m tip diameter, approximately 200 cells were injected in the common cardinal vein, as previously described. After injection, larvae were incubated at 28.5°C for 2 h to recover. Following this, larvae were treated with Sq 1000  $\mu$ M via waterborne administration and incubated at 32°C to assess Sq effectiveness on reducing the tumor mass in comparison to the control. At 3 days post-injection (dpi), larvae were placed in the imaging chambers (70326-12, Electron Microscopy Sciences), and fluorescent z-stack images were acquired using Zeiss LSM700 confocal microscope at 555 nm. The total fluorescent area of CM-Dil-labeled lymphoma cells was analyzed using ImageJ software.

#### **4.3.8 Statistical analysis**

All the data were analyzed and plotted as mean  $\pm$  SD using GraphPad Prism. To compare the control group (n=9) to Sq treated group (n=9) in toxicity and effectiveness studies, two-tailed Student's t-test was used. The level of significance for all analyses was  $p < 0.05$ . (\*\*\*) indicates statistical significance  $p < 0.005$ , (\*\*)  $p < 0.01$ , (\*)  $p < 0.05$ .

### **4.4 Results**

#### **4.4.1 Sahaquine toxicity in zebrafish larvae evaluated by two exposure routes**

Zebrafish larvae at 2 dpf were treated with Sq either via waterborne exposure or IV microinjections. Larvae were evaluated at 1 and 3 days after Sq treatments for lethal, sublethal and developmental toxicity. Endpoints of toxicity included mortality, malformation, heartbeats and body length.

Sq did not induce mortality in the case of 1, 10, 100, 1000 and 2000  $\mu\text{M}$  waterborne exposure and 800  $\mu\text{M}$  injection, and the larvae well-tolerated Sq after three days of treatment. However, at higher concentrations (1600  $\mu\text{M}$  injection), Sq produced 100 % mortality after two days of injection(Figure S1a).

Morphological malformations were observed and recorded under microscope. No obvious abnormalities (body axis, eye, jaw, heart, brain, fin, yolk sac, trunk, circulation, pigment and swim bladder) were observed in 1, 10, 100, 1000 and 2000  $\mu\text{M}$  waterborne (Figure 1a, S1b) and 800  $\mu\text{M}$  injection groups (Figure 1d). The larvae appeared healthy until the end of the experiment. However, in the 1600  $\mu\text{M}$  injection group (Figure 1g) at 1

dpi, larvae exhibited severe morphological anomalies represented by yolk retention, pericardial edema, opaque tissue, bent spine, tail malformation and absence of blood circulation, while DMSO-injected larvae had minor abnormalities represented by pericardial edema. The positive control 5Z-7-oxozeaenol (2  $\mu$ M) produced severe phenotypic toxicity (Figure S1c).

Heartbeats were visually counted at 1 dpt. Results showed no significant differences between Sq-treated groups and controls in both 1, 10, 100, 1000 and 2000  $\mu$ M waterborne (Figure S1d) and 800  $\mu$ M injection experiments (Figure S1e). In contrast, Sq 1600  $\mu$ M injection caused cardiotoxicity symptoms ranging from slow to absence of heartbeats.

Sq injected into zebrafish larvae (800  $\mu$ M, vol 2 nl) disturbed their development leading to a decreased body length. The mean body length of zebrafish larvae at 1 (Figure 1e) and 3 (Figure 1f) dpi were significantly shorter, 94.43 % and 95.57 %, compared to the controls 3.5 mm and 4 mm, respectively. Nonetheless, length measurement of larvae exposed to Sq 1000  $\mu$ M via waterborne at 1 (Figure 1b) and 3 dpt (Figure 1c) demonstrated no significant differences in the body length, 97.86 % and 98.86 %, in comparison to the controls 3.3 mm and 3.9 mm, respectively.

Taken together these results establish a gross morphological profile of drug toxicity but do not inform on the spatial drug distribution and its local accumulation, key factors in studying drug safety. In order to do this, we adapted MALDI MSI to study Sq tissue distribution.

**Fig. 1**

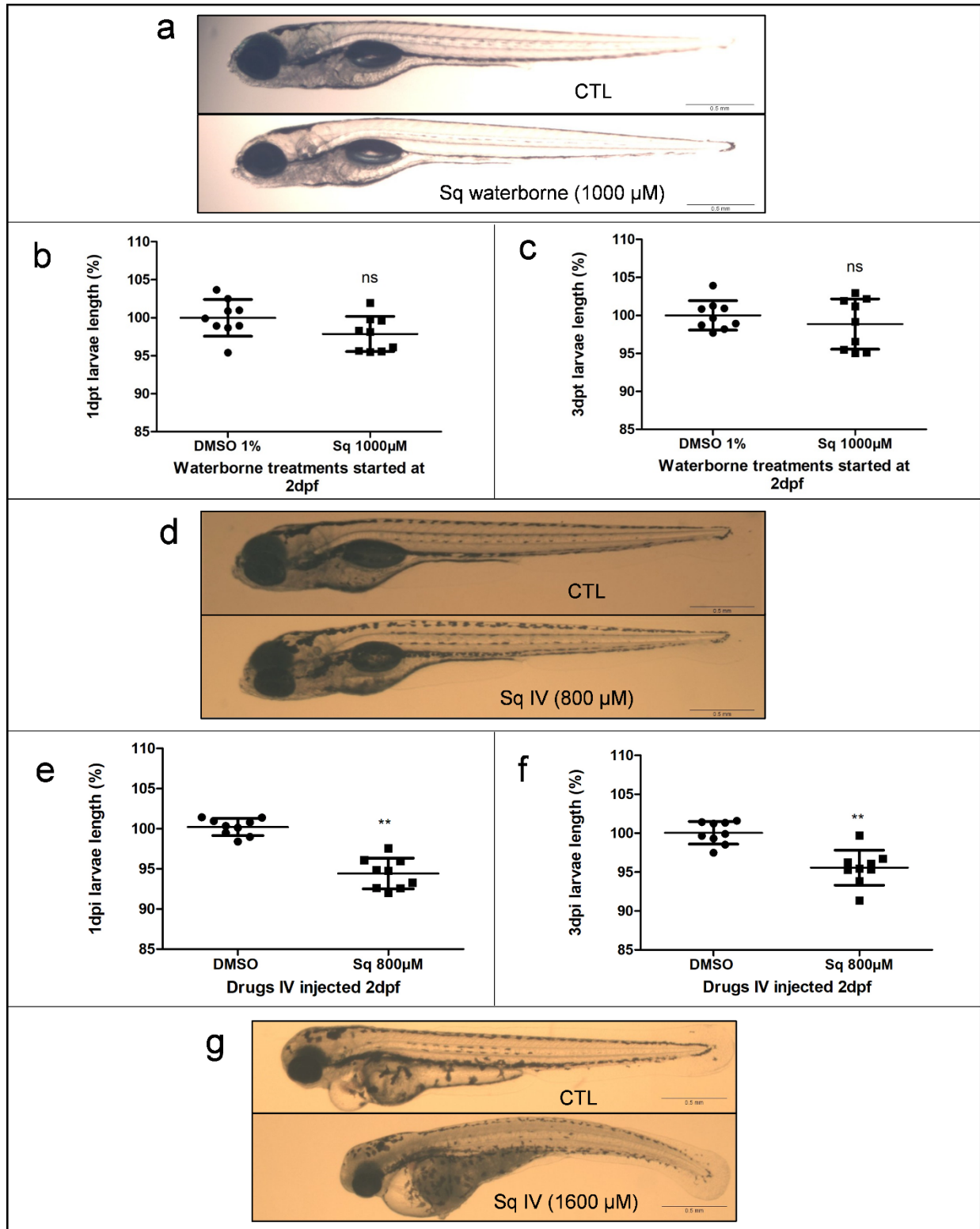


### **Fig. 1 Sahaquine toxicity assessment in zebrafish larvae model.**

(a) Representative micrographs of 5 dpf zebrafish larvae (lateral position), following the administration of DMSO 1 % (CTL) or Sq (1000  $\mu$ M) via waterborne starting at 2 dpf. Percent larvae length at 1 dpt (b) and 3 dpt (c) determined from (a) micrographs. (d) Representative micrographs of 5 dpf larvae, following the injection of DMSO 2 nl (CTL) or Sq (800  $\mu$ M) at 2 dpf. Percent larvae length at 1 dpi (e) and 3 dpi (f) determined from (d) micrographs. (g) Representative micrographs of 3 dpf larvae following the injection of DMSO 4 nl (CTL) or Sq (1600  $\mu$ M) at 2 dpf. Brightfield images were captured using Motic Images Plus 2.0 software, then larvae length was measured. Data presented as mean  $\pm$  SD with n=9 in each group (\*\*p < 0.01, two-tailed Student's t-test). Intravenous (IV).

#### **4.4.2 Development of a MALDI MSI method to study Sq tissue distribution**

MALDI MSI is a state-of-the-art bioanalytical technology that requires several preparatory steps to visualize compound spatial distribution in zebrafish larva tissue sections.

##### **4.4.2.1 DAN matrix was identified as the most suitable matrix for Sq detection**

The first step is the identification of the most suitable matrix for specific analyte detection, in this case Sq. To select the appropriate matrix for the detection of Sq, multiple criteria were evaluated: the sensitivity, the formation of sodium (Na<sup>+</sup>) and potassium (K<sup>+</sup>) adducts, the matrix background noise and the matrix interference peaks. Four matrices were tested: CHCA, DHB, MBT and DAN, using positive and

negative ion modes. In the positive ion mode, the detection of Sq was possible with the four matrices, with CHCA being moderately more sensitive, followed by DHB, MBT and DAN — which all showed similar sensitivity towards Sq (Figure 2a). Interestingly, using the DAN matrix, Sq could also be observed as a radical ion [47], which explains the enhanced Sq  $[M]^{\bullet+}$  signal ( $m/z$  388.2) in comparison to the other matrices. In the negative ion mode, deprotonated Sq was only detected using the DAN matrix with a similar intensity compared to the positive ion mode (Figure S2a).

Looking for the presence of adducts, such as  $Na^+$  and  $K^+$ , in the spectra can provide important insights during method development. In fact, lowering the capacity of salt adduct formation can greatly increase the sensitivity for detecting protonated compounds on tissue because the majority of the signal will be associated with one ion. Results showed that Sq was detected as  $Na^+$  and  $K^+$  adducts using the four matrices (Figure 2b). However, DAN induced the lowest portion of  $Na^+/K^+$  adducts and was the best matrix for promoting the formation of protonated ions.

Background noise and interference peaks were also evaluated to select the best matrix (Figure S3). DHB produced higher background noise possibly due to the necessary higher laser intensity compared to MBT, CHCA and DAN. For the remaining three matrices, a similar level of background noise was observed, but only the DAN matrix was free of interference at  $m/z$  389.2 (Figure S3b). Assuming that Sq can be detected at very low intensity on the zebrafish larvae, the presence of matrix interference could lead to a false interpretation of the MSI results. Additionally, if this interference is present in

the minimal detection window of  $\pm 1$  Da required for MS/MS, it could be problematic for accurate Sq identification.

Based on the above observations, the DAN matrix was chosen for this study. Since Sq was detectable using both ionization modes, MS/MS was performed to evaluate the best fragmentation pattern (Figure S2b). As a result, the positive mode showed greater signal intensity and number of fragment ions, which increases the possibility of identifying Sq on-tissue. Hence, DAN matrix in the positive ion mode was used to analyze Sq distribution in zebrafish larvae.

**Fig. 2**

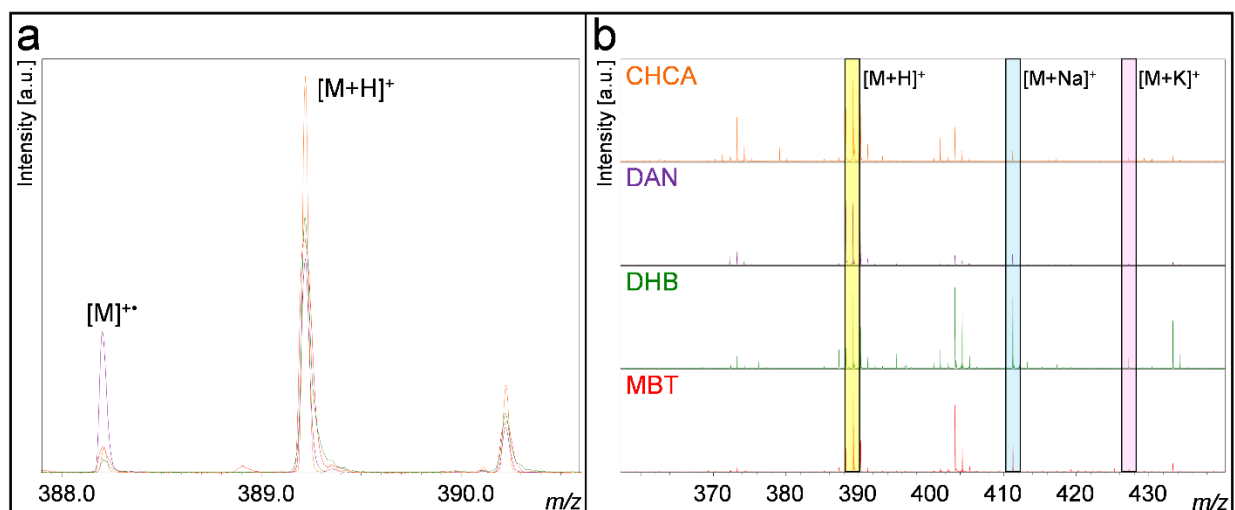


**Fig. 2 MALDI matrix evaluation for the detection of protonated sahaquine.** (a) Magnified spectra of the protonated sahaquine presented with the respective matrix colors: CHCA (orange), DAN (purple), DHB (green) and MBT (red). (b) Relative

abundance of sahaquine protonated (yellow rectangle), sodiated (blue rectangle) and potassiated (pink rectangle) using different matrices.

#### **4.4.2.2 Optimizing matrix deposition and hexane washes using zebrafish homogenate spiked with Sq**

The second step is determining the optimal matrix thickness and the number of washes yielding the best signal. Zebrafish homogenate (approximately 100  $\mu$ l) was prepared using 400 larvae at 5 dpf using a Bead-Based Homogenizer (Next Advance Bullet Blender<sup>24</sup>). Sq was added to reach a final concentration of 260  $\mu$ M. The homogenate was pipetted into homemade molds made of 10 % gelatin and containing holes formed by PCR tubes. The homogenate block was then cryosectioned as previously described. To optimize the matrix thickness, DAN was spray deposited using 18, 22, 26 and 30 passes. Figure 3a shows the results after MSI analysis where 26 passes led to the highest mean intensity, whereas 30 passes dramatically decreased Sq signal.

Since lipids are highly abundant in tissues and might cause ion suppression, the effect of tissue washing on Sq signal intensity was also assessed. Hexane washing has already been shown to enhance the sensitivity of drug on-tissue detection prior to MALDI MSI analysis [48]. For slightly lipophilic compounds, like Sq ( $\log P = 0.921$ ), hexane is a solvent that can be used to safely remove highly lipophilic compounds on-tissue without affecting the compound of interest. To further evaluate the effectiveness of hexane washing, one, two and three 30 second washes were performed (Figure 3b). The results demonstrated that a single hexane wash greatly enhanced Sq sensitivity

and removed almost half of phospholipids on-tissue (Figure S4), while two and three washes slightly reduced Sq sensitivity. Of note, in figure 3b, an air bubble was observed on the zebrafish homogenate. This issue commonly occurs when filling the molds with the homogenate solution. To overcome this issue, regions of interest (ROIs) were drawn using the SCiLS software to exclude the air bubble and generate representative mean intensities.

**Fig. 3**

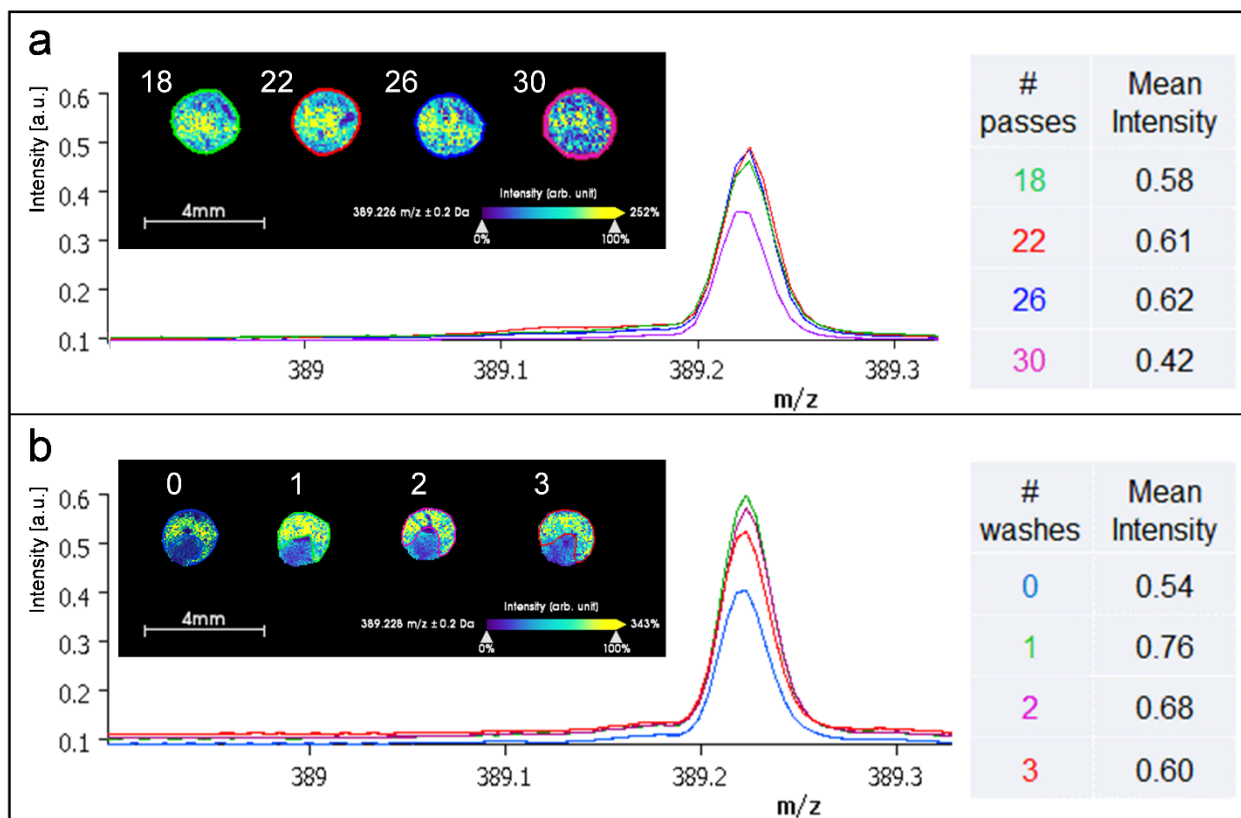


**Fig. 3 Optimization of sahaquine detection on-tissue using thin sections of zebrafish larvae homogenate. (a) Evaluation of the optimal number of DAN spray**

deposition passes using the TM-Sprayer. (b) Evaluation of the optimal number of hexane washes (30 sec each) before DAN deposition.

#### **4.4.2.3 MS/MS identification of Sq injected into larvae yolk**

The last step carried out to confirm the results using MS/MS. Due to the relatively low Sq signal from the tissue sections ( $S/N < 10$ ), MS/MS analyses failed to identify the compound directly on the treated larvae. As an alternative, Sq was injected into 2 dpf zebrafish larvae yolk to concentrate the compound in one area, leading to signal enhancement. Larvae were embedded in the mold immediately after yolk injection. The sample was then used to generate the Sq on-tissue fragmentation pattern and compare it to the MS/MS results from the Sq standard (Figure S5). The fragmentation pattern obtained from the Sq injected into the yolk revealed the same signature peaks as the Sq standard.

Once the adaptation of MALDI MSI for the detection of Sq in zebrafish larvae was completed, it became possible to carry out the drug safety and metabolism analysis *in vivo*.

#### **4.4.3 Sq did not induce tissue specific toxicity**

MALDI MSI analyses were performed on zebrafish larvae to evaluate the possible accumulation of Sq in vital organs, such as the heart and the brain (Figure S6), leading to tissue specific toxicity. Larvae were collected at different time points following the administration of Sq via waterborne or IV injection. Larvae were cryosectioned and the histological aspects of the sections were identified by utilizing the autofluorescent

properties of the zebrafish larval tissue to acquire images using a confocal microscope (Figure 4a). The spatial distribution of Sq across thin tissue sections was visualized using MALDI MSI (Figure 4b). Following 24 h of Sq waterborne exposure (1000  $\mu$ M), Sq at low abundance was detected mainly in the yolk. After Sq microinjections (800  $\mu$ M), larvae were collected at 2, 24, 48, and 72 h. Within 2 hours post-injection (hpi), Sq was observed in the circulatory system, including brain vessels, with a higher signal around the heart (located next to the injection site in the common cardinal vein). By 24 hpi, Sq was mainly distributed throughout the yolk and was absent or not detected (below the limit of detection) in larvae collected at 48 and 72 hpi.

**Fig. 4**

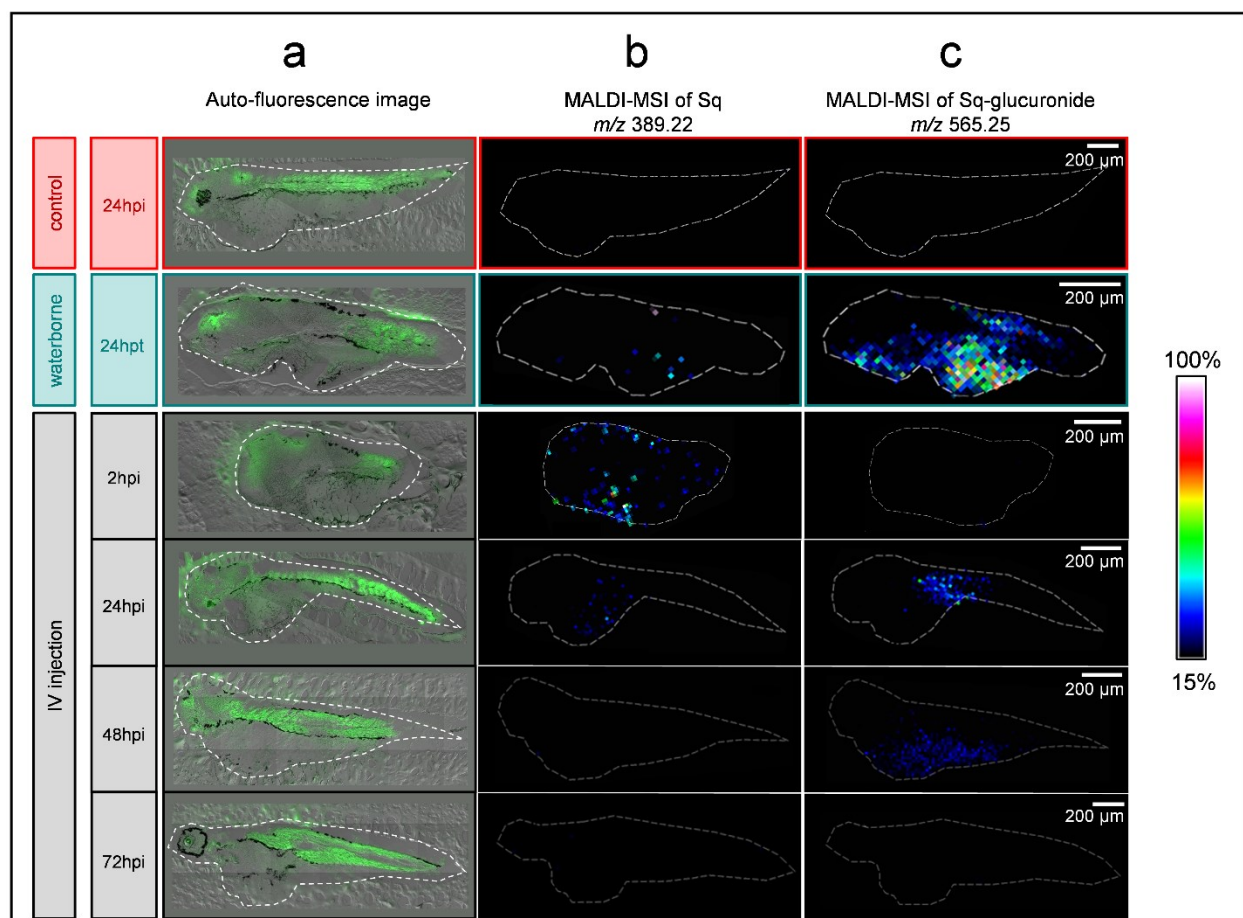


**Fig. 4 MALDI-TOF MSI showing the tissue distribution of sahaquine (Sq) and its glucuronide metabolite (Sq-glu) in zebrafish larvae sections acquired at 20 μm spatial resolution.** Column (a) shows the auto-fluorescence images of larvae tissue sections, while columns (b) and (c) show ion images of Sq ( $m/z$  389.22) and Sq-glu ( $m/z$  565.25), respectively from the same tissue section. Zebrafish larvae were divided into three group to be treated via DMSO injection (red box), Sq 1000 μM waterborne exposure (green box), or Sq 800 μM injection (gray box). Larvae were collected at different time points for MALDI MSI. Each section was collected from one representative

larva per group (n=9). The rainbow bar on the right indicates the relative intensity across the entire cohort increasing from black (no signal) to white (most intense signal).

#### **4.4.4 Glucuronidated Sq was formed and excreted within 72 hpi**

Sq is a hybrid molecule synthesized by combining hydroxamic acid — the active moiety of suberoylanilide hydroxamic acid (SAHA, vorinostat) — with primaquine. To assess Sq elimination, the structures of potential Sq metabolites (Figure S7) were predicted based on the SAHA [49] and primaquine [50] metabolites. Potential metabolites with their respective m/z, such as  $[M+H]^+$  and  $[M+Na]^+$ , were screened in the entire MSI data set. Consequently, a peak was detected at m/z 565.255, which may correspond to Sq-glucuronide (Sq-glu) with a theoretical m/z of 565.2504 (Err/ppm = 8.1). Further MS/MS analyses could not confirm the identity of Sq-glu due to the relatively low signal ( $S/N < 10$ ). However, the absence of interferences at the respective m/z in the entire data set and the presence of Sq-glu radical  $[M]^+\bullet$  strongly support our findings (Figure S8). Following Sq waterborne administration (1000  $\mu$ M), the glucuronidated form was observed at low abundance in the YSL and accumulated at a much higher abundance in the newly formed gastrointestinal tract (Figure 4c). In the case of microinjections at 2 hpi, Sq-glu was not detected in the larvae tissue sections. Interestingly, at 24 and 48 hpi, Sq-glu was observed in the gut. At 72 hpi, Sq-glu was possibly eliminated and no longer detected (Figure 4c).

#### 4.4.5 Waterborne exposure was not adequate for Sq to reach therapeutic concentrations in the larval body

Next, we investigated whether Sq, after waterborne administration, accumulated at therapeutic concentrations in the larvae circulatory system before being metabolized in the gut. At 2 dpf, labeled lymphoma cells (OCI-LY2) were IV injected. The xenografted larvae were then treated with Sq 1000  $\mu$ M for three consecutive days, with daily replacement of media. To assess the ability of Sq to decrease tumor mass at 3 dpt, the total fluorescence area was measured in larvae using confocal z-stack imaging (Figure 5a). Sq treatment did not induce a significant reduction of tumor mass in treated xenografts compared to untreated (Figure 5b). The positive control 5Z-7-oxozeaenol (1  $\mu$ M) significantly reduced tumor mass in treatment-group compared to control-group (Figure S9).

**Fig. 5**

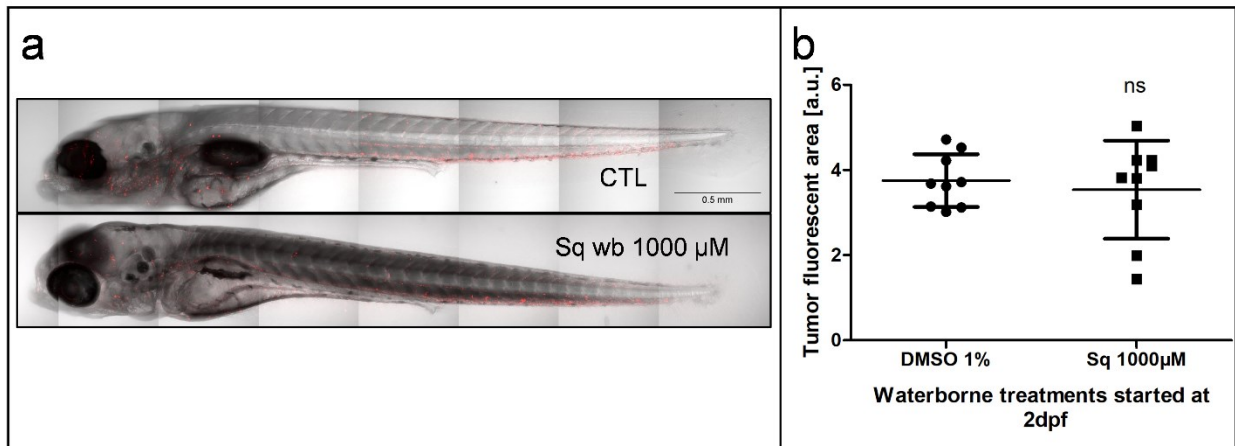


**Fig. 5 Assessment of tumor mass after Sahaquine waterborne administration in zebrafish xenograft model.** (a) Representative fluorescence z-stack images of 5 dpf zebrafish larvae, injected with fluorescently labeled OCI-LY2 lymphoma cells, and treated with DMSO 1 %(CTL) or Sq (1000  $\mu$ M) via waterborne exposure for 3 days. (b) Quantification of total fluorescence area at 3 dpt. Xenografted larvae were imaged with a confocal microscope, and fluorescence area was measured using ImageJ. Data presented as mean  $\pm$  SD with n=9 in each group (two-tailed Student's t-test).

## 4.5 Discussion

The main objective of this study was to develop MALDI MSI to study drug safety and metabolism of a histone deacetylase inhibitor Sq, in zebrafish larvae. Several structurally similar compounds are proposed for clinical studies but their distribution and elimination in an aquatic environment has not been previously investigated. Considering that many pharmaceutical products are found in water, we assessed if MALDI MSI could be a useful way to investigate possible deleterious effects of SAHA derivative, Sq, in zebrafish. We successfully optimized MALDI MSI protocol to study Sq tissue distribution and metabolism, demonstrating that this strategy can enhance currently available methods to study the metabolic fate and distribution of clinically used and new candidate drugs.

In particular, we found that Sq via waterborne exposure did not induce any visible toxicity, while via 800  $\mu$ M injection caused developmental toxicity. However, Sq after 1600  $\mu$ M injection produced lethal toxicity. MALDI MSI analyses showed the spatial distribution of Sq after treatment and revealed a potential metabolite — Sq-glu.

Following 24 h of Sq administration, it was mainly distributed throughout the yolk. After 48 and 72 h of Sq injection, it was absent from larvae tissues. Sq-glu was detected mainly in the gut after 24 h of Sq treatment and eliminated within 72 hpi.

Based on the results obtained from waterborne treatment, Sq appears not to be toxic at the highest concentrations tested here, because the compound did not reach the larva body. These results are in accordance with recent publications where distinct distribution patterns were observed between the larval body and the yolk following waterborne exposure. This was accomplished by separating the yolk from the body and analyzing compound concentrations using either LC–MS [51] or radioactivity analyses [52]. In this study, we evaluated the distribution profile of Sq for the first time by combining a zebrafish safety study with MSI and a zebrafish xenograft model. A partition coefficient ( $\log P$ ) of Sq is 0.921 which favors its absorption and trapping by the lipid-rich yolk [51-53]. This prevents it from reaching the bloodstream at detectable concentrations as shown here by MALDI MSI analysis. To further assess if Sq reached the circulatory system at therapeutic concentrations lower than the detection limit, a zebrafish xenograft model was used. Xenografted larvae treated with 1000  $\mu\text{M}$  Sq showed no significant differences in tumor mass area in comparison to the control group treated with DMSO 1 %. These results confirm that although Sq was distributed throughout the yolk, it did not reach the larva body at therapeutic concentrations. Hence, understanding the distribution pattern is crucial to avoid overestimating compound concentrations in the larva body.

Sq is a novel hybrid molecule based on primaquine and SAHA motifs [42]. To gain a better insight into potential metabolites, we assessed the metabolism of both primaquine and SAHA. Primaquine undergoes oxidative deamination to carboxyprimaquine, its main metabolite. This is also the major metabolite in mice [54], dogs [55] and primates [56]. Other than carboxyprimaquine, thirty-four metabolites can be detected in humans. They include products of direct glucuronidation of primaquine and hydroxylation of the quinoline ring, however, these metabolites are formed to a lesser extent [50]. SAHA has two main metabolites - SAHA-glucuronide and 4-anilino-4-oxobutanoic acid [57]. SAHA-glucuronide is formed after direct glucuronidation by the UDP-glucuronosyltransferase (UGT) family of enzymes, whereas the enzymes involved in the formation of 4-anilino-4-oxobutanoic acid are still unknown [49].

The only potential Sq metabolite detected was the glucuronidated form. This was probably due to the presence of the OH-group in its active moiety (hydroxamic acid), making phase II (conjugative) metabolism more favorable than phase I (oxidative) [58]. The glucuronidated form was also present in the metabolism of SAHA, a drug bearing the same pharmacophore, i.e., hydroxamic acid. In comparison to primaquine, which is mostly metabolised at its terminal amine group, the nitrogen present in the Sq's structure forms an amide bond and cannot undergo oxidative deamination. In addition, zebrafish have glucuronidation enzymes (UGT) [59] and they are biologically active at a very early stages of larval development [58].

It has previously been shown that adult zebrafish glucuronidation enzymes are present in the liver, intestine, brain and gonads [60]. However, MALDI MSI results showed, for the first time, that larvae Sq-glu was mainly formed in the intestine and slightly in YSL. Therefore, we believe that after waterborne exposure a small portion of Sq can be glucuronidated in the YSL while it is absorbed from media to the yolk. These results are consistent with another study done in Medaka embryos (another teleost fish) suggesting that the YSL has the ability to perform phase II (sulfation and glucuronidation) metabolism reactions [61]. These findings are critical to explain the presence of different metabolites depending on administration routes, in some cases as shown by Park et al. [62]. Future studies using waterborne treatment should consider the YSL metabolic activity and its effects on xenobiotic metabolism after waterborne administration.

We assume that the majority of Sq is absorbed from the media without glucuronide conjugation. Sq is then translocated from the yolk to the gastrointestinal tract, in a similar way to fatty acids reabsorption from yolk to gut [63, 64]. Finally, Sq is mainly metabolized in the gastrointestinal tract that features high expression of glucuronidation enzymes (Ugt1a and Ugt1b) from 3 to 5 dpf [60]. The larval elimination pathway discovered here was further supported by the results from MALDI MSI following IV injection. After Sq yolk-enrichment at 1 dpi, the majority of Sq was translocated to the newly formed guts to be metabolized and stored until the gastrointestinal tract is completely open (4 dpf, 2 dpi) [65, 66], and can be excreted. Hence, by 3 dpi, Sq was mostly excreted as Sq-glu and not detected. This translocation process from yolk to gut

represents a distinct protection mechanism that enables larvae to eliminate xenobiotics after accumulating them in the yolk.

To ensure accurate dose delivery to the bloodstream, larvae were microinjected with 800  $\mu\text{M}$  of Sq in the common cardinal vein. Although Sq distributed throughout blood vessels after IV injection, it did not cause lethal toxicity or phenotypic abnormalities. At 24 hpi, Sq did not accumulate in any vital organs and it was generally detected in the yolk. However, larvae injected with 800  $\mu\text{M}$  of Sq were shorter than control larvae injected with 2 nl of DMSO. This delay in development can be explained for the first time according to the MALDI MSI data by the fact that Sq after a single injection is enriched in the yolk. Sq enrichment in the yolk disturbs the absorption of nutrients needed for larval growth, leading to larvae malnutrition and late development. These findings are in contrast to waterborne treatment where Sq's gradual uptake led to gradual enrichment in the yolk. Hence, it did not affect nutrient uptake remarkably and caused no obvious reduction of body growth.

We also investigated Sq toxicity at a higher concentration (1600  $\mu\text{M}$ ) and found that Sq caused severe abnormalities leading to 100 % lethality compared to the control group injected with 4 nl of DMSO. Injection of DMSO at this large volume is expected to induce minor toxicity. However, Sq injections (1600  $\mu\text{M}$ ) caused lethal toxicity.

Interestingly, the yolk was not depleted in all Sq-treated larvae, indicating a severe interruption in nutrients utilization. These findings can be explained by the possibility of an excessive accumulation of Sq in the yolk after IV injection in high concentration. Sq

accumulation impairs yolk absorption and leads to a starvation environment which can result in larval death [53].

Taken together, these results suggest that Sq has a good safety profile in concentrations around 40x higher than those needed for in vitro anticancer effect using zebrafish larvae models. We show that MALDI MSI applied in a zebrafish safety studies provides the means of better understanding xenobiotics distribution and their potential consequences on species in the aquatic environment. MALDI MSI data showed a potential Sq metabolite. To confirm this finding, complementary toxicokinetic studies are needed. Toxicokinetic approaches using highly sensitive LC-MS/MS [67] may confirm the presence of Sq-glu and possibly identify other metabolites that were not detected by MALDI-TOF MSI. Future studies will be needed after confirming Sq metabolites, to assess the anticancer activity of Sq using zebrafish tumor-bearing transgenic model [68]. Additional animal models may be required to further study Sq safety and effectiveness.

## **Declarations**

Conflicts of interest: The authors have no conflicts of interest.

Ethics approval: Ethics approval for experimentation reported herein was obtained from the Animal compliance office (McGill University) protocol #7438.

Funding: This work was supported by NSERC Discovery grant RGPIN-2015-06768 (SR) and RGPIN-2020-07011 (DM). SR is supported by a Chercheur-Boursier Senior salary award from the Fonds de Recherche du Québec – Santé. MA has been supported by awards from the Dep. Of Pharmacology and Experimental therapeutics - McGill University, the Faculty of Medicine - McGill University and the Research Institute of the McGill University Health Centre (RI-MUHC).

Availability of data and material: All data generated or analyzed during this study are included in this article and electronic supplementary information files.

## 4.6 References

1. Li AP. Accurate prediction of human drug toxicity: a major challenge in drug development. *Chemico-Biological Interactions*. 2004;150(1):3-7.
2. Parng C, Seng WL, Semino C, McGrath P. Zebrafish: A Preclinical Model for Drug Screening. *ASSAY and Drug Development Technologies*. 2002;1(1):41-8.
3. Pritchard JF, Jurima-Romet M, Reimer MLJ, Mortimer E, Rolfe B, Cayen MN. Making Better Drugs: Decision Gates in Non-Clinical Drug Development. *Nature Reviews Drug Discovery*. 2003;2(7):542-53.
4. DiMasi JA, Hansen RW, Grabowski HG. The price of innovation: new estimates of drug development costs. *Journal of Health Economics*. 2003;22(2):151-85.

5. Paul SM, Mytelka DS, Dunwiddie CT, Persinger CC, Munos BH, Lindborg SR, et al. How to improve R&D productivity: the pharmaceutical industry's grand challenge. *Nature Reviews Drug Discovery*. 2010;9(3):203-14.
6. Teame T, Zhang Z, Ran C, Zhang H, Yang Y, Ding Q, et al. The use of zebrafish (*Danio rerio*) as biomedical models. *Animal Frontiers*. 2019;9(3):68-77.
7. Gomes MC, Mostowy S. The Case for Modeling Human Infection in Zebrafish. *Trends in Microbiology*. 2020;28(1):10-8.
8. Carmona-Aldana F, Nuñez-Martinez HN, Peralta-Alvarez CA, Tapia-Urzua G, Recillas-Targa F. Generation of Functional Genetic Study Models in Zebrafish Using CRISPR-Cas9. In: Robles-Flores M, editor. *Cancer Cell Signaling: Methods and Protocols*. New York, NY: Springer US; 2021. p. 255-62.
9. Cassar S, Adatto I, Freeman JL, Gamse JT, Iturria I, Lawrence C, et al. Use of Zebrafish in Drug Discovery Toxicology. *Chem Res Toxicol*. 2020;33(1):95-118.
10. MacRae CA, Peterson RT. Zebrafish as tools for drug discovery. *Nature Reviews Drug Discovery*. 2015;14(10):721-31.
11. Howe K, Clark MD, Torroja CF, Torrance J, Berthelot C, Muffato M, et al. The zebrafish reference genome sequence and its relationship to the human genome. *Nature*. 2013;496(7446):498-503.
12. Spitsbergen JM, Kent ML. The State of the Art of the Zebrafish Model for Toxicology and Toxicologic Pathology Research—Advantages and Current Limitations. *Toxicol Pathol*. 2003;31(1\_suppl):62-87.

13. Lessman CA. The developing zebrafish (*Danio rerio*): A vertebrate model for high-throughput screening of chemical libraries. *Birth Defects Research Part C: Embryo Today: Reviews*. 2011;93(3):268-80.
14. Rubinstein AL. Zebrafish: from disease modeling to drug discovery. *Current Opinion in Drug Discovery and Development*. 2003;6(2):218-23.
15. Veinotte CJ, Dellaire G, Berman JN. Hooking the big one: the potential of zebrafish xenotransplantation to reform cancer drug screening in the genomic era. *Dis Model Mech*. 2014;7(7):745-54.
16. Tonon F, Zennaro C, Dapas B, Carraro M, Mariotti M, Grassi G. Rapid and cost-effective xenograft hepatocellular carcinoma model in Zebrafish for drug testing. *International Journal of Pharmaceutics*. 2016;515(1):583-91.
17. Zhang B, Shimada Y, Kuroyanagi J, Nishimura Y, Umemoto N, Nomoto T, et al. Zebrafish xenotransplantation model for cancer stem-like cell study and high-throughput screening of inhibitors. *Tumor Biology*. 2014;35(12):11861-9.
18. Konantz M, Balci TB, Hartwig UF, Dellaire G, André MC, Berman JN, et al. Zebrafish xenografts as a tool for in vivo studies on human cancer. *Annals of the New York Academy of Sciences*. 2012;1266(1):124-37.
19. de Souza Anselmo C, Sardela VF, de Sousa VP, Pereira HMG. Zebrafish (*Danio rerio*): A valuable tool for predicting the metabolism of xenobiotics in humans? *Comparative Biochemistry and Physiology Part C: Toxicology & Pharmacology*. 2018;212:34-46.
20. Hung MW, Zhang ZJ, Li S, Lei B, Yuan S, Cui GZ, et al. From Omics to Drug Metabolism and High Content Screen of Natural Product in Zebrafish: A New Model for

Discovery of Neuroactive Compound. Evidence-Based Complementary and Alternative Medicine. 2012;2012:605303.

21. Quinlivan VH, Farber SA. Lipid Uptake, Metabolism, and Transport in the Larval Zebrafish. 2017;8(319).

22. Carvalho L, Heisenberg C-P. The yolk syncytial layer in early zebrafish development. Trends in Cell Biology. 2010;20(10):586-92.

23. Berghmans S, Butler P, Goldsmith P, Waldron G, Gardner I, Golder Z, et al. Zebrafish based assays for the assessment of cardiac, visual and gut function — potential safety screens for early drug discovery. Journal of Pharmacological and Toxicological Methods. 2008;58(1):59-68.

24. Hill AJ, Teraoka H, Heideman W, Peterson RE. Zebrafish as a Model Vertebrate for Investigating Chemical Toxicity. Toxicological Sciences. 2005;86(1):6-19.

25. Milan David J, Peterson Travis A, Ruskin Jeremy N, Peterson Randall T, MacRae Calum A. Drugs That Induce Repolarization Abnormalities Cause Bradycardia in Zebrafish. Circulation. 2003;107(10):1355-8.

26. Bhusnure OG, Mane JM, Gholve SB, Thonte SS, Giram PS. Drug target screening and its validation by zebrafish as a novel tool. Pharm Anal Acta. 2015;6(426):10-4172.

27. Zon LI, Peterson RT. In vivo drug discovery in the zebrafish. Nature Reviews Drug Discovery. 2005;4(1):35-44.

28. Bugel SM, Tanguay RL, Planchart A. Zebrafish: A Marvel of High-Throughput Biology for 21st Century Toxicology. Curr Environ Health Rep. 2014;1(4):341-52.

29. Prideaux B, Stoeckli M. Mass spectrometry imaging for drug distribution studies. Journal of Proteomics. 2012;75(16):4999-5013.

30. Aichler M, Walch A. MALDI Imaging mass spectrometry: current frontiers and perspectives in pathology research and practice. *Laboratory Investigation*. 2015;95(4):422-31.
31. Kirla KT, Groh KJ, Poetzsch M, Banote RK, Stadnicka-Michalak J, Eggen RIL, et al. Importance of Toxicokinetics to Assess the Utility of Zebrafish Larvae as Model for Psychoactive Drug Screening Using Meta-Chlorophenylpiperazine (mCPP) as Example. *Front Pharmacol*. 2018;9:414-.
32. Walch A, Rauser S, Deininger S-O, Höfler H. MALDI imaging mass spectrometry for direct tissue analysis: a new frontier for molecular histology. *Histochemistry and Cell Biology*. 2008;130(3):421.
33. Kirla KT, Groh KJ, Steuer AE, Poetzsch M, Banote RK, Stadnicka-Michalak J, et al. From the Cover: Zebrafish Larvae Are Insensitive to Stimulation by Cocaine: Importance of Exposure Route and Toxicokinetics. *Toxicological Sciences*. 2016;154(1):183-93.
34. Reyzer ML, Caprioli RM. MALDI-MS-based imaging of small molecules and proteins in tissues. *Current Opinion in Chemical Biology*. 2007;11(1):29-35.
35. Dueñas ME, Essner JJ, Lee YJ. 3D MALDI Mass Spectrometry Imaging of a Single Cell: Spatial Mapping of Lipids in the Embryonic Development of Zebrafish. *Scientific Reports*. 2017;7(1):14946.
36. Villacrez M, Hellman K, Ono T, Sugihara Y, Rezeli M, Ek F, et al. Evaluation of Drug Exposure and Metabolism in Locust and Zebrafish Brains Using Mass Spectrometry Imaging. *ACS Chemical Neuroscience*. 2018;9(8):1994-2000.

37. Castellino S, Groseclose MR, Wagner D. MALDI imaging mass spectrometry: bridging biology and chemistry in drug development. *Bioanalysis*. 2011;3(21):2427-41.
38. Prideaux B, Lenaerts A, Dartois V. Imaging and spatially resolved quantification of drug distribution in tissues by mass spectrometry. *Current Opinion in Chemical Biology*. 2018;44:93-100.
39. McLaughlin N, Bielinski TM, Tressler CM, Barton E, Glunde K, Stumpo KA. Pneumatically Sprayed Gold Nanoparticles for Mass Spectrometry Imaging of Neurotransmitters. *Journal of the American Society for Mass Spectrometry*. 2020;31(12):2452-61.
40. Buchberger AR, DeLaney K, Johnson J, Li L. Mass Spectrometry Imaging: A Review of Emerging Advancements and Future Insights. *Analytical Chemistry*. 2018;90(1):240-65.
41. Zhang I, Beus M, Stochaj U, Le PU, Zorc B, Rajić Z, et al. Inhibition of glioblastoma cell proliferation, invasion, and mechanism of action of a novel hydroxamic acid hybrid molecule. *Cell Death Discov*. 2018;4:41-.
42. Beus M, Rajić Z, Maysinger D, Mlinarić Z, Antunović M, Marijanović I, et al. SAHAQuines, Novel Hybrids Based on SAHA and Primaquine Motifs, as Potential Cytostatic and Antiplasmodial Agents. *ChemistryOpen*. 2018;7(8):624-38.
43. Lawrence C. The husbandry of zebrafish (*Danio rerio*): A review. *Aquaculture*. 2007;269(1):1-20.
44. Kimmel CB, Ballard WW, Kimmel SR, Ullmann B, Schilling TF. Stages of embryonic development of the zebrafish. *Developmental Dynamics*. 1995;203(3):253-310.

45. Hallare A, Nagel K, Köhler H-R, Triebkorn R. Comparative embryotoxicity and proteotoxicity of three carrier solvents to zebrafish (*Danio rerio*) embryos. *Ecotoxicology and Environmental Safety*. 2006;63(3):378-88.
46. Dannhorn A, Kazanc E, Ling S, Nikula C, Karali E, Serra MP, et al. Universal Sample Preparation Unlocking Multimodal Molecular Tissue Imaging. *Analytical Chemistry*. 2020;92(16):11080-8.
47. Calvano CD, Capozzi MAM, Punzi A, Farinola GM, Cataldi TRI, Palmisano F. 1,5-Diaminonaphtalene is a Highly Performing Electron-Transfer Secondary-Reaction Matrix for Laser Desorption Ionization Mass Spectrometry of Indolenine-Based Croconaines. *ACS Omega*. 2018;3(12):17821-7.
48. Sharifi Z, Abdulkarim B, Meehan B, Rak J, Daniel P, Schmitt J, et al. Mechanisms and Antitumor Activity of a Binary EGFR/DNA–Targeting Strategy Overcomes Resistance of Glioblastoma Stem Cells to Temozolomide. *Clinical Cancer Research*. 2019;25(24):7594.
49. Balliet RM, Chen G, Gallagher CJ, Dellinger RW, Sun D, Lazarus P. Characterization of UGTs active against SAHA and association between SAHA glucuronidation activity phenotype with UGT genotype. *Cancer Res*. 2009;69(7):2981-9.
50. Avula B, Tekwani BL, Chaurasiya ND, Fasinu P, Dhammika Nanayakkara NP, Bhandara Herath HMT, et al. Metabolism of primaquine in normal human volunteers: investigation of phase I and phase II metabolites from plasma and urine using ultra-high performance liquid chromatography-quadrupole time-of-flight mass spectrometry. *Malaria Journal*. 2018;17(1):294.

51. Halbach K, Ulrich N, Goss K-U, Seiwert B, Wagner S, Scholz S, et al. Yolk Sac of Zebrafish Embryos as Backpack for Chemicals? *Environmental Science & Technology*. 2020;54(16):10159-69.
52. Souder JP, Gorelick DA. Quantification of Estradiol Uptake in Zebrafish Embryos and Larvae. *Toxicological Sciences*. 2017;158(2):465-74.
53. Sant KE, Timme-Laragy AR. Zebrafish as a Model for Toxicological Perturbation of Yolk and Nutrition in the Early Embryo. *Curr Environ Health Rep*. 2018;5(1):125-33.
54. Avula B, Khan SI, Tekwani BL, Dhammika Nanayakkara NP, McChesney JD, Walker LA, et al. Analysis of primaquine and its metabolite carboxyprimaquine in biological samples: enantiomeric separation, method validation and quantification. *Biomedical Chromatography*. 2011;25(9):1010-7.
55. Nanayakkara NPD, Tekwani BL, Herath HMTB, Sahu R, Gettayacamin M, Tungtaeng A, et al. Scalable preparation and differential pharmacologic and toxicologic profiles of primaquine enantiomers. *Antimicrob Agents Chemother*. 2014;58(8):4737-44.
56. Saunders D, Vanachayangkul P, Imerbsin R, Khemawoot P, Siripokasupkul R, Tekwani BL, et al. Pharmacokinetics and pharmacodynamics of (+)-primaquine and (-)-primaquine enantiomers in rhesus macaques (*Macaca mulatta*). *Antimicrob Agents Chemother*. 2014;58(12):7283-91.
57. Du L, Musson DG, Wang AQ. High turbulence liquid chromatography online extraction and tandem mass spectrometry for the simultaneous determination of suberoylanilide hydroxamic acid and its two metabolites in human serum. *Rapid Communications in Mass Spectrometry*. 2005;19(13):1779-87.

58. Le Fol V, Brion F, Hillenweck A, Perdu E, Bruel S, Aït-Aïssa S, et al. Comparison of the In Vivo Biotransformation of Two Emerging Estrogenic Contaminants, BP2 and BPS, in Zebrafish Embryos and Adults. *Int J Mol Sci.* 2017;18(4):704.
59. van Wijk RC, Krekels EHJ, Hankemeier T, Spaink HP, van der Graaf PH. Systems pharmacology of hepatic metabolism in zebrafish larvae. *Drug Discovery Today: Disease Models.* 2016;22:27-34.
60. Christen V, Fent K. Tissue-, sex- and development-specific transcription profiles of eight UDP-glucuronosyltransferase genes in zebrafish (*Danio rerio*) and their regulation by activator of aryl hydrocarbon receptor. *Aquatic Toxicology.* 2014;150:93-102.
61. Hornung MW, Cook PM, Fitzsimmons PN, Kuehl DW, Nichols JW. Tissue Distribution and Metabolism of Benzo[a]pyrene in Embryonic and Larval Medaka (*Oryzias latipes*). *Toxicological Sciences.* 2007;100(2):393-405.
62. Park YM, Meyer MR, Müller R, Herrmann J. Drug Administration Routes Impact the Metabolism of a Synthetic Cannabinoid in the Zebrafish Larvae Model. *Molecules.* 2020;25(19).
63. Miyares RL, de Rezende VB, Farber SA. Zebrafish yolk lipid processing: a tractable tool for the study of vertebrate lipid transport and metabolism. *Disease Models & Mechanisms.* 2014;7(7):915.
64. García Hernández MP, Lozano MT, Elbal MT, Agulleiro B. Development of the digestive tract of sea bass (*Dicentrarchus labrax* L). Light and electron microscopic studies. *Anatomy and Embryology.* 2001;204(1):39-57.
65. Strähle U, Scholz S, Geisler R, Greiner P, Hollert H, Rastegar S, et al. Zebrafish embryos as an alternative to animal experiments—A commentary on the definition of the

onset of protected life stages in animal welfare regulations. *Reproductive Toxicology*. 2012;33(2):128-32.

66. Ng ANY, de Jong-Curtain TA, Mawdsley DJ, White SJ, Shin J, Appel B, et al. Formation of the digestive system in zebrafish: III. Intestinal epithelium morphogenesis. *Developmental Biology*. 2005;286(1):114-35.

67. Kantae V, Krekels EHJ, Ordas A, González O, van Wijk RC, Harms AC, et al. Pharmacokinetic Modeling of Paracetamol Uptake and Clearance in Zebrafish Larvae: Expanding the Allometric Scale in Vertebrates with Five Orders of Magnitude. *Zebrafish*. 2016;13(6):504-10.

68. Gutierrez A, Pan L, Groen RWJ, Baleyrier F, Kentsis A, Marineau J, et al. Phenothiazines induce PP2A-mediated apoptosis in T cell acute lymphoblastic leukemia. *The Journal of Clinical Investigation*. 2014;124(2):644-55.

#### **4.7 Supplementary data**

**Fig. S1**

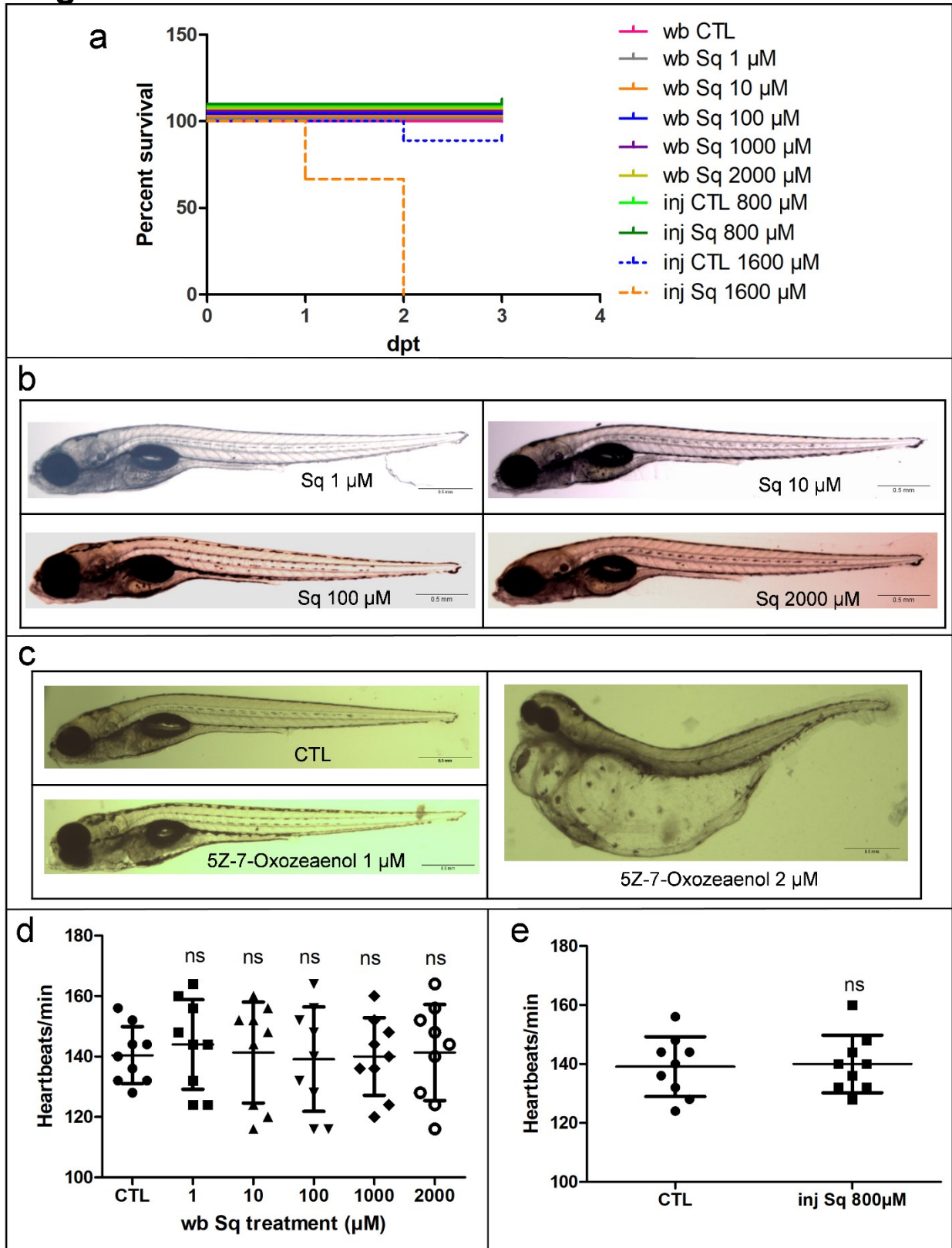


**Fig. S1 Evaluating zebrafish larvae survival, malformations and heartbeats rate, after Sahaquine treatment.** (a) Survival was assessed daily under an inverted microscope for 3 days of Sq treatment (n=9 in each group). Representative micrographs of 5 dpf zebrafish larvae (lateral position), following the administration of Sq (b) or the positive control 5Z-7-oxozeaenol (c) via waterborne starting at 2 dpf. Heartbeats were visually counted under an inverted microscope at 1 dpt, in both (d) waterborne and (e) 800  $\mu$ M injection experiments. Data presented as mean  $\pm$  SD with n=9 in each group (two-tailed Student's t-test). Waterborne (wb), injection (inj).

**Fig. S2**

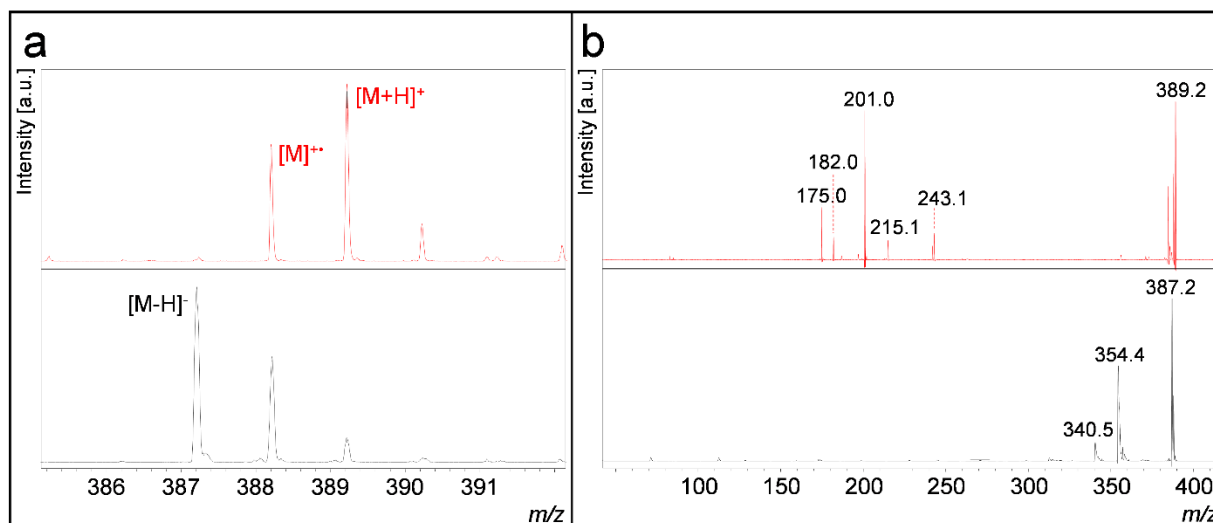


**Fig. S2 MS spectra of sahaquine in the positive (red) and negative (black) ion modes using DAN matrix (a) and corresponding MS/MS fragment ion patterns (b).**

**Fig. S3**

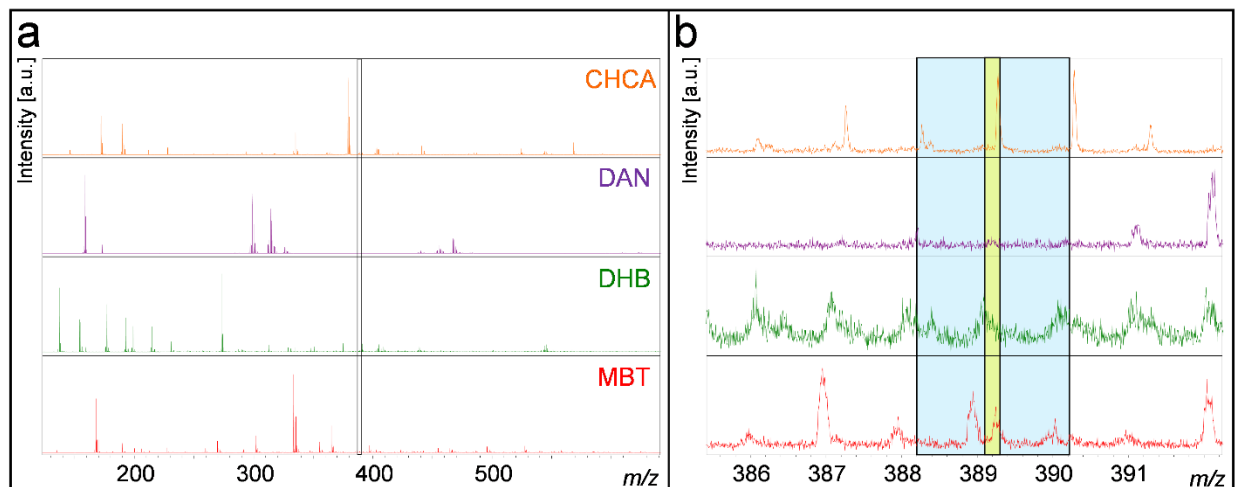


**Fig. S3 Evaluation of matrix interference for the detection of protonated sahaquine.**

(a) MS spectra overview in the low mass range with the different matrices. (b) Magnified spectra of protonated sahaquine at  $m/z\ 389.22 \pm 0.1$  (yellow rectangle) and MS/MS minimal detection window (blue rectangle). Matrix colors: CHCA (orange), DAN (purple), DHB (green) and MBT (red).

**Fig. S4**

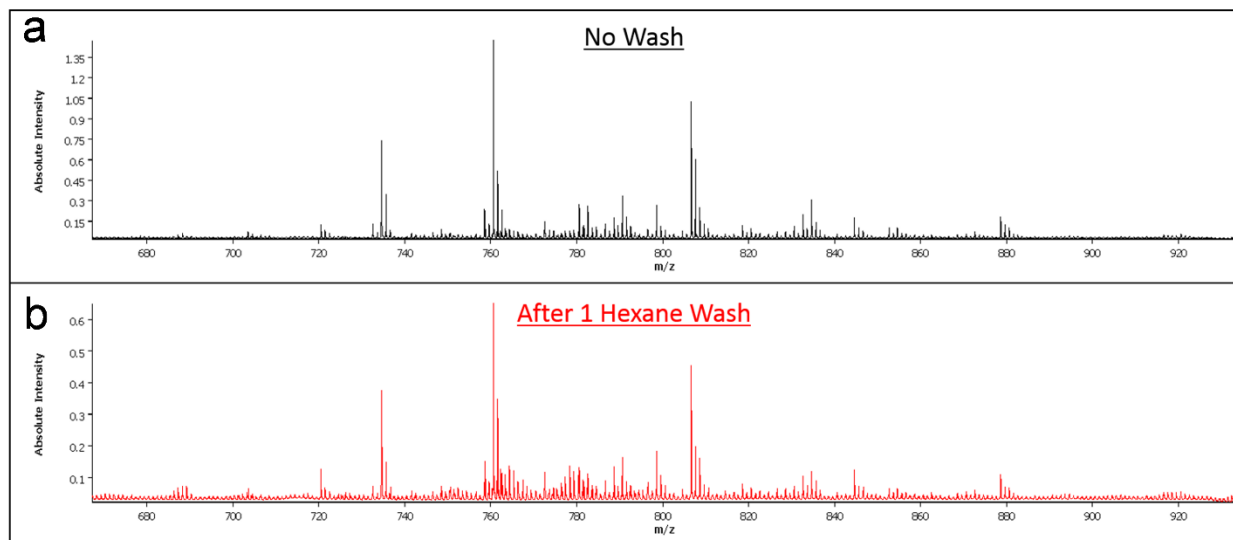


**Fig. S4 MS spectra of phospholipids in zebrafish larvae homogenate in a mass range of 680 to 920 Da using the DAN matrix in the positive ion mode before hexane wash (a) and after one hexane wash (b).**

**Fig. S5**

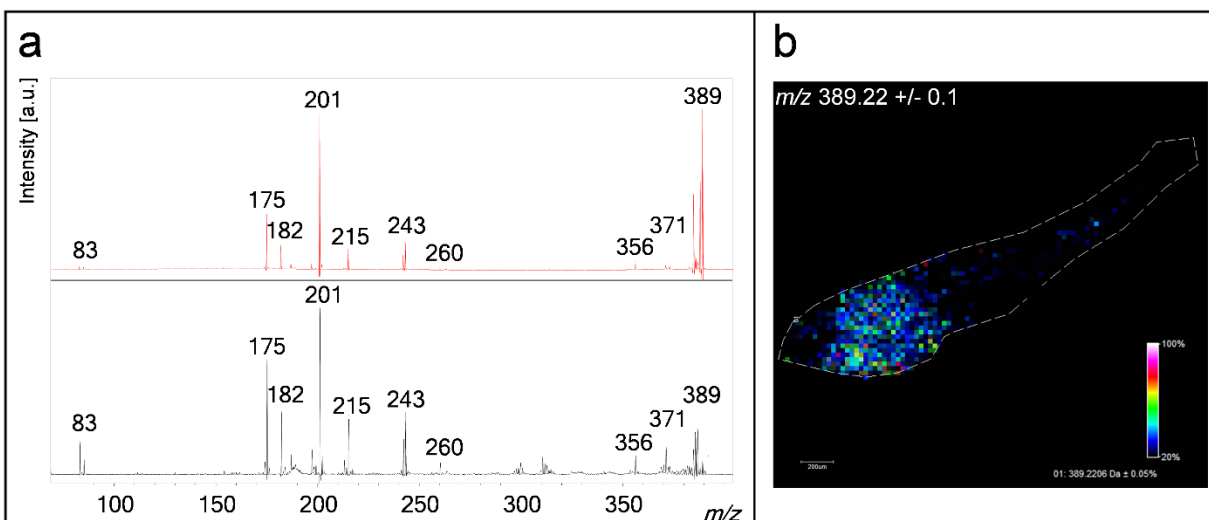


**Fig. S5 (a) MS/MS identification of sahaquine in the zebrafish larvae yolk (black spectrum) and its comparison to the standard off-tissue (red spectrum). (b) MSI distribution of sahaquine on-tissue.**

**Fig. S6**

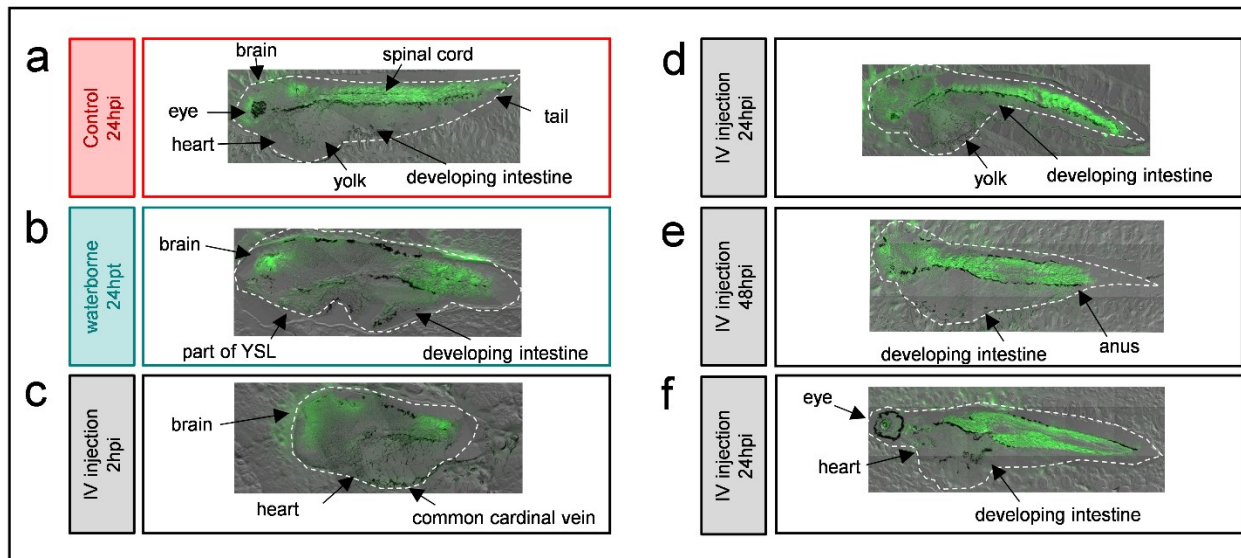


**Fig. S6 Auto-fluorescence images showing the anatomy of larvae tissue sections.**

**Fig. S7**

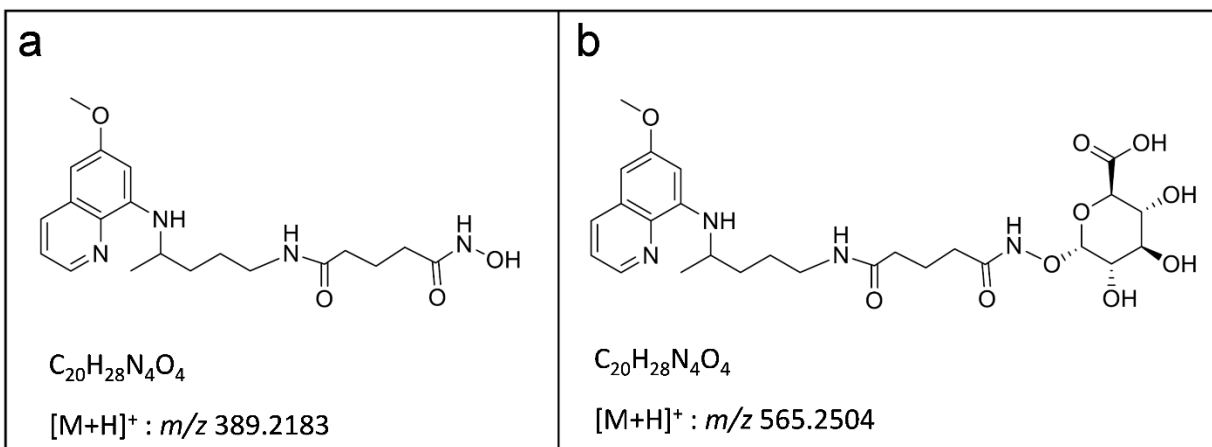


**Fig. S7 Molecular structures of (a) sahaquine and (b) sahaquine glucuronide, with their respective protonated m/z.**

**Fig. S8**

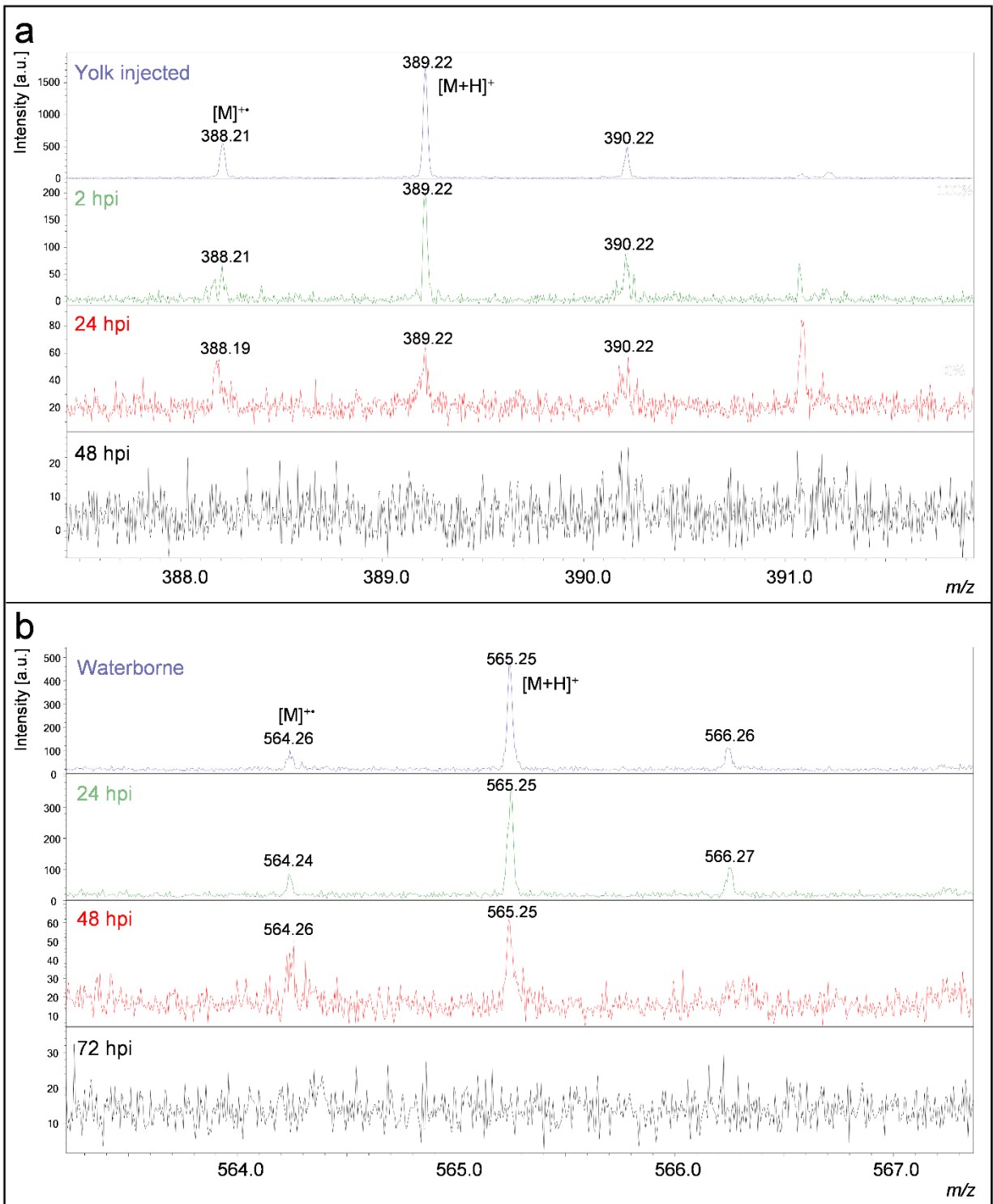


**Fig. S8 MS spectra of sahaquine (m/z 389.22) and sahaquine glucuronide (m/z 565.25).**

The similarities between both isotopic pattern ( $[M]^+\bullet / [M+H]^+$ ) and the exact mass were used for their on-tissue identification. (a) MS spectrum of sahaquine at high concentration after its injection in the yolk (blue), at medium concentration in the IV sample of 2 hpi (green), low concentration in the IV sample of 24 hpi (red) and their absence in the IV sample of 48 hpi (black). (b) MS spectrum of sahaquine glucuronide at high concentration in the waterborne sample (blue), at medium concentration for the IV sample of 24 hpi (green), at low concentration for the IV sample of 48 hpi (red) and their absence in the IV sample of 72 hpi (black).

**Fig. S9**

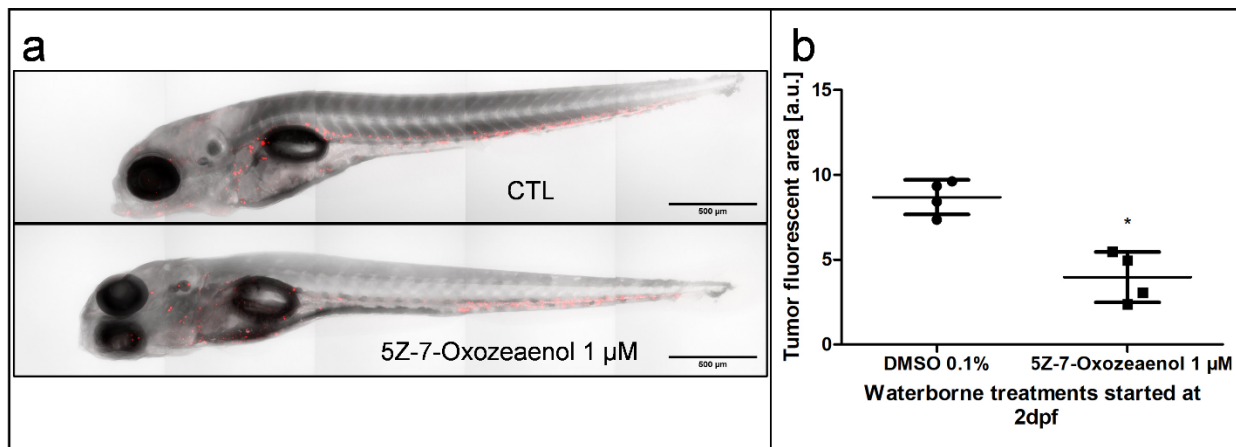


**Fig. S9 Assessing tumor mass after 5Z-7-oxozeaenol waterborne administration in zebrafish xenograft model.**

(a) Representative fluorescence z-stack images of 5 dpf zebrafish larvae, injected with fluorescently labeled OCI-LY2 lymphoma cells, and treated with DMSO 0.1 % (CTL) or 5Z-7-oxozeaenol (1  $\mu$ M) via waterborne exposure for 3 days. (b) Quantification of total fluorescence area at 3 dpt. Xenografted larvae were imaged with a confocal microscope, and fluorescence area was measured using ImageJ. Data presented as mean  $\pm$  SD with n=4 in each group (\*p < 0.05, two-tailed Student's t-test).

## Chapter 5: Scholarly Discussion and Conclusion

In this project, we studied the anti-lymphoma activity of both ERK1/2 pathway inhibitors including Compound 1 (TPL2 inhibitor) and PD184352 (MKK1/2 inhibitor), and HDAC6 inhibitors, namely Sahaquine (in-house inhibitor) and ACY1215 (commercial inhibitor) in immortalized non-Hodgkin B-cell lymphoma cell lines. Additionally, the combined effects of dual MKK1/2-HDAC6 inhibition was assessed and quantified *in vitro*. Finally, Sahaquine safety and metabolism was investigated in the zebrafish larvae model using optimized MALDI MSI protocol.

Results from this project show that single inhibition of either HDAC6 or ERK1/2 (via TPL2 or MKK1/2 inhibitors) can inhibit the growth of several B-cell NHL cell lines, namely DLBCL, Burkitt lymphoma, and Waldenstrom Macroglobulinemia (WM). The combination of HDAC6 and ERK1/2 inhibitors enhanced the single therapies cytostatic effects and induced cytotoxic effects (apoptosis) in the cell culture model. We propose the combination mechanisms of action to involve disrupting DNA damage response via targeting ARPC2 and SPNO1, in addition to reducing metabolic energy production by interfering with cathepsin D and ECH1 functions. Safety study in zebrafish larvae has indicated that Sahaquine was well tolerated and did not induce tissue-specific toxicity since it was metabolized to glucuronidated form and excreted, as shown by the optimized MALDI MSI protocol.

In this section, we will discuss

1. The modes of action involved in MKK1/2-HDAC6 combination cytotoxic effects based on the proteomic data analysis.

2 Mechanisms of resistance to NHL first line treatments as drug resistance is the major reason for treatment failure.

## **5.1 Mechanisms of action involved in cytotoxic effects of dual MKK1/2-HDAC6 inhibition**

Chemotherapies possess DNA-damaging properties enabling them to kill cancer cells. However, tumors can activate DNA repair responses to reduce the effectiveness of chemotherapy drugs [224]. The activity of DNA repairing proteins is controlled by post-translational modifications such as phosphorylation, ubiquitylation, and acetylation [225-227], in addition to sensor proteins that detect DNA damage, including poly (ADP-ribose) polymerase (PARP) [228]. Currently, the only FDA approved therapeutics targeting DNA damage response are PARP inhibitors [229]; however, after initial therapy, cancer cells can develop PARP inhibitor resistance [230]. Targeting other DNA repairing mechanisms is being investigated and tested in clinical trials [231].

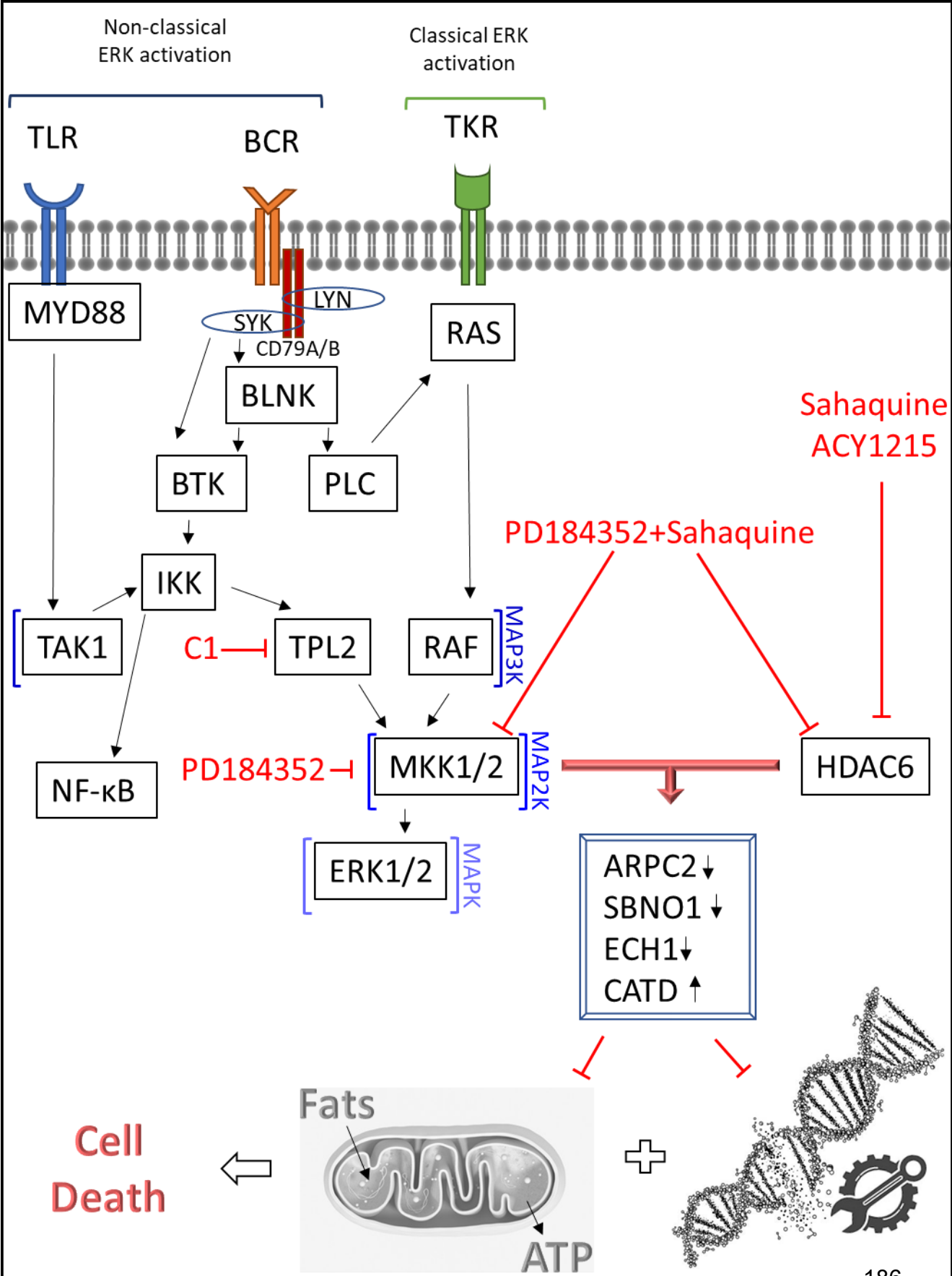
Interestingly, our study showed that dual MKK1/2-HDAC6 inhibition increased the acetylation of ARPC2, a protein that plays key roles in DNA damage repair [232]. Moreover, blocking MKK1/2-HDAC6 led to SBNO1 acetylation. SBNO1 is a novel transcriptional factor that belongs to the helicase superfamily 2, which is involved in development and likely contributes to DNA repair functions [233]. This modulation of

ARPC2 and SBNO1 acetylation probably inhibits DNA repair leading to cell death. Deeper investigation of ARPC2 and SBNO1 acetylation impact on DNA repair mechanisms is needed. For instance, to measure the efficiency of DNA repair mechanisms following dual MKK1/2-HDAC6 inhibition, cells can be transfected with DNA plasmids containing damaged DNA in the transcribed strand of EGFP. Then we will measure the intensity of EGFP expression levels, which is proportional to the DNA repair efficiency.

Failure in repairing damaged DNA induces apoptosis and stimulates cathepsin D activation, a lysosomal aspartic protease [234-237]. Cathepsin D can cleave and degrade functional and structural proteins such as cytoskeletal proteins including tubulin [238, 239]. Thus, we speculate that cathepsin D presence in the acetylation enrichment experiment is due to its conjugation with acetylated tubulin, as currently cathepsin D has no reported acetylation site. Moreover, the activation of cathepsin D negatively regulates lipid metabolism [240], which is a major pathway to generate energy [241].

Cancer cells need a sustained source of energy for their rapid growth, division, and survival. To meet this high energy demand, tumors alter their lipid metabolism to generate a larger quantity of ATP [242]. Fatty acid beta oxidation is the most energy-efficient metabolic pathway to produce ATP; therefore, cancer cells utilize it to satisfy their energy needs [243, 244]. Previous studies have shown that blocking lipid oxidation decreased cellular viability of several cancers, including hematologic malignancies [245-248]. Results from this project have revealed that the combination of PD184352 and Sahaquine targeted ECH1 protein which is involved in the fatty acid beta oxidation pathway [249], in addition to cathepsin D activation. Hence, it will be of

interest to study lipid metabolic fate following treatment with MKK1/2-HDAC6 inhibitors. For instance, to evaluate the abundance of fatty acids following the combined treatment, mass spectrometry approaches can be used, such as MALDI MSI or liquid chromatography. Technically, MALDI MSI requires less sample preparation compared to liquid chromatography. Hence basically, following treatment, intact cells will be collected and placed on indium tin oxide (ITO)-coated glass slides using the cytopsin technique. Then MALDI matrix technique will be applied and the slides will be analyzed. However, if absolute quantification is needed then liquid chromatography will be preferable, as MALDI MSI is usually used for relative quantification.



### **Mechanisms of action involved in cytotoxic effects of dual MKK1/2-HDAC6**

**inhibition.** Combined treatment with PD184352 (MKK1/2 inhibitor) and Sahaquinone (HDAC6 inhibitor) increased the acetylation levels of Actin-related protein 2/3 complex subunit 2 (ARPC2); Strawberry notch homolog 1 (SBNO1); and Delta(3,5)-Delta(2,4)-dienoyl-CoA isomerase mitochondrial (ECH1) leading to downregulation of their activities, in addition to activating Cathepsin D (CATD/CTSD). As a result, DNA damage response and fatty acid beta oxidation were interrupted, leading to cell death.

Mechanisms under this heading include Toll-like receptor (TLR); Myeloid differentiation primary response 88 (MYD88); TGF- $\beta$ -activated kinase 1 (TAK1); I $\kappa$ B kinase (IKK); Nuclear Factor  $\kappa$ B (NF- $\kappa$ B); B-cell receptor (BCR); Lck/Yes novel tyrosine kinase (LYN); Spleen tyrosine kinase (SYK); B-cell linker protein (BLNK); Bruton's tyrosine kinase (BTK); Phospholipase C (PLC); Rat sarcoma virus (RAS); Rapidly Accelerated Fibrosarcoma (RAF); Tumor Promoting Locus 2 (TPL2); Mitogen-activated protein kinase kinase 1 and 2 (MKK1/2); Extracellular signal-regulated kinase 1 and 2 (ERK1/2); and histone deacetylase 6 (HDAC6).

## **5.2 Mechanisms of resistance following NHL first line treatments**

NHLs develop resistance to first line treatment, which is a primary cause of treatment failure [250]. Resistance can arise by way of several mechanisms, including changes in drug influx or efflux pathways, alterations in drug targets or metabolism, activation of alternative signaling pathways, and influence of tumor microenvironment [251, 252].

The increase in drug efflux occurs via modulation of drug efflux pump activity such as P-glycoprotein, a multidrug resistance transporter belonging to the ATP-binding cassette family [253]. P-glycoprotein is overexpressed in the subpopulation of NHL patients [254]; therefore, targeting P-glycoprotein activity can enhance therapeutic responses. Previously, P-glycoprotein inhibitors such as primaquine (anti-malarial drug) sensitized malignant cells to anti-cancer treatments [255]. Sahaquine contains the primaquine group in its structure; therefore it has an inhibitory effect on P-glycoprotein [198], which probably increases its biological activity and reduces the risk of drug resistance.

Another resistance factor is the tumor microenvironment, which has immunosuppressive properties that enable malignant cells to evade immune detection [256]. The rapid growth of tumor cells creates hypoxia, oxidative stress, and acidosis in a tumor microenvironment [257], leading to chronic inflammation [258] which affects components of the tumor microenvironment, including immune cells (T and B lymphocytes, natural killer cells, and Tumor-associated macrophages); stromal cells (fibroblasts, mesenchymal stromal cells, blood and lymphatic vascular networks); and the extracellular matrix [257].

Chronic inflammation exhausts T cells, leading them to lose effector functions and the expression of multiple inhibitory receptors such as programmed cell death protein 1 (PD1); T-cell immunoglobulin and mucin-domain containing protein 3 (TIM3); Cytotoxic T-lymphocyte antigen 4 (CTLA4); and lymphocyte-activation gene 3 (LAG3) on their surface [259]. The state of T cell exhaustion contributes to tumor microenvironment immune suppression. Therefore, restoring antitumor immune responses is a crucial step towards the development of more efficient NHL therapies. Currently, several

immunotherapeutic approaches are available to target B-cell NHL, including antibody and cellular immunotherapies [260, 261]. We believe that combining immunotherapies with dual MKK1/2-HDAC6 inhibition will play a complementary role in boosting antitumor immune responses. This triple combination can reduce T cell exhaustion by decreasing the levels of inflammatory cytokines in a tumor microenvironment as a result of ERK1/2 inhibition because ERK1/2 plays an essential role downstream of immune receptors to stimulate inflammatory gene expression in response to infection or cellular damage. Further studies should investigate the addition of Immunotherapy to MKK1/2-HDAC6 inhibitors in order to improve the therapeutic efficacy of the PD184352 and Sahaquine combination.

## **Limitations and future directions**

A number of limitations and future directions have already been mentioned throughout this thesis with respect to our focus of study. Herein we also studied the anti-lymphoma activity of several SMIs, namely Compound 1 (TPL2 inhibitor), PD184352 (MKK1/2 inhibitor), Sahaquine (HDAC6 inhibitor), and ACY1215 (HDAC6 inhibitor) alone or in combination using a cell culture model which itself has several limitations. One of the main limitations of cell culture is the absence of tumor microenvironment interaction. Therefore, it will be of interest to test these single or dual therapies in animal models to reflect the complex roles of interaction with such a microenvironment. If promising results are obtained, it will be ideal to test this combination in B cell NHL patients, knowing that safety information from previous clinical trials is already available for

PD184352 and ACY1215, in addition to Sahaquine preliminary safety information, which can accelerate the phase of drug development.

This work illustrated that the combination of MEK1/2 and HDAC6 inhibitors induced killing effects by interfering with ARPC2, SBNO1, CATD, and ECH1 proteins. Therefore, studying the roles of these proteins in B cell NHL pathogenesis and progression merits future investigations as they can be potential targets for therapeutic interventions in lymphoma treatment. One possible strategy to evaluate the effects of these proteins on malignant B cell survival is by a systematic knockout of these genes using the LentiCRISPR/Cas9 system, as these cells are hard to transfect by non-viral techniques such as calcium phosphate exposure, electroporation, and liposome-based transfection. Gene knockout results will be confirmed by T7 Endonuclease I (T7E1) mutation mismatch assay followed with PCR. T7E1 assay is a precise method to recognize and cleave imperfectly matched DNA, resulting from CRISPR indel mutations, as sometimes the indel mutations will not significantly change the product size to be detected by PCR alone.

## **Conclusion**

This project enhances our knowledge of the roles of the TPL2-ERK1/2 pathway and HDAC6 activity in B cell NHL proliferation and survival. Moreover, it emphasizes the importance of targeting multiple oncogenic pathways as a preferable strategy compared to monotherapies as a means of effectively eliminating malignant cells.

The MALDI MSI technique combined with zebrafish larvae safety studies represents a powerful approach to studying SMI safety and metabolism in vertebrate models for rapid SMI development.

The promising results enumerated herein raise hopes that dual ERK1/2-HDAC6 inhibition can achieve clinical activity. Therefore, it can be a potential therapeutic strategy for B cell NHL patients.

## Reference list

1. Kubik S. The Anatomy of the Lymphatic System. In: Musshoff K, editor. *Diagnosis and Therapy of Malignant Lymphoma*. Berlin, Heidelberg: Springer Berlin Heidelberg; 1974. p. 5-17.
2. Alitalo K, Carmeliet P. Molecular mechanisms of lymphangiogenesis in health and disease. *Cancer Cell*. 2002;1(3):219-27.
3. Ling K-W, Dzierzak E. Ontogeny and genetics of the hemato/lymphopoietic system. *Current Opinion in Immunology*. 2002;14(2):186-91.
4. Melchers F, Jüvelier H. Checkpoints that control B cell development. *Nature Reviews Immunology*. 2015;15(6):2203-10.
5. Janeway Jr CA, Travers P, Walport M, Shlomchik MJ. *The components of the immune system*. Immunobiology: The Immune System in Health and Disease 5th edition: Garland Science; 2001.
6. Shaffer AL, Rosenwald A, Staudt LM. Lymphoid Malignancies: the dark side of B-cell differentiation. *Nature Reviews Immunology*. 2002;2(12):920-33.
7. Burger JA, Wiestner A. Targeting B cell receptor signalling in cancer: preclinical and clinical advances. *Nature Reviews Cancer*. 2018;18(3):148-67.
8. Küppers R. The biology of Hodgkin's lymphoma. *Nature Reviews Cancer*. 2009;9(1):15-27.
9. Küppers R. Mechanisms of B-cell lymphoma pathogenesis. *Nature Reviews Cancer*. 2005;5(4):251-62.

10. Klein U, Dalla-Favera R. Germinal centres: role in B-cell physiology and malignancy. *Nature Reviews Immunology*. 2008;8(1):22-33.
11. Young RM, Shaffer AL, 3rd, Phelan JD, Staudt LM. B-cell receptor signaling in diffuse large B-cell lymphoma. *Seminars in hematology*. 2015;52(2):77-85.
12. Roco JA, Mesin L, Binder SC, Nefzger C, Gonzalez-Figueroa P, Canete PF, et al. Class-Switch Recombination Occurs Infrequently in Germinal Centers. *Immunity*. 2019;51(2):337-50.e7.
13. Young RM, Staudt LM. Targeting pathological B cell receptor signalling in lymphoid malignancies. *Nature Reviews Drug Discovery*. 2013;12(3):229-43.
14. Davis RE, Ngo VN, Lenz G, Tolar P, Young RM, Romesser PB, et al. Chronic active B-cell-receptor signalling in diffuse large B-cell lymphoma. *Nature*. 2010;463(7277):88-92.
15. Gauld SB, Cambier JC. Src-family kinases in B-cell development and signaling. *Oncogene*. 2004;23(48):8001-6.
16. Dal Porto JM, Gauld SB, Merrell KT, Mills D, Pugh-Bernard AE, Cambier J. B cell antigen receptor signaling 101. *Molecular Immunology*. 2004;41(6):599-613.
17. Wen T, Wang J, Shi Y, Qian H, Liu P. Inhibitors targeting Bruton's tyrosine kinase in cancers: drug development advances. *Leukemia*. 2021;35(2):312-32.
18. Jacob A, Cooney D, Pradhan M, Coggeshall KM. Convergence of Signaling Pathways on the Activation of ERK in B Cells\*. *Journal of Biological Chemistry*. 2002;277(26):23420-6.
19. Kaminski D, Wei C, Qian Y, Rosenberg A, Sanz I. Advances in Human B Cell Phenotypic Profiling. 2012;3.
20. Sanz I, Wei C, Jenks SA, Cashman KS, Tipton C, Woodruff MC, et al. Challenges and Opportunities for Consistent Classification of Human B Cell and Plasma Cell Populations. 2019;10.
21. Morgan D, Tergaonkar VJ. Unraveling B cell trajectories at single cell resolution. 2022.
22. Connors JM, Cozen W, Steidl C, Carbone A, Hoppe RT, Flechtner H-H, et al. Hodgkin lymphoma. *Nature Reviews Disease Primers*. 2020;6(1):61.
23. Zhang J, Grubor V, Love CL, Banerjee A, Richards KL, Mieczkowski PA, et al. Genetic heterogeneity of diffuse large B-cell lymphoma. 2013;110(4):1398-403.
24. De Paepe P, De Wolf-Peeters C. Diffuse large B-cell lymphoma: a heterogeneous group of non-Hodgkin lymphomas comprising several distinct clinicopathological entities. *Leukemia*. 2007;21(1):37-43.
25. Bakhshi TJ, Georgel PT. Genetic and epigenetic determinants of diffuse large B-cell lymphoma. *Blood Cancer Journal*. 2020;10(12):123.
26. Pasqualucci L, Trifonov V, Fabbri G, Ma J, Rossi D, Chiarenza A, et al. Analysis of the coding genome of diffuse large B-cell lymphoma. *Nature Genetics*. 2011;43(9):830-7.
27. Morin RD, Mendez-Lago M, Mungall AJ, Goya R, Mungall KL, Corbett RD, et al. Frequent mutation of histone-modifying genes in non-Hodgkin lymphoma. *Nature*. 2011;476(7360):298-303.
28. Lohr JG, Stojanov P, Lawrence MS, Auclair D, Chapuy B, Sougnez C, et al. Discovery and prioritization of somatic mutations in diffuse large B-cell lymphoma (DLBCL) by whole-exome sequencing. 2012;109(10):3879-84.

29. Pasqualucci L, Dominguez-Sola D, Chiarenza A, Fabbri G, Grunn A, Trifonov V, et al. Inactivating mutations of acetyltransferase genes in B-cell lymphoma. *Nature*. 2011;471(7337):189-95.
30. Challa-Malladi M, Lieu Yen K, Califano O, Holmes AB, Bhagat G, Murty Vundavalli V, et al. Combined Genetic Inactivation of  $\beta$ 2-Microglobulin and CD58 Reveals Frequent Escape from Immune Recognition in Diffuse Large B Cell Lymphoma. *Cancer Cell*. 2011;20(6):728-40.
31. Alizadeh AA, Eisen MB, Davis RE, Ma C, Lossos IS, Rosenwald A, et al. Distinct types of diffuse large B-cell lymphoma identified by gene expression profiling. *Nature*. 2000;403(6769):503-11.
32. Lenz G, Nagel I, Siebert R, Roschke AV, Sanger W, Wright GW, et al. Aberrant immunoglobulin class switch recombination and switch translocations in activated B cell-like diffuse large B cell lymphoma. *Journal of Experimental Medicine*. 2007;204(3):633-43.
33. Bea S, Zettl A, Wright G, Salaverria I, Jehn P, Moreno V, et al. Diffuse large B-cell lymphoma subgroups have distinct genetic profiles that influence tumor biology and improve gene-expression-based survival prediction. *Blood*. 2005;106(9):3183-90.
34. Huang JZ, Sanger WG, Greiner TC, Staudt LM, Weisenburger DD, Pickering DL, et al. The t(14;18) defines a unique subset of diffuse large B-cell lymphoma with a germinal center B-cell gene expression profile. *Blood*. 2002;99(7):2285-90.
35. Rosenwald A, Wright G, Chan WC, Connors JM, Campo E, Fisher RI, et al. The use of molecular profiling to predict survival after chemotherapy for diffuse large-B-cell lymphoma. 2002;346(25):1937-47.
36. Shaffer AL, 3rd, Young RM, Staudt LM. Pathogenesis of human B cell lymphomas. *Annual review of immunology*. 2012;30:565-610.
37. Xu Y, Xu L, Zhao M, Xu C, Fan Y, Pierce SK, et al. No receptor stands alone: IgG B-cell receptor intrinsic and extrinsic mechanisms contribute to antibody memory. *Cell Research*. 2014;24(6):651-64.
38. Wakabayashi C, Adachi T, Wienands J, Tsubata TJS. A distinct signaling pathway used by the IgG-containing B cell antigen receptor. 2002;298(5602):2392-5.
39. Ngo VN, Young RM, Schmitz R, Jhavar S, Xiao W, Lim K-H, et al. Oncogenically active MYD88 mutations in human lymphoma. *Nature*. 2011;470(7332):115-9.
40. Dekker JD, Park D, Shaffer AL, Kohlhammer H, Deng W, Lee B-K, et al. Subtype-specific addiction of the activated B-cell subset of diffuse large B-cell lymphoma to FOXP1. 2016;113(5):E577-E86.
41. Friedberg JW. Relapsed/Refractory Diffuse Large B-Cell Lymphoma. *Hematology*. 2011;2011(1):498-505.
42. Gisselbrecht C, Glass B, Mounier N, Singh Gill D, Linch DC, Trneny M, et al. Salvage regimens with autologous transplantation for relapsed large B-cell lymphoma in the rituximab era. *Journal of clinical oncology : official journal of the American Society of Clinical Oncology*. 2010;28(27):4184-90.
43. Zinzani PL, Pellegrini C, Gandolfi L, Stefoni V, Quirini F, Derenzini E, et al. Combination of Lenalidomide and Rituximab in Elderly Patients With Relapsed or Refractory Diffuse Large B-Cell Lymphoma: A Phase 2 Trial. *Clinical Lymphoma Myeloma and Leukemia*. 2011;11(6):462-6.

44. Wang M, Fowler N, Wagner-Bartak N, Feng L, Romaguera J, Neelapu SS, et al. Oral lenalidomide with rituximab in relapsed or refractory diffuse large cell, follicular and transformed lymphoma: a phase II clinical trial. *Leukemia*. 2013;27(9):1902-9.
45. Feldman T, Mato AR, Chow KF, Protomastro EA, Yannotti KML, Bhattacharyya P, et al. Addition of lenalidomide to rituximab, ifosfamide, carboplatin, etoposide (RICER) in first-relapse/primary refractory diffuse large B-cell lymphoma. 2014;166(1):77-83.
46. Martín A, Redondo AM, Dlouhy I, Salar A, González-Barca E, Canales M, et al. Lenalidomide in combination with R-ESHAP in patients with relapsed or refractory diffuse large B-cell lymphoma: a phase 1b study from GELTAMO group. 2016;173(2):245-52.
47. Vitolo U, Chiappella A, Franceschetti S, Carella AM, Baldi I, Inghirami G, et al. Lenalidomide plus R-CHOP21 in elderly patients with untreated diffuse large B-cell lymphoma: results of the REAL07 open-label, multicentre, phase 2 trial. *The Lancet Oncology*. 2014;15(7):730-7.
48. Reddy NM, Greer JP, Morgan DS, Chen H, Park SI, Richards KL. A phase II randomized study of lenalidomide or lenalidomide and rituximab as maintenance therapy following standard chemotherapy for patients with high/high-intermediate risk diffuse large B-cell lymphoma. *Leukemia*. 2017;31(1):241-4.
49. Evens AM, Rosen ST, Helenowski I, Kline J, Larsen A, Colvin J, et al. A phase I/II trial of bortezomib combined concurrently with gemcitabine for relapsed or refractory DLBCL and peripheral T-cell lymphomas. 2013;163(1):55-61.
50. Ruan J, Martin P, Furman RR, Lee SM, Cheung K, Vose JM, et al. Bortezomib plus CHOP-rituximab for previously untreated diffuse large B-cell lymphoma and mantle cell lymphoma. 2011;29(6):690-7.
51. Sauter CS, Matasar MJ, Schoder H, Devlin SM, Drullinsky P, Gerecitano J, et al. A phase 1 study of ibrutinib in combination with R-ICE in patients with relapsed or primary refractory DLBCL. *Blood*. 2018;131(16):1805-8.
52. Younes A, Sehn LH, Johnson P, Zinzani PL, Hong X, Zhu J, et al. Randomized phase III trial of ibrutinib and rituximab plus cyclophosphamide, doxorubicin, vincristine, and prednisone in non-germinal center B-cell diffuse large B-cell lymphoma. 2019;37(15):1285.
53. Ramchandren R, Johnson P, Ghosh N, Ruan J, Ardeshta KM, Johnson R, et al. The iR2 Regimen (Ibrutinib, Lenalidomide, and Rituximab) Is Active with a Manageable Safety Profile in Patients with Relapsed/Refractory Non-Germinal Center-like Diffuse Large B-Cell Lymphoma. *Blood*. 2018;132:402.
54. de Vos S, Swinnen LJ, Wang D, Reid E, Fowler N, Cordero J, et al. Venetoclax, bendamustine, and rituximab in patients with relapsed or refractory NHL: a phase Ib dose-finding study. *Annals of Oncology*. 2018;29(9):1932-8.
55. Morschhauser F, Salles G, Le Gouill S, Tilly H, Thieblemont C, Bouabdallah K, et al. An open-label phase 1b study of obinutuzumab plus lenalidomide in relapsed/refractory follicular B-cell lymphoma. *Blood*. 2018;132(14):1486-94.
56. Barnes JA, Jacobsen E, Feng Y, Freedman A, Hochberg EP, LaCasce AS, et al. Everolimus in combination with rituximab induces complete responses in heavily pretreated diffuse large B-cell lymphoma. 2013;98(4):615.
57. Fenske TS, Shah NM, Kim KM, Saha S, Zhang C, Baim AE, et al. A phase 2 study of weekly temsirolimus and bortezomib for relapsed or refractory B-cell non-Hodgkin lymphoma: A Wisconsin Oncology Network study. 2015;121(19):3465-71.

58. Bende RJ, Smit LA, van Noesel CJM. Molecular pathways in follicular lymphoma. *Leukemia*. 2007;21(1):18-29.
59. Dreyling M, Ghielmini M, Rule S, Salles G, Ladetto M, Tonino S, et al. Newly diagnosed and relapsed follicular lymphoma: ESMO Clinical Practice Guidelines for diagnosis, treatment and follow-up†☆. 2021;32(3):298-308.
60. Carbone A, Roulland S, Gloghini A, Younes A, von Keudell G, López-Guillermo A, et al. Follicular lymphoma. *Nature Reviews Disease Primers*. 2019;5(1):83.
61. Bouska A, Bi C, Lone W, Zhang W, Kedwaili A, Heavican T, et al. Adult high-grade B-cell lymphoma with Burkitt lymphoma signature: genomic features and potential therapeutic targets. *Blood*. 2017;130(16):1819-31.
62. Schmitz R, Young RM, Ceribelli M, Jhavar S, Xiao W, Zhang M, et al. Burkitt lymphoma pathogenesis and therapeutic targets from structural and functional genomics. *Nature*. 2012;490(7418):116-20.
63. Molyneux EM, Rochford R, Griffin B, Newton R, Jackson G, Menon G, et al. Burkitt's lymphoma. *The Lancet*. 2012;379(9822):1234-44.
64. Casulo C, Friedberg JW. Burkitt lymphoma- a rare but challenging lymphoma. *Best Practice & Research Clinical Haematology*. 2018;31(3):279-84.
65. Zhang J, Meng L, Jiang W, Zhang H, Zhou A, Zeng N. Identification of clinical molecular targets for childhood Burkitt lymphoma. *Translational Oncology*. 2020;13(12):100855.
66. Burkhardt B, Michgehl U, Rohde J, Erdmann T, Berning P, Reutter K, et al. Clinical relevance of molecular characteristics in Burkitt lymphoma differs according to age. *Nature communications*. 2022;13(1):3881.
67. Johnson PC, Abramson JSJO. Current Treatment of Burkitt Lymphoma and High-Grade B-Cell Lymphomas. 2022;36(8).
68. Harker-Murray PD, Pommert L, Barth MJJJotNCCN. Novel therapies potentially available for pediatric B-cell non-Hodgkin lymphoma. 2020;18(8):1125-34.
69. Sander S, Calado Dinis P, Srinivasan L, Köchert K, Zhang B, Rosolowski M, et al. Synergy between PI3K Signaling and MYC in Burkitt Lymphomagenesis. *Cancer Cell*. 2012;22(2):167-79.
70. Bhatti M, Ippolito T, Mavis C, Gu J, Cairo MS, Lim MS, et al. Pre-clinical activity of targeting the PI3K/Akt/mTOR pathway in Burkitt lymphoma. *Oncotarget*. 2018;9(31):21820-30.
71. Simmons JK, Patel J, Michalowski A, Zhang S, Wei B-R, Sullivan P, et al. TORC1 and class I HDAC inhibitors synergize to suppress mature B cell neoplasms. *Molecular Oncology*. 2014;8(2):261-72.
72. Tomska K, Kurilov R, Lee KS, Hüllelein J, Lukas M, Sellner L, et al. Drug-based perturbation screen uncovers synergistic drug combinations in Burkitt lymphoma. *Scientific Reports*. 2018;8(1):12046.
73. Mertz JA, Conery AR, Bryant BM, Sandy P, Balasubramanian S, Mele DA, et al. Targeting MYC dependence in cancer by inhibiting BET bromodomains. 2011;108(40):16669-74.
74. Ghobrial IM, Gertz MA, Fonseca R. Waldenström macroglobulinaemia. *The Lancet Oncology*. 2003;4(11):679-85.

75. Rousseau S, Martel G. Gain-of-Function Mutations in the Toll-Like Receptor Pathway: TPL2-Mediated ERK1/ERK2 MAPK Activation, a Path to Tumorigenesis in Lymphoid Neoplasms? 2016;4.
76. Oza A, Rajkumar SV. Waldenstrom macroglobulinemia: prognosis and management. *Blood Cancer J.* 2015;5(3):e394.
77. Treon SP. How I treat Waldenström macroglobulinemia. *Blood.* 2015;126(6):721-32.
78. Fonseca R, Hayman S. Waldenström macroglobulinaemia. 2007;138(6):700-20.
79. Cargnello M, Roux PP. Activation and function of the MAPKs and their substrates, the MAPK-activated protein kinases. *Microbiology and molecular biology reviews* : MMBR. 2011;75(1):50-83.
80. Guo YJ, Pan WW, Liu SB, Shen ZF, Xu Y, Hu LL. ERK/MAPK signalling pathway and tumorigenesis (Review). *Exp Ther Med.* 2020;19(3):1997-2007.
81. Dhillon AS, Hagan S, Rath O, Kolch W. MAP kinase signalling pathways in cancer. *Oncogene.* 2007;26(22):3279-90.
82. Burotto M, Chiou VL, Lee J-M, Kohn EC. The MAPK pathway across different malignancies: A new perspective. 2014;120(22):3446-56.
83. Vendramini E, Bomben R, Pozzo F, Bittolo T, Tissino E, Gattei V, et al. KRAS and RAS-MAPK Pathway Deregulation in Mature B Cell Lymphoproliferative Disorders. *Cancers.* 2022;14(3).
84. Dai B, Zhao XF, Mazan-Mamczarz K, Hagner P, Corl S, Bahassi el M, et al. Functional and molecular interactions between ERK and CHK2 in diffuse large B-cell lymphoma. *Nature communications.* 2011;2:402.
85. Dhanasekaran N, Reddy EP. Signaling by dual specificity kinases. *Oncogene.* 1998;17(11):1447-55.
86. Avruch J. MAP kinase pathways: The first twenty years. *Biochimica et Biophysica Acta (BBA) - Molecular Cell Research.* 2007;1773(8):1150-60.
87. Keshet Y, Seger R. The MAP Kinase Signaling Cascades: A System of Hundreds of Components Regulates a Diverse Array of Physiological Functions. In: Seger R, editor. *MAP Kinase Signaling Protocols: Second Edition.* Totowa, NJ: Humana Press; 2010. p. 3-38.
88. Mebratu Y, Tesfaigzi Y. How ERK1/2 activation controls cell proliferation and cell death: Is subcellular localization the answer? *Cell cycle (Georgetown, Tex).* 2009;8(8):1168-75.
89. Soares-Silva M, Diniz FF, Gomes GN, Bahia D. The Mitogen-Activated Protein Kinase (MAPK) Pathway: Role in Immune Evasion by Trypanosomatids. 2016;7.
90. Cuevas BD. Mitogen-Activated Protein Kinase Kinases. In: Schwab M, editor. *Encyclopedia of Cancer.* Berlin, Heidelberg: Springer Berlin Heidelberg; 2017. p. 2872-6.
91. Pearson G, Robinson F, Beers Gibson T, Xu B-e, Karandikar M, Berman K, et al. Mitogen-Activated Protein (MAP) Kinase Pathways: Regulation and Physiological Functions\*. *Endocrine Reviews.* 2001;22(2):153-83.
92. Cuevas BD, Abell AN, Johnson GL. Role of mitogen-activated protein kinase kinase kinases in signal integration. *Oncogene.* 2007;26(22):3159-71.
93. Roskoski R. RAF protein-serine/threonine kinases: Structure and regulation. *Biochemical and Biophysical Research Communications.* 2010;399(3):313-7.

94. Davies H, Bignell GR, Cox C, Stephens P, Edkins S, Clegg S, et al. Mutations of the BRAF gene in human cancer. *Nature*. 2002;417(6892):949-54.
95. Wellbrock C, Karasarides M, Marais R. The RAF proteins take centre stage. *Nature Reviews Molecular Cell Biology*. 2004;5(11):875-85.
96. Lavoie H, Therrien M. Regulation of RAF protein kinases in ERK signalling. *Nature Reviews Molecular Cell Biology*. 2015;16(5):281-98.
97. Marais R, Light Y, Paterson HF, Mason CS, Marshall CJ. Differential Regulation of Raf-1, A-Raf, and B-Raf by Oncogenic Ras and Tyrosine Kinases\*. *Journal of Biological Chemistry*. 1997;272(7):4378-83.
98. Takaesu G, Surabhi RM, Park K-J, Ninomiya-Tsuji J, Matsumoto K, Gaynor RB. TAK1 is Critical for I $\kappa$ B Kinase-mediated Activation of the NF- $\kappa$ B Pathway. *Journal of Molecular Biology*. 2003;326(1):105-15.
99. Shi J-H, Sun S-C. Tumor Necrosis Factor Receptor-Associated Factor Regulation of Nuclear Factor  $\kappa$ B and Mitogen-Activated Protein Kinase Pathways. 2018;9.
100. Blonska M, Shambharkar PB, Kobayashi M, Zhang D, Sakurai H, Su B, et al. TAK1 Is Recruited to the Tumor Necrosis Factor- $\alpha$  (TNF- $\alpha$ ) Receptor 1 Complex in a Receptor-interacting Protein (RIP)-dependent Manner and Cooperates with MEKK3 Leading to NF- $\kappa$ B Activation\*. *Journal of Biological Chemistry*. 2005;280(52):43056-63.
101. Irie T, Muta T, Takeshige K. TAK1 mediates an activation signal from toll-like receptor(s) to nuclear factor- $\kappa$ B in lipopolysaccharide-stimulated macrophages. 2000;467(2-3):160-4.
102. Kawasaki T, Kawai T. Toll-like receptor signaling pathways. *Frontiers in immunology*. 2014;5:461.
103. Troutman TD, Bazan JF, Pasare C. Toll-like receptors, signaling adapters and regulation of the pro-inflammatory response by PI3K. *Cell cycle (Georgetown, Tex)*. 2012;11(19):3559-67.
104. Lin W-W, Karin MJ. A cytokine-mediated link between innate immunity, inflammation, and cancer. 2007;117(5):1175-83.
105. Rousseau S, Martel G. Gain-of-Function Mutations in the Toll-Like Receptor Pathway: TPL2-Mediated ERK1/ERK2 MAPK Activation, a Path to Tumorigenesis in Lymphoid Neoplasms? *Frontiers in cell and developmental biology*. 2016;4:50.
106. Farias R, Rousseau S. The TAK1 $\rightarrow$ IKK $\beta$  $\rightarrow$ TPL2 $\rightarrow$ MKK1/MKK2 Signaling Cascade Regulates IL-33 Expression in Cystic Fibrosis Airway Epithelial Cells Following Infection by *Pseudomonas aeruginosa*. 2016;3.
107. Gantke T, Sriskantharajah S, Ley SC. Regulation and function of TPL-2, an I $\kappa$ B kinase-regulated MAP kinase kinase. *Cell Res*. 2011;21(1):131-45.
108. Waterfield M, Jin W, Reiley W, Zhang M, Sun S-C. I $\kappa$ B Kinase Is an Essential Component of the Tpl2 Signaling Pathway. 2004;24(13):6040-8.
109. Beinke S, Deka J, Lang V, Belich MP, Walker PA, Howell S, et al. NF- $\kappa$ B1 p105 Negatively Regulates TPL-2 MEK Kinase Activity. 2003;23(14):4739-52.
110. Oeckinghaus A, Ghosh S. The NF- $\kappa$ B family of transcription factors and its regulation. *Cold Spring Harbor perspectives in biology*. 2009;1(4):a000034.
111. Perkins ND. Post-translational modifications regulating the activity and function of the nuclear factor  $\kappa$ B pathway. *Oncogene*. 2006;25(51):6717-30.

112. Waterfield MR, Zhang M, Norman LP, Sun S-C. NF- $\kappa$ B1/p105 Regulates Lipopolysaccharide-Stimulated MAP Kinase Signaling by Governing the Stability and Function of the Tpl2 Kinase. *Molecular cell*. 2003;11(3):685-94.
113. Banerjee A, Gugasyan R, McMahon M, Gerondakis S. Diverse Toll-like receptors utilize Tpl2 to activate extracellular signal-regulated kinase (ERK) in hemopoietic cells. 2006;103(9):3274-9.
114. Alessi DR, Saito Y, Campbell DG, Cohen P, Sithanandam G, Rapp U, et al. Identification of the sites in MAP kinase kinase-1 phosphorylated by p74raf-1. *The EMBO journal*. 1994;13(7):1610-9.
115. Zheng CF, Guan KL. Activation of MEK family kinases requires phosphorylation of two conserved Ser/Thr residues. *The EMBO journal*. 1994;13(5):1123-31.
116. Coulombe P, Meloche S. Atypical mitogen-activated protein kinases: Structure, regulation and functions. *Biochimica et Biophysica Acta (BBA) - Molecular Cell Research*. 2007;1773(8):1376-87.
117. Cargnello M, Roux PP. Activation and Function of the MAPKs and Their Substrates, the MAPK-Activated Protein Kinases. 2011;75(1):50-83.
118. Fan H-Y, Sun Q-Y. Involvement of Mitogen-Activated Protein Kinase Cascade During Oocyte Maturation and Fertilization in Mammals<sup>1</sup>. *Biology of Reproduction*. 2004;70(3):535-47.
119. Dumitru CD, Ceci JD, Tsatsanis C, Kontoyiannis D, Stamatakis K, Lin J-H, et al. TNF- $\alpha$  Induction by LPS Is Regulated Posttranscriptionally via a Tpl2/ERK-Dependent Pathway. *Cell*. 2000;103(7):1071-83.
120. Waetzig V, Herdegen T. MEKK1 controls neurite regrowth after experimental injury by balancing ERK1/2 and JNK2 signaling. *Molecular and Cellular Neuroscience*. 2005;30(1):67-78.
121. Jacobs D, Glossip D, Xing H, Muslin AJ, Kornfeld K. Multiple docking sites on substrate proteins form a modular system that mediates recognition by ERK MAP kinase. *Genes & development*. 1999;13(2):163-75.
122. Morrison DK, Davis RJ. Regulation of MAP kinase signaling modules by scaffold proteins in mammals. *Annual review of cell and developmental biology*. 2003;19:91-118.
123. Zhou B, Zhang J, Liu S, Reddy S, Wang F, Zhang Z-Y. Mapping ERK2-MKP3 Binding Interfaces by Hydrogen/Deuterium Exchange Mass Spectrometry\*. *Journal of Biological Chemistry*. 2006;281(50):38834-44.
124. Yoon S, Seger R. The extracellular signal-regulated kinase: Multiple substrates regulate diverse cellular functions. *Growth Factors*. 2006;24(1):21-44.
125. Friday BB, Adjei AA. Advances in Targeting the Ras/Raf/MEK/Erk Mitogen-Activated Protein Kinase Cascade with MEK Inhibitors for Cancer Therapy. *Clinical Cancer Research*. 2008;14(2):342-6.
126. Burotto M, Chiou VL, Lee JM, Kohn EC. The MAPK pathway across different malignancies: a new perspective. *Cancer*. 2014;120(22):3446-56.
127. Plataniias LC. Map kinase signaling pathways and hematologic malignancies. *Blood*. 2003;101(12):4667-79.
128. Proietti I, Skroza N, Michellini S, Mambrin A, Balduzzi V, Bernardini N, et al. BRAF Inhibitors: Molecular Targeting and Immunomodulatory Actions. *Cancers*. 2020;12(7).
129. Roskoski R. Targeting oncogenic Raf protein-serine/threonine kinases in human cancers. *Pharmacological Research*. 2018;135:239-58.

130. Yang L, Zheng L, Chng WJ, Ding JLJTips. Comprehensive analysis of ERK1/2 substrates for potential combination immunotherapies. 2019;40(11):897-910.
131. Han J, Liu Y, Yang S, Wu X, Li H, Wang Q. MEK inhibitors for the treatment of non-small cell lung cancer. *Journal of Hematology & Oncology*. 2021;14(1):1.
132. Shin MH, Kim J, Lim SA, Kim J, Lee KM. Current Insights into Combination Therapies with MAPK Inhibitors and Immune Checkpoint Blockade. *Int J Mol Sci*. 2020;21(7).
133. Mandalà M, De Logu F, Merelli B, Nassini R, Massi D. Immunomodulating property of MAPK inhibitors: from translational knowledge to clinical implementation. *Laboratory Investigation*. 2017;97(2):166-75.
134. Frémin C, Meloche S. From basic research to clinical development of MEK1/2 inhibitors for cancer therapy. *Journal of Hematology & Oncology*. 2010;3(1):8.
135. Valentini E, Di Martile M, Brignone M, Di Caprio M, Manni I, Chiappa M, et al. Bcl-2 family inhibitors sensitize human cancer models to therapy. *Cell Death & Disease*. 2023;14(7):441.
136. Lina H, Qi Z, Monique D, Ce S, Antonio C, Vivian RR, et al. Concomitant targeting of BCL2 with venetoclax and MAPK signaling with cobimetinib in acute myeloid leukemia models. *Haematologica*. 2020;105(3):697-707.
137. Lomonosova E, Chinnadurai G. BH3-only proteins in apoptosis and beyond: an overview. *Oncogene*. 2008;27(1):S2-S19.
138. Giam M, Huang DCS, Bouillet P. BH3-only proteins and their roles in programmed cell death. *Oncogene*. 2008;27(1):S128-S36.
139. Letai AG. Diagnosing and exploiting cancer's addiction to blocks in apoptosis. *Nature Reviews Cancer*. 2008;8(2):121-32.
140. Roberts AW, Huang D. Targeting BCL2 With BH3 Mimetics: Basic Science and Clinical Application of Venetoclax in Chronic Lymphocytic Leukemia and Related B Cell Malignancies. *Clinical pharmacology and therapeutics*. 2017;101(1):89-98.
141. Schuetz JM, Johnson NA, Morin RD, Scott DW, Tan K, Ben-Nierah S, et al. BCL2 mutations in diffuse large B-cell lymphoma. *Leukemia*. 2012;26(6):1383-90.
142. de Jong MRW, Langendonk M, Reitsma B, Nijland M, van den Berg A, Ammatuna E, et al. Heterogeneous Pattern of Dependence on Anti-Apoptotic BCL-2 Family Proteins upon CHOP Treatment in Diffuse Large B-Cell Lymphoma. 2019;20(23):6036.
143. Cang S, Iragavarapu C, Savooji J, Song Y, Liu D. ABT-199 (venetoclax) and BCL-2 inhibitors in clinical development. *Journal of Hematology & Oncology*. 2015;8(1):129.
144. Roberts AW. Therapeutic development and current uses of BCL-2 inhibition. *Hematology*. 2020;2020(1):1-9.
145. Itchaki G, Brown JR. The potential of venetoclax (ABT-199) in chronic lymphocytic leukemia. *Therapeutic advances in hematology*. 2016;7(5):270-87.
146. Airiau K, Prouzet-Mauléon V, Rousseau B, Pigneux A, Jeanneteau M, Giraudon M, et al. Synergistic cooperation between ABT-263 and MEK1/2 inhibitor: effect on apoptosis and proliferation of acute myeloid leukemia cells. *Oncotarget*. 2016;7(1):845-59.
147. Sale Matthew J, Cook Simon J. The BH3 mimetic ABT-263 synergizes with the MEK1/2 inhibitor selumetinib/AZD6244 to promote BIM-dependent tumour cell death and inhibit acquired resistance. *Biochemical Journal*. 2013;450(2):285-94.

148. Tan N, Wong M, Nannini MA, Hong R, Lee LB, Price S, et al. Bcl-2/Bcl-xL Inhibition Increases the Efficacy of MEK Inhibition Alone and in Combination with PI3 Kinase Inhibition in Lung and Pancreatic Tumor Models. *Molecular Cancer Therapeutics*. 2013;12(6):853-64.
149. Ansell SM, Hodge LS, Secreto FJ, Manske M, Braggio E, Price-Troska T, et al. Activation of TAK1 by MYD88 L265P drives malignant B-cell Growth in non-Hodgkin lymphoma. *Blood Cancer J*. 2014;4(2):e183.
150. Avbelj M, Wolz OO, Fekonja O, Benčina M, Repič M, Mavri J, et al. Activation of lymphoma-associated MyD88 mutations via allosterically-induced TIR-domain oligomerization. *Blood*. 2014;124(26):3896-904.
151. Gruosso T, Garnier C, Abelanet S, Kieffer Y, Lemesre V, Bellanger D, et al. MAP3K8/TPL-2/COT is a potential predictive marker for MEK inhibitor treatment in high-grade serous ovarian carcinomas. *Nature communications*. 2015;6(1):8583.
152. Newman S, Fan L, Pribnow A, Silkov A, Rice SV, Lee S, et al. Clinical genome sequencing uncovers potentially targetable truncations and fusions of MAP3K8 in spitzoid and other melanomas. *Nature Medicine*. 2019;25(4):597-602.
153. Chorzalska A, Ahsan N, Rao RSP, Roder K, Yu X, Morgan J, et al. Overexpression of Tpl2 is linked to imatinib resistance and activation of MEK-ERK and NF- $\kappa$ B pathways in a model of chronic myeloid leukemia. 2018;12(5):630-47.
154. Green N, Hu Y, Janz K, Li H-Q, Kaila N, Guler S, et al. Inhibitors of Tumor Progression Loci-2 (Tpl2) Kinase and Tumor Necrosis Factor  $\alpha$  (TNF- $\alpha$ ) Production: Selectivity and in Vivo Antiinflammatory Activity of Novel 8-Substituted-4-anilino-6-aminoquinoline-3-carbonitriles. *Journal of Medicinal Chemistry*. 2007;50(19):4728-45.
155. Hall JP, Kurdi Y, Hsu S, Cuzzo J, Liu J, Telliez J-B, et al. Pharmacologic Inhibition of Tpl2 Blocks Inflammatory Responses in Primary Human Monocytes, Synoviocytes, and Blood\*. *Journal of Biological Chemistry*. 2007;282(46):33295-304.
156. Struhl KJG, development. Histone acetylation and transcriptional regulatory mechanisms. 1998;12(5):599-606.
157. Wade PA, Pruss D, Wolffe AP. Histone acetylation: chromatin in action. *Trends in Biochemical Sciences*. 1997;22(4):128-32.
158. Marks PA, Miller T, Richon VM. Histone deacetylases. *Current Opinion in Pharmacology*. 2003;3(4):344-51.
159. RUIJTER AJMd, GENNIP AHv, CARON HN, KEMP S, KUILENBURG ABPv. Histone deacetylases (HDACs): characterization of the classical HDAC family. *Biochemical Journal*. 2003;370(3):737-49.
160. Seto E, Yoshida MJCSHpib. Erasers of histone acetylation: the histone deacetylase enzymes. 2014;6(4):a018713.
161. Dali-Youcef N, Lagouge M, Froelich S, Koehl C, Schoonjans K, Auwerx J. Sirtuins: The 'magnificent seven', function, metabolism and longevity. *Annals of Medicine*. 2007;39(5):335-45.
162. Trapp J, Jung MJCdt. The role of NAD<sup>+</sup> dependent histone deacetylases (sirtuins) in ageing. 2006;7(11):1553-60.
163. Yanginlar C, Logie C. HDAC11 is a regulator of diverse immune functions. *Biochimica et Biophysica Acta (BBA) - Gene Regulatory Mechanisms*. 2018;1861(1):54-9.

164. Kelly RD, Cowley SM. The physiological roles of histone deacetylase (HDAC) 1 and 2: complex co-stars with multiple leading parts. *Biochemical Society transactions*. 2013;41(3):741-9.
165. Millard CJ, Watson PJ, Fairall L, Schwabe JWJ. Targeting class I histone deacetylases in a “complex” environment. 2017;38(4):363-77.
166. Jamaladdin S, Kelly RDW, O'Regan L, Dovey OM, Hodson GE, Millard CJ, et al. Histone deacetylase (HDAC) 1 and 2 are essential for accurate cell division and the pluripotency of embryonic stem cells. 2014;111(27):9840-5.
167. Li Y, Seto E. HDACs and HDAC Inhibitors in Cancer Development and Therapy. *Cold Spring Harbor perspectives in medicine*. 2016;6(10).
168. Montgomery RL, Hsieh J, Barbosa AC, Richardson JA, Olson EN. Histone deacetylases 1 and 2 control the progression of neural precursors to neurons during brain development. 2009;106(19):7876-81.
169. Guardiola AR, Yao T-P. Molecular cloning and characterization of a novel histone deacetylase HDAC10. 2002;277(5):3350-6.
170. Kawaguchi Y, Kovacs JJ, McLaurin A, Vance JM, Ito A, Yao T-P. The Deacetylase HDAC6 Regulates Aggresome Formation and Cell Viability in Response to Misfolded Protein Stress. *Cell*. 2003;115(6):727-38.
171. Magiera MM, Janke C. Post-translational modifications of tubulin. *Current Biology*. 2014;24(9):R351-R4.
172. Hubbert C, Guardiola A, Shao R, Kawaguchi Y, Ito A, Nixon A, et al. HDAC6 is a microtubule-associated deacetylase. *Nature*. 2002;417(6887):455-8.
173. Eshun-Wilson L, Zhang R, Portran D, Nachury MV, Toso DB, Löhr T, et al. Effects of  $\alpha$ -tubulin acetylation on microtubule structure and stability. 2019;116(21):10366-71.
174. Portran D, Schaedel L, Xu Z, Théry M, Nachury Maxence V. Tubulin acetylation protects long-lived microtubules against mechanical ageing. *Nature Cell Biology*. 2017;19(4):391-8.
175. Xu Z, Schaedel L, Portran D, Aguilar A, Gaillard J, Marinkovich MP, et al. Microtubules acquire resistance from mechanical breakage through intraluminal acetylation. 2017;356(6335):328-32.
176. Haggarty SJ, Koeller KM, Wong JC, Grozinger CM, Schreiber SL. Domain-selective small-molecule inhibitor of histone deacetylase 6 (HDAC6)-mediated tubulin deacetylation. 2003;100(8):4389-94.
177. Perdiz D, Mackeh R, Poüs C, Baillet A. The ins and outs of tubulin acetylation: More than just a post-translational modification? *Cellular Signalling*. 2011;23(5):763-71.
178. Wu JY, Xiang S, Zhang M, Fang B, Huang H, Kwon OK, et al. Histone deacetylase 6 (HDAC6) deacetylates extracellular signal-regulated kinase 1 (ERK1) and thereby stimulates ERK1 activity. *The Journal of biological chemistry*. 2018;293(6):1976-93.
179. Li Y, Zhang X, Polakiewicz RD, Yao TP, Comb MJ. HDAC6 is required for epidermal growth factor-induced beta-catenin nuclear localization. *The Journal of biological chemistry*. 2008;283(19):12686-90.
180. Zhang W, Kone BC. NF-kappaB inhibits transcription of the H(+)-K(+)-ATPase alpha(2)-subunit gene: role of histone deacetylases. *American journal of physiology Renal physiology*. 2002;283(5):F904-11.
181. Adcock IM. HDAC inhibitors as anti-inflammatory agents. *British journal of pharmacology*. 2007;150(7):829-31.

182. Kee HJ, Kook H. Roles and Targets of Class I and IIa Histone Deacetylases in Cardiac Hypertrophy. *Journal of Biomedicine and Biotechnology*. 2011;2011:928326.
183. Fischer A, Sananbenesi F, Mungenast A, Tsai L-H. Targeting the correct HDAC(s) to treat cognitive disorders. *Trends in Pharmacological Sciences*. 2010;31(12):605-17.
184. Glozak MA, Seto E. Histone deacetylases and cancer. *Oncogene*. 2007;26(37):5420-32.
185. Choi J-H, Kwon HJ, Yoon B-I, Kim J-H, Han SU, Joo HJ, et al. Expression Profile of Histone Deacetylase 1 in Gastric Cancer Tissues. 2001;92(12):1300-4.
186. Zhang Z, Yamashita H, Toyama T, Sugiura H, Ando Y, Mita K, et al. Quantitation of HDAC1 mRNA Expression in Invasive Carcinoma of the Breast\*. *Breast Cancer Research and Treatment*. 2005;94(1):11-6.
187. Wilson AJ, Byun D-S, Popova N, Murray LB, L'Italien K, Sowa Y, et al. Histone deacetylase 3 (HDAC3) and other class I HDACs regulate colon cell maturation and p21 expression and are deregulated in human colon cancer. 2006;281(19):13548-58.
188. Adams H, Fritzsche FR, Dirnhofer S, Kristiansen G, Tzankov A. Class I histone deacetylases 1, 2 and 3 are highly expressed in classical Hodgkin's lymphoma. *Expert Opinion on Therapeutic Targets*. 2010;14(6):577-84.
189. Skov V, Larsen TS, Thomassen M, Riley CH, Jensen MK, Bjerrum OW, et al. Increased gene expression of histone deacetylases in patients with Philadelphia-negative chronic myeloproliferative neoplasms. *Leukemia & Lymphoma*. 2012;53(1):123-9.
190. Barneda-Zahonero B, Parra M. Histone deacetylases and cancer. *Molecular Oncology*. 2012;6(6):579-89.
191. Hagelkruys A, Sawicka A, Rennmayr M, Seiser CJHDtB, Implication C. The biology of HDAC in cancer: the nuclear and epigenetic components. 2011:13-37.
192. Yoon S, Eom GH. HDAC and HDAC Inhibitor: From Cancer to Cardiovascular Diseases. *Chonnam medical journal*. 2016;52(1):1-11.
193. Chun P. Histone deacetylase inhibitors in hematological malignancies and solid tumors. *Archives of Pharmacal Research*. 2015;38(6):933-49.
194. Mehrpouri M, Pourbagheri-Sigaroodi A, Bashash D. The contributory roles of histone deacetylases (HDACs) in hematopoiesis regulation and possibilities for pharmacologic interventions in hematologic malignancies. *International Immunopharmacology*. 2021;100:108114.
195. Mottamal M, Zheng S, Huang TL, Wang G. Histone Deacetylase Inhibitors in Clinical Studies as Templates for New Anticancer Agents. 2015;20(3):3898-941.
196. Rajak H, Singh A, Raghuwanshi K, Kumar R, Dewangan P, Veerasamy R, et al. A structural insight into hydroxamic acid based histone deacetylase inhibitors for the presence of anticancer activity. 2014;21(23):2642-64.
197. Targeting Histone Deacetylases in Diseases: Where Are We? 2015;23(1):99-126.
198. Zhang I, Beus M, Stochaj U, Le PU, Zorc B, Rajić Z, et al. Inhibition of glioblastoma cell proliferation, invasion, and mechanism of action of a novel hydroxamic acid hybrid molecule. *Cell Death Discov*. 2018;4:41.
199. Bass AS, Cartwright ME, Mahon C, Morrison R, Snyder R, McNamara P, et al. Exploratory drug safety: A discovery strategy to reduce attrition in development. *Journal of Pharmacological and Toxicological Methods*. 2009;60(1):69-78.

200. Kramer JA, Sagartz JE, Morris DL. The application of discovery toxicology and pathology towards the design of safer pharmaceutical lead candidates. *Nature Reviews Drug Discovery*. 2007;6(8):636-49.
201. Lindgren S, Bass AS, Briscoe R, Bruse K, Friedrichs GS, Kallman MJ, et al. Benchmarking Safety Pharmacology regulatory packages and best practice. *Journal of Pharmacological and Toxicological Methods*. 2008;58(2):99-109.
202. Kola I, Landis J. Can the pharmaceutical industry reduce attrition rates? *Nature Reviews Drug Discovery*. 2004;3(8):711-6.
203. Zachariah CJ, Kamaraj RJ, JoP, Technology. Regulatory Drug Approval Process in Canada. 2020;13(4):2040-4.
204. Grössmann N, Robausch M, Rosian K, Wild C, Simon J. Monitoring evidence on overall survival benefits of anticancer drugs approved by the European Medicines Agency between 2009 and 2015. *European Journal of Cancer*. 2019;110:1-7.
205. Fielden MR, Kolaja KL. The role of early in vivo toxicity testing in drug discovery toxicology. *Expert Opinion on Drug Safety*. 2008;7(2):107-10.
206. Taškova K, Fontaine J-F, Mrowka R, Andrade-Navarro MA. Evaluation of in vivo and in vitro models of toxicity by comparison of toxicogenomics data with the literature. *Methods*. 2018;132:57-65.
207. Zon LI, Peterson RT. In vivo drug discovery in the zebrafish. *Nature Reviews Drug Discovery*. 2005;4(1):35-44.
208. Sieber S, Grossen P, Bussmann J, Campbell F, Kros A, Witzigmann D, et al. Zebrafish as a preclinical in vivo screening model for nanomedicines. *Advanced Drug Delivery Reviews*. 2019;151-152:152-68.
209. Delvecchio C, Tiefenbach J, Krause HM. The Zebrafish: A Powerful Platform for In Vivo, HTS Drug Discovery. *ASSAY and Drug Development Technologies*. 2011;9(4):354-61.
210. Saleem S, Kannan RR. Zebrafish: an emerging real-time model system to study Alzheimer's disease and neurospecific drug discovery. *Cell Death Discov*. 2018;4:45.
211. Strähle U, Scholz S, Geisler R, Greiner P, Hollert H, Rastegar S, et al. Zebrafish embryos as an alternative to animal experiments—A commentary on the definition of the onset of protected life stages in animal welfare regulations. *Reproductive Toxicology*. 2012;33(2):128-32.
212. MacRae CA, Peterson RT. Zebrafish as tools for drug discovery. *Nature Reviews Drug Discovery*. 2015;14(10):721-31.
213. Cassar S, Adatto I, Freeman JL, Gamse JT, Iturria I, Lawrence C, et al. Use of Zebrafish in Drug Discovery Toxicology. *Chem Res Toxicol*. 2020;33(1):95-118.
214. Rajan V, Dellaire G, Berman JNJZM, Protocols. Modeling leukemogenesis in the zebrafish using genetic and xenograft models. 2016:171-89.
215. Howe K, Clark MD, Torroja CF, Torrance J, Berthelot C, Muffato M, et al. The zebrafish reference genome sequence and its relationship to the human genome. *Nature*. 2013;496(7446):498-503.
216. Milazzo G, Mercatelli D, Di Muzio G, Triboli L, De Rosa P, Perini G, et al. Histone Deacetylases (HDACs): Evolution, Specificity, Role in Transcriptional Complexes, and Pharmacological Actionability. *Genes*. 2020;11(5).

217. Osko JD, Porter NJ, Narayana Reddy PA, Xiao Y-C, Rokka J, Jung M, et al. Exploring Structural Determinants of Inhibitor Affinity and Selectivity in Complexes with Histone Deacetylase 6. *Journal of Medicinal Chemistry*. 2020;63(1):295-308.
218. Olaoye OO, Watson PR, Nawar N, Geletu M, Sedighi A, Bukhari S, et al. Unique Molecular Interaction with the Histone Deacetylase 6 Catalytic Tunnel: Crystallographic and Biological Characterization of a Model Chemotype. *Journal of Medicinal Chemistry*. 2021;64(5):2691-704.
219. van Wijk RC, Krekels EHJ, Hankemeier T, Spaik HP, van der Graaf PH. Systems pharmacology of hepatic metabolism in zebrafish larvae. *Drug Discovery Today: Disease Models*. 2016;22:27-34.
220. Goldstone JV, McArthur AG, Kubota A, Zanette J, Parente T, Jönsson ME, et al. Identification and developmental expression of the full complement of Cytochrome P450 genes in Zebrafish. *BMC Genomics*. 2010;11(1):643.
221. McGrath P, Li C-Q. Zebrafish: a predictive model for assessing drug-induced toxicity. *Drug Discovery Today*. 2008;13(9):394-401.
222. Ščupáková K, Balluff B, Tressler C, Adelaja T, Heeren RMA, Glunde K, et al. Cellular resolution in clinical MALDI mass spectrometry imaging: the latest advancements and current challenges. 2020;58(6):914-29.
223. Trim PJ, Snel MF. Small molecule MALDI MS imaging: Current technologies and future challenges. *Methods*. 2016;104:127-41.
224. Cheung-Ong K, Giaever G, Nislow C. DNA-Damaging Agents in Cancer Chemotherapy: Serendipity and Chemical Biology. *Chemistry & Biology*. 2013;20(5):648-59.
225. Bouwman P, Jonkers J. The effects of deregulated DNA damage signalling on cancer chemotherapy response and resistance. *Nature Reviews Cancer*. 2012;12(9):587-98.
226. Piekna-Przybylska D, Bambara RA, Balakrishnan L. Acetylation regulates DNA repair mechanisms in human cells. *Cell cycle (Georgetown, Tex)*. 2016;15(11):1506-17.
227. Sommers JA, Suhasini AN, Brosh RM. Protein Degradation Pathways Regulate the Functions of Helicases in the DNA Damage Response and Maintenance of Genomic Stability. 2015;5(2):590-616.
228. Caron M-C, Sharma AK, O'Sullivan J, Myler LR, Ferreira MT, Rodrigue A, et al. Poly(ADP-ribose) polymerase-1 antagonizes DNA resection at double-strand breaks. *Nature communications*. 2019;10(1):2954.
229. Yap TA, Plummer R, Azad NS, Helleday T. The DNA Damaging Revolution: PARP Inhibitors and Beyond. 2019(39):185-95.
230. Jurkovicova D, Neophytou CM, Gašparović AČ, Gonçalves AC. DNA Damage Response in Cancer Therapy and Resistance: Challenges and Opportunities. 2022;23(23):14672.
231. Chen T, Tongpeng S, Lu Z, Topatana W, Juengpanich S, Li S, et al. DNA damage response inhibition-based combination therapies in cancer treatment: Recent advances and future directions. 2022;3(1):44-67.
232. Schrank BR, Aparicio T, Li Y, Chang W, Chait BT, Gundersen GG, et al. Nuclear ARP2/3 drives DNA break clustering for homology-directed repair. *Nature*. 2018;559(7712):61-6.

233. Watanabe Y, Miyasaka KY, Kubo A, Kida YS, Nakagawa O, Hirate Y, et al. Notch and Hippo signaling converge on Strawberry Notch 1 (Sbno1) to synergistically activate Cdx2 during specification of the trophectoderm. *Sci Rep.* 2017;7:46135.
234. Emert-Sedlak L, Shangary S, Rabinovitz A, Miranda MB, Delach SM, Johnson DE. Involvement of cathepsin D in chemotherapy-induced cytochrome c release, caspase activation, and cell death. *Molecular Cancer Therapeutics.* 2005;4(5):733-42.
235. Minarowska A, Minarowski L, Karwowska A, Gacko M. Regulatory role of cathepsin D in apoptosis. *Folia histochemica et cytobiologica.* 2007;45(3):159-63.
236. Mijanovic O, Petushkova AI, Brankovic A, Turk B, Solovieva AB, Nikitkina AI, et al. Cathepsin D-Managing the Delicate Balance. *Pharmaceutics.* 2021;13(6).
237. Kågedal K, Johansson U, Öllinger K. The lysosomal protease cathepsin D mediates apoptosis induced by oxidative stress. 2001;15(9):1592-4.
238. Banay-Schwartz M, Bracco F, DeGuzman T, Lajtha A. Developmental changes in the breakdown of brain tubulin by cerebral cathepsin D. *Neurochemical Research.* 1983;8(1):51-61.
239. Benes P, Vetvicka V, Fusek M. Cathepsin D--many functions of one aspartic protease. *Critical reviews in oncology/hematology.* 2008;68(1):12-28.
240. Houben T, Oligschläeger Y, Hendrikx T, Bitorina AV, Walenbergh SMA, van Gorp PJ, et al. Cathepsin D regulates lipid metabolism in murine steatohepatitis. *Scientific Reports.* 2017;7(1):3494.
241. Liu K, Czaja MJ. Regulation of lipid stores and metabolism by lipophagy. *Cell Death & Differentiation.* 2013;20(1):3-11.
242. Koundouros N, Pouligiannis G. Reprogramming of fatty acid metabolism in cancer. *British Journal of Cancer.* 2020;122(1):4-22.
243. Lee JS, Oh SJ, Choi HJ, Kang JH, Lee SH, Ha JS, et al. ATP Production Relies on Fatty Acid Oxidation Rather than Glycolysis in Pancreatic Ductal Adenocarcinoma. *Cancers.* 2020;12(9).
244. Monaco ME. Fatty acid metabolism in breast cancer subtypes. *Oncotarget.* 2017;8(17):29487-500.
245. Ma Y, Temkin SM, Hawkrigde AM, Guo C, Wang W, Wang XY, et al. Fatty acid oxidation: An emerging facet of metabolic transformation in cancer. *Cancer Lett.* 2018;435:92-100.
246. Schlaepfer IR, Rider L, Rodrigues LU, Gijón MA, Pac CT, Romero L, et al. Lipid Catabolism via CPT1 as a Therapeutic Target for Prostate Cancer. *Molecular Cancer Therapeutics.* 2014;13(10):2361-71.
247. Ricciardi MR, Mirabilii S, Allegretti M, Licchetta R, Calarco A, Torrisi MR, et al. Targeting the leukemia cell metabolism by the CPT1a inhibition: functional preclinical effects in leukemias. *Blood.* 2015;126(16):1925-9.
248. Pacilli A, Calienni M, Margarucci S, D'Apolito M, Petillo O, Rocchi L, et al. Carnitine-Acyltransferase System Inhibition, Cancer Cell Death, and Prevention of Myc-Induced Lymphomagenesis. *JNCI: Journal of the National Cancer Institute.* 2013;105(7):489-98.
249. Zhang D, Liang X, He X-Y, Alipui OD, Yang S-Y, Schulz HJJJoBC.  $\Delta^3, 5, \Delta^2, 4$ -dienoyl-CoA Isomerase is a multifunctional isomerase: a structural and mechanistic study. 2001;276(17):13622-7.

250. Klener P, Klanova M. Drug Resistance in Non-Hodgkin Lymphomas. *Int J Mol Sci.* 2020;21(6).
251. Cree IA, Charlton P. Molecular chess? Hallmarks of anti-cancer drug resistance. *BMC Cancer.* 2017;17(1):10.
252. Mansoori B, Mohammadi A, Davudian S, Shirjang S, Baradaran B. The Different Mechanisms of Cancer Drug Resistance: A Brief Review. *Advanced pharmaceutical bulletin.* 2017;7(3):339-48.
253. Gottesman MMJArom. Mechanisms of cancer drug resistance. 2002;53(1):615-27.
254. Rodriguez C, Commes T, Robert J, Rossi J-F. Expression of P-glycoprotein and anionic glutathione S-transferase genes in non-hodgkin's lymphoma. *Leukemia Research.* 1993;17(2):149-56.
255. Kim J-H, Choi A-R, Kim YK, Yoon S. Co-treatment with the anti-malarial drugs mefloquine and primaquine highly sensitizes drug-resistant cancer cells by increasing P-gp inhibition. *Biochemical and Biophysical Research Communications.* 2013;441(3):655-60.
256. Marshall HT, Djamgoz MBA. Immuno-Oncology: Emerging Targets and Combination Therapies. *Frontiers in oncology.* 2018;8:315.
257. Roma-Rodrigues C, Mendes R, Baptista PV, Fernandes AR. Targeting Tumor Microenvironment for Cancer Therapy. 2019;20(4):840.
258. Reuter S, Gupta SC, Chaturvedi MM, Aggarwal BB. Oxidative stress, inflammation, and cancer: How are they linked? *Free Radical Biology and Medicine.* 2010;49(11):1603-16.
259. Wherry EJ, Kurachi M. Molecular and cellular insights into T cell exhaustion. *Nature Reviews Immunology.* 2015;15(8):486-99.
260. Bezombes C, Pérez-Galán P. Immunotherapies in Non-Hodgkin's Lymphoma. *Cancers.* 2021;13(14).
261. Brudno JN, Kochenderfer JN. Chimeric antigen receptor T-cell therapies for lymphoma. *Nature Reviews Clinical Oncology.* 2018;15(1):31-46.